THÈSE

présentée en vue d'obtenir le grade de Docteur de l'Université de Lille en
Sciences et technologies de l'information et de la communication
École Doctorale: **072 Sciences pour l'Ingénieur**

par

Michel SAIDEH

Contributions on Radio Access Techniques for Future Railway Communications System

Soutenue le 05/12/2019 à Villeneuve d'Ascq,
devant le jury composé de :

Rapporteurs

- M. Michel TERRE	Professeur, CNAM
- Mme Karine AMIS	Professeur, IMT atlantique, Brest

Examinateurs

- M. Kosai RAOOF	Professeur, Université du Mans
- M. Loïc BRUNEL	Dr, Mitsubishi Electric R&D Centre Europe

Directeurs de thèse

- Mme Marion BERBINEAU	Directrice de Recherche, IFSTTAR, COSYS, LEOST, Villeneuve d'ascq
- M. Iyad DAYOUB	Professeur, UPHF

Acknowledgments

Throughout this Ph.D journey, I have passed through many life changing experiences where the support and guidance of too many people were of major importance.

I would like to start by thanking my Ph.D directors, Mme Marion BERBINEAU and M. Iyad DAYOUB, for their support during my Ph.D study. The realisation of this work could have not been possible without their guidance.

I exploit this opportunity to thank my scholorship donors, IFSTTAR and the region "Hauts de France" for their financial support that allowed me to conduct my Ph.D.

I would like to thank M. Michel TERRE and Mme Karine AMIS for accepting to review and evaluate the thesis. Also, I thank M. Kosai RAOOF and M. Loïc Brunel for accepting to be members of the jury.

Special thanks to my friends and colleagues at IFSTTAR and Railenium: Anthony, Mouna, Mohamed, Romain, Sana, Yamen, Kawtar, Céline, Ali, Luca, Olivier, Julien, Maha, Nicolas, Enjy, Verina, Mathieu, Elisa, Malik, Sebastien and many other names that are written in my memories. Thank you for the time we spent together which made this Ph.D a nice adventure.

I thank my Dad and Mum, my sisters Laura and Joelle, and my brothers Georges and Marc for being my family. I thank them for their prayers and encouragements during the hardest times, for the laughs and joys.

In the end, I would like to thank my best friend, my fiance, my wife and my life partner, Roula, for being with me.

Abstract

Nowadays, a huge amount of data exchanges is needed in the railway system. This is particularly to support autonomous train, reduce operation and maintenance costs, increase safety and security. In the same time, many new services are offered to passengers. There is no unique technology that can satisfy all these needs. Consequently, different industrial and academical research projects are on-going at European and International levels to develop the Future Railway Mobile Communications System (FRMCS). FRMCS will be IP-based, adaptable, agnostic to radio technology and resilient to technological evolutions. In addition, it should support high data rate, low latency, large bandwidth, and efficient spectrum utilization.

The FRMCS is expected to be able to choose in real time between different available radio access technologies in function of applications needs and the surrounding railway environment. Among these technologies, we can mention the Wi-Fi, LTE, satellites and the 5G NR standard in development. Thus, the contributions of this PhD thesis are part of the development of an Adaptable Communication System (ACS) for the railway by considering cutting-edge technologies of the future 5G NR system and beyond.

Different key enabling technologies have been proposed recently under the umbrella of 5G and Beyond communication systems. Among which, radio access techniques play major role over key metrics, such as the efficient utilization of the available spectrum, the high data rates, and the computational complexity of the transceiver system. One of the major technological evolution in that domain concerns the introduction of different Multi-Carrier Modulation (MCM) and Non-Orthogonal Multiple Access (NOMA) techniques.

In this Ph.D thesis, we start by considering the MCM technology in the context of high speed railway. A performance evaluation study is conducted where different MCM schemes are highlighted in different scenarios. The Filtered Bank Multi-Carrier (FBMC) waveform presents high robustness to high mobility scenarios while exploiting the available spectrum efficiently. However, FBMC advantages come with additional built-in interference that challenges traditional transceiver design techniques. Thereby, we propose different contributions that handle the channel estimation and equalization aspects of the FBMC waveform. The contributions aims to assure better performance at the cost of negligible additional

complexity compared with the literature.

Finally, to exploit the data rate gains accompanied with the emerging NOMA technology, we consider the overall MCM based NOMA system. We start by emphasizing the accompanied gains of the different MCM based NOMA schemes compared with the traditional orthogonal multiple access schemes. Thereafter, and to handle the MCM and NOMA induced interference in MCM based NOMA systems, we propose a joint iterative interference cancellation scheme that deals with both interference components. We evaluate this study in different channel scenarios and present accompanied improvements.

Keywords : High Speed Rail, 5G and Beyond, MCM, NOMA, Channel Estimation, Equalization, Interference Cancellation.

Résumé

Avec l'automatisation croissante des fonctions de contrôle commande dans le domaine ferroviaire, on assiste aujourd'hui à une augmentation drastique des échanges d'information. Ces échanges sont cruciaux pour le déploiement du train autonome, la réduction des coûts d'exploitation et de maintenance, l'amélioration de la sécurité. En même temps, de nombreux nouveaux services d'information et de divertissement s'appuyant sur des systèmes de communication sont proposés aux passagers. Pourtant, il n'y a pas aujourd'hui de technologie unique qui puisse satisfaire tous les besoins exigeants en termes de performances. En conséquence, différents projets de recherche industrielle et académique sont en cours aux niveaux européen et international pour développer le système de communication mobile ferroviaire de demain (ou Future Railway Mobile Communication Système – FRMCS). Ce système s'appuiera sur la technologie IP et sera adaptatif, agnostique à la technologie radio et résilient aux évolutions technologiques. En outre, il devra offrir des débits de données élevés, une faible latence, une large bande passante et une utilisation efficace du spectre.

Le FRMCS devra être en mesure de choisir en temps réel entre différentes technologies d'accès radio disponibles en fonction des besoins des applications et de l'environnement ferroviaire. Parmi les technologies d'accès disponibles, on peut citer le Wi-Fi, le LTE, les satellites et le standard 5G NR en cours de développement. Ainsi, les contributions de cette thèse de doctorat s'inscrivent dans le cadre du développement d'un système de communication adaptatif (ACS-Adaptable Communication System) pour le ferroviaire en considérant des technologies de pointe du futur standard 5G NR et au-delà.

Différentes technologies clef ont récemment été proposées dans le cadre de la standardisation 5G et au-delà. Parmi celles-ci, les techniques d'accès radio jouent un rôle majeur sur les métriques clés, telles que l'utilisation efficace du spectre disponible, les débits de données élevés et la complexité du système émetteur-récepteur. Une des évolutions technologiques majeure dans ce domaine consiste en l'introduction de différentes techniques de modulation multi-porteuses (MCM-Multi-Carrier Modulation) et des techniques d'accès multiple non orthogonales (NOMA- Non-Orthogonal Multiple Access).

Dans ce mémoire de thèse de doctorat, nous commençons par étudier les techniques MCM dans le contexte des défis posés par la grande vitesse ferroviaire.

Une évaluation des performances est réalisée en considérant différents systèmes multi porteuses dans différents scénarios. La forme d'ondes FBMC (Filtered Bank Multi-Carrier) offre une grande robustesse dans des scénarios de forte mobilité tout en exploitant efficacement le spectre disponible. Cependant, les avantages de la modulation FBMC s'accompagnent d'interférences intrinsèques supplémentaires qui remettent en question les techniques de conception des émetteurs-récepteurs traditionnels. Ainsi, nous proposons différentes contributions qui concernent les techniques d'estimation et d'égalisation du canal pour la forme d'onde FBMC. Les contributions visent à augmenter les performances finales au prix d'une complexité supplémentaire négligeable si on compare à la littérature existante.

Enfin, pour exploiter les gains de débit associés à la technique d'accès multiple émergente, NOMA, nous avons considéré un système NOMA global associé aux techniques multi porteuses Nous mettons d'abord en évidence les avantages des différents systèmes NOMA associés aux techniques multi porteuses par rapport au système d'accès multiple orthogonal traditionnel associé aux techniques multi porteuses. Cependant, les systèmes d'accès multiple non orthogonaux associés aux techniques multi porteuses (NOMA-MCM) souffrent de deux types d'interférences intrinsèques qui proviennent respectivement de la techniques NOMA et de la technique MCM. Partant de ce constat, nous avons proposé un schéma d'annulation d'interférence itératif commun. Ce schéma est évalué dans différents scénarios de canaux de propagation ferroviaires et nous présentons les améliorations de performances obtenues.

Mots-clés : Train à grande vitesse, 5G et au-delà, MCM, NOMA, Estimation de canal, Egalisation, Annulation d'interférence.

Contents

List of Figures

List of Tables

Mathematical Notations and Acronyms

List of Mathematical Notations and Operators

$(.)^*$	Conjugate operation.
$(.)^T$	Transpose operation.
$(.)^H$	Hermitian conjugate transpose.
$(.)^\dagger$	Pseudo inverse operation.
$E(.)$	Expectation operator.
$\|.\|$	Absolute value operator.
$Tr(.)$	Matrix trace operator.
$diag(.)$	Matlab diag function.
$\otimes$	Kronecker product.
$\mathbb{C}$	Set of complex numbers.
$\mathbb{R}$	Set of real numbers.
$\Re$	Real part of complex number or matrix.
$\Im$	Imaginary part of complex number of matrix.
$\odot$	Matrix Hermitian product.
$\boldsymbol{I}_N$	The $N \times N$ identity matrix.

$J_0(.)$	The Bessel function of the first kind with zero order.
$\mathcal{M}(.)$	Nearest neighbor detection function.

List of Notations

f_c	Carrier frequency.
f_d	Maximum Doppler frequency.
$\boldsymbol{G}$	The MCM modulation matrix.
$\boldsymbol{Q}$	The MCM Demodulation matrix.
$\boldsymbol{x}$	The transmitted data symbols.
M	The number of subcarriers.
K	The number of transmitted time domain symbols.
N	The total number of samples.
F	Frequency spacing between subcarriers.
T	The MCM symbol duration.

List of Acronyms

AP	Auxiliary Pilot.
BEM	Bases Expansion Model.
BER	Bit Error Rate.
BLT	Balian Low Theorem.
CP	Cyclic Prefix.
CR	Cognitive Radio.
CSI	Channel State Information.

DFT	Discrete Fourier Transform.
ECM	Error Covariance Matrix.
FFT	Fast Fourier Transform.
F-OFDM	Filtered- Orthogonal Frequency Division Modulation.
FBMC	Filter Bank Multi-Carrier.
FDD	Frequency Division Duplex.
FDM	Frequency Division Multiplexing.
FDMA	Frequency Division Multiple Access.
GSM	Global System for Mobile communications.
GSNR	Generalized Signal to Noise Ratio.
HSR	High Speed Railway.
IFFT	Inverse Fast Fourier Transform.
ICI	Inter-Carrier Interference.
IID	Independent and Identical Distribution.
IN	Impulsive Noise.
ISI	Inter-Symbol Interference.
LMMSE	Linear Minimum Mean Square Error.
LS	Least Square.
LTE	Long Term Evolution.
MCM	Multi-Carrier Modulation.
MSE	Mean Square Error.
NOMA	Non-Orthogonal Multiple Access.
OFDM	Orthogonal Frequency Division Modulation.

OOB	Out Of Band.
OQAM	Offset Quadrature Amplitude Modulation.
OMA	Orthogonal Multiple Access.
PAM	Pulse Amplitude Modulation.
PDF	Probability Distribution Function.
PSD	Power Spectral Density.
PSIC	Perfect Successive Interference Cancellation.
QAM	Quadrature Amplitude Modulation.
RRC	Root-Raised Cosine.
SC	Superposition Coding.
SIC	Successive Interference Cancellation.
SIMO	Single Input Multiple Output.
SINR	Signal to Interference plus Noise Ration.
SNR	Signal to Noise Ratio.
STM	System Transmission Matrix.
TDD	Time Division Duplex.
TDMA	Time Division Multiple Access.
TFL	Time Frequency Localization.
UFMC	Universal Filtered Multi-Carrier.
WGN	White Gaussian Noise.
WOLA	Weighted Overlap and Add.
WSSUS	Wide Sense Stationary Uncorrelated Scattering.

General Introduction

Context and Motivations

To increase railway attractivity, accessibility and productivity, it is necessary to increase safety, reduce operation and maintenance costs, and offer new services to passengers. To reach this goal, the generalization of information exchange among railway stakeholders is mandatory. These data fluxes must cover the increasing demands in the railway domain including safety-related applications, Internet access for passengers and embedded real-time video transmission for surveillance, *etc.* To answer all these needs, a lot of different wireless communication devices that operate at different frequencies, in the trains and along its infrastructures, are deployed. There is no single technology that can replace all the other ones while still supporting the multitude of usages and needs. Thus, the integration of all these heterogeneous railway-dedicated radio services is unavoidable to improve the global efficiency of the railway system.

In this context, the Railway industry has launched innovative research programs in order to develop a new IP-based Adaptable Communication System (ACS). This ACS should be able to answer all the needs of the railway domain in different sectors (urban, regional, inter-city, high speed and freight). The adaptability of the system is based on the cohabitation of different radio access technology (RAT) bearers. Among them, one can find existing standards such as Wi-Fi, LTE, satellite systems and future ones such as 5G NR and beyond. In this context, the PhD work has focused on key enabling technologies such as Multi Carrier Modulation (MCM) technique combined with Non orthogonal Multiple Access (NOMA) technology. This happens while taking into account the time and frequency selectivity (doubly selectivity) of the HSR channel, in addition to considering Alpha-stable model for the impulsive noise.

Thesis Organization

This thesis is divided into five Chapters. The addressed problem is founded in Chapter 1. Thereafter, we present in Chapter 2 the MCM techniques in details

and we evaluate their performance in doubly selective wireless channel. In Chapter 3, two contributions are detailed. The first one consists in the generalization of the sliding-window TD-LMMSE channel estimation technique so that it might be implemented on different MCM techniques. The second contribution includes the proposal of a pattern based LMMSE channel estimator that exploits the power spread pattern of different prototype filters. The effects of FBMC-OQAM non-orthogonality on the equalization block are treated in Chapter 4. We propose an efficient equalizer that considers the imperfect channel estimation aspect and tries to exploit it while causing no additional complexity. In Chapter 5, we consider the MCM based NOMA combined technologies where we start by presenting their advantages compared to the traditional orthogonal multiple access system. The FBMC-OQAM based NOMA will be highlighted due to its superiority compared to other MCM based NOMA schemes. In addition, we have proposed an iterative inter-user (MOMA induced) and intra-user(MCM and Channel induced) interference cancellation scheme. Finally, we conclude the thesis and give perspectives.

Thesis Contributions

International Journal papers

- **M. Saideh**, Y. Alsaba, I. Dayoub, M. Berbineau and M. Berbineau, "Joint Interference Cancellation for Multi-Carrier Modulation Based Non-Orthogonal Multiple Access," in 2019 IEEE Communications Letters.
  doi: 10.1109/LCOMM.2019.2933817

- **M. Saideh**, I. Dayoub and M. Berbineau, "Efficient Equalization for FBMC-OQAM Under Doubly Selective Channel Estimation Errors," in IEEE Communications Letters, vol. 23, no. 5, pp. 863-866, May 2019.
  doi: 10.1109/LCOMM.2019.2907938

- **M. Saideh**, M. Berbineau and I. Dayoub, "On the Performance of Sliding Window TD-LMMSE Channel Estimation for 5G Waveforms in High Mobility Scenario," in IEEE Transactions on Vehicular Technology, vol. 67, no. 9, pp. 8974-8977, Sept. 2018. doi: 10.1109/TVT.2018.2845551

International Conference Papers

- Y. Alsaba, **M. Saideh**, I. Dayoub and M. Berbineau, "On the Sum Rate of MCM-Based NOMA and MCM-Based OMA Systems," 2020 IEEE International Conference on Communications (ICC) (Submitted).

- **M. Saideh**, Y. Alsaba, I. Dayoub and M. Berbineau, "Performance Evaluation of Multi-Carrier Modulation Techniques in High Speed Railway En-

vironment with Impulsive Noise," In 2019 2nd 5G World Forum (5GWF), Dresden, 2019, pp. 1-5.

- **M. Saideh**, M. Berbineau and I. Dayoub, "On Doubly selective Channel Estimation for FBMC-OQAM using the LMMSE Filter for Future Railway Communications," 2018 16th International Conference on Intelligent Transportation Systems Telecommunications (ITST), Lisboa, 2018, pp. 1-6. doi: 10.1109/ITST.2018.8566706

- **M. Saideh**, M. Berbineau and I. Dayoub, "5G waveforms for Railway," 2017 15th International Conference on ITS Telecommunications (ITST), Warsaw, 2017, pp. 1-5. doi: 10.1109/ITST.2017.7972208

Miscellaneous Publications

Reports

- **Saideh, M.** Rapport d'avencement de thèse, IFSTTAR, June 2019.

- **Saideh, M.** Rapport d'avencement de thèse, IFSTTAR, July 2018.

- **Saideh, M.** Rapport régional d'avencement de thèse, April 2018.

Posters and Presentations

- **Saideh, M.** "Contributions on Filter Bank Multi Carrier System for Future High Speed Railway Communications", SMARTIES 2nd workshop, IFSTTAR, Villeneuve d'Ascq, February 2019.

- **Saideh, M.** "On doubly selective channel estimation for FBMC-OQAM", LEOST seminar, IFSTTAR, Villeneuve d'Ascq, January 2019.

- **Saideh, M.** 2nd Journée des doctorants du département COSYS, IFSTTAR, Paris, July 2018.

- **Saideh, M.** "5G waveforms", SMARTIES 1st workshop, IFSTTAR, Villeneuve d'Ascq, January, 2018.

- **Saideh, M.** "FBMC channel estimation in high mobility environment", SMARTIES 1st workshop, IFSTTAR, Villeneuve d'Ascq, January 2018.

- **Saideh, M.** 1st Journée des doctorants du département COSYS, IFSTTAR, Paris, June 2017.

Chapter 1

Problem Foundation

1.1 Introduction

The railway sector needs new wireless communications systems that could answer all the different applications and services requirements. To do so, future railway communications systems are envisioned to allow the cooperation and exploitation of the available and the upcoming wireless communications technologies, *e.g.*, Wi-Fi, 4G, 5G and Beyond, Satellites communications. Within the research framework of 5G and Beyond, many enabling technologies have been recently developed and analyzed. In this chapter, we present a set of different 5G and Beyond key enabling technologies to end up highlighting the power of the multi-carrier modulation technique as a major player in assuring an efficient spectrum utilization of the railway available spectrum. In addition, we emphasise the high data rate advantages that the non-orthogonal multiple access technology can provide. This will shape the motivations beyond later analysis and developments in the Ph.D thesis.

This chapter is organized as follows. In Section 1.2 we present the motivations and needs that have caused the launch of different industrial and academical projects. These projects aim to replace the current railway communication system, the GSM-R, with an adaptable railway communication system. Section 1.3 recalls different enabling technologies that have been proposed within the framework of 5G and Beyond wireless communications systems. Together, these enabling technologies could satisfy the railway sector needs. In Section 1.4, we present the focus of the Ph.D thesis and the motivations beyond the adoption of the Multi-Carrier Modulation (MCM) and the Non-Orthogonal Multiple-Access (NOMA) techniques.

1.2 Wireless Communications for Railways

With the development of train automation, driverless and autonomous systems, exchanges of information between the different railway stakeholders are growing continuously. Train-to-Ground (T2G), Train-to-Train (T2T) and Intra-Train (InT) wireless communications aim to support a wide variety of applications. This necessitates the existence of high-performance communications technologies that are able to answer the different exigencies, *e.g.*, robustness, reliability, high data rate, high capacity everywhere, spectral efficiency, optimization of radio resource usages, low latency, low energy consumption, resilience to any kind of interference and to technological evolution [1].

Nowadays, the Railway version of the Global System for Mobile communications (GSM-R) is used in the European railway sector for the control and command of high speed trains. GSM-R was built on the GSM phase2+ system while taking into considerations the train control and command requirements of high speed lines crossing Europe. Its date of obsolescence is predicted by 2030 [2] where the industry is expected to stop providing its related products and maintenance support, hence leading to major challenges. In this context, a lot of different wireless communications systems that are based on different technologies have been deployed at different frequency bands, ranging from several MHz to several GHz.

In order to anticipate the GSM-R obsolescence, and to allow the convergence between all existing systems, different European bodies of the railway sector, such as the International Railway Union (UIC), and the European Railway Agency (ERA), have started working toward a new wireless communication system. This system should replace the GSM-R [3, 4] and satisfy all the identified additional needs. Compared to GSM-R, the most important and mandatory characteristics of this new wireless communication system are: Internet Protocol (IP) based communications, bearer agnostic, flexibility and resilience to technological evolution.

In 2007, the European project, named as the Next Generation of Train Control System (NGTC) [5], was launched in the Framework Program 7 (FP7). This project considered the possible convergence between different systems in the railway sector. Preliminary performance evaluations of different wireless technologies were conducted. NGTC project has paved the way for the Future Railway Mobile Communication System (FRMCS) project to be launched by UIC in 2014. FRMCS aims to provide a technology independent plan of user needs and functional specifications concerning the future railway communications system. For example, FRMCS should satisfy all the needs for existing critical communications but also new ones related to driverless trains, virtual coupling and decoupling of trains, and communications with sensors along the tracks. In addition, non-critical applications such as real time video calls, augmented reality data communication, and wireless internet on-train for passengers, should be supported [6].

To offer this wide range of applications and services, the FRMCS has to exhibit

outstanding features such as high data rate, large bandwidth, efficient exploitation of the available bandwidth, flexibility and a low latency. In addition, FRMCS should be resilient to technology evolution in order to cope with long life cycle of railway domain ($\sim$ 30 years is the the average life time of a train) as opposite to the short product life cycle of the public telecommunication industry. To this end, different studies have been conducted in the literature to evaluate the performance of candidate systems. The Long Term Evolution (LTE) system has been particularly studied [7, 8] as a serious candidate to replace GSM-R associated with other systems. However, the fact that FRMCS requires higher data rate and higher bandwidths due to real time HD video transmission for example, has pushed researchers and industry to envision the recently standardized 5G wireless communication system as another alternative [9, 10].

In 2016, the Innovation Program 2 (IP2) of the Horizon 2020 Shift2Rail initiative [11] has gone even further by willing to set up various prototypes to be tested in 2022. In the shift2rail framework, these prototypes are under development today within the X2RAIL-1 [12] and X2RAIL-3 [13] projects. Their aim is to combine different wireless communication systems *e.g.,* 4G, 5G, Wi-Fi and Satellite communications, within the so called Adaptable Communication System (ACS) [14]. In figure 1.1, we present the ACS architecture presented recently by the Shift2Rail annual plan [15]. Different radio access modules will cooperate to provide the required communication needs of the different applications. On-board and track-side applications are considered such as the Automatic Trains Protection (ATP), Automatic Train Operation (ATO), Train Control and Monitoring System (TCMS) and critical voice between driver and signalling teams.

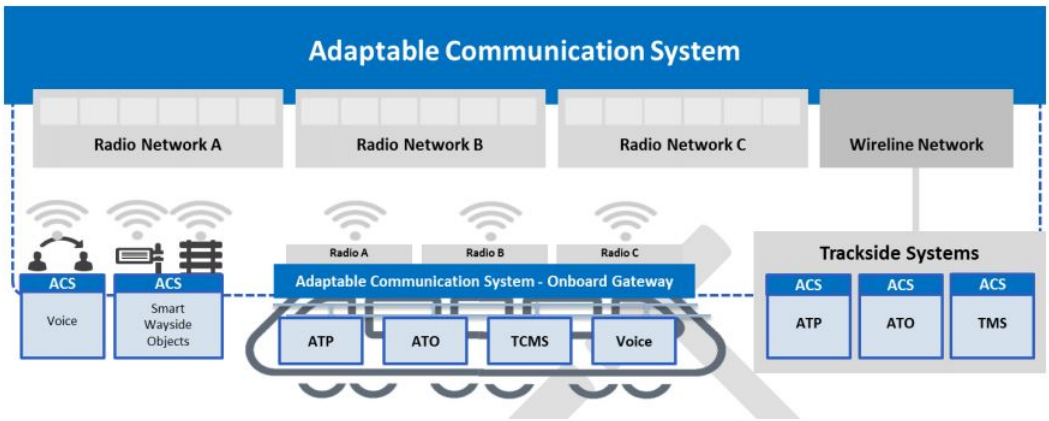

Figure 1.1: ACS architecture [15]

In late 2017, 5GPPP provided its vision of a 5G adaptive communication system where different transceivers coexist to support different radio access technologies. Figure 1.2 shows the 5GPPP presented Medium Access Control (MAC) architecture. The system will be sensing its surrounding environment to be able to exploit both licensed and unlicensed spectrum in an adaptable manner. A centralized Radio Resource Management (cRRM) is used to allow the intelligent and efficient use of the available radio resources from different spectrum bands.

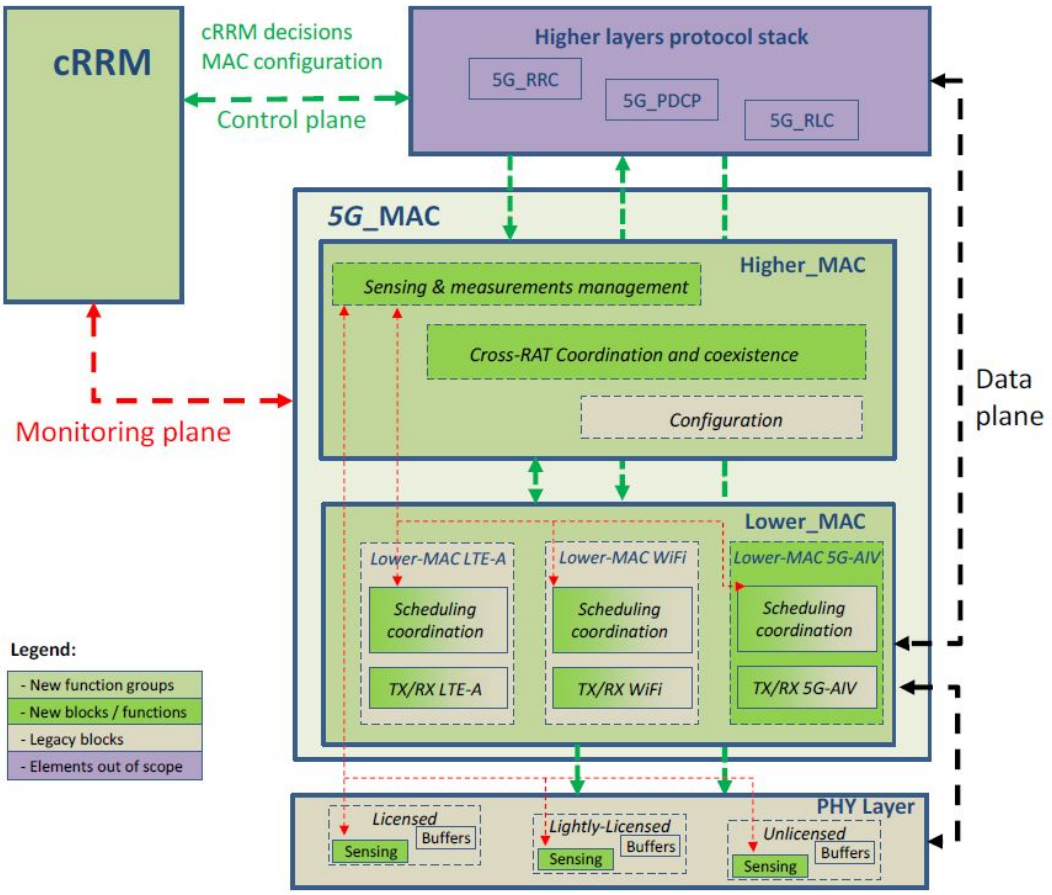

Figure 1.2: 5GPPP MAC architecture [16]

cRRM will help in the coordination process between the supported radio access technologies.

These dynamic spectrum access schemes and different radio access technologies are among many other key enabling technologies that have been recently proposed and studied while witnessing different technical evolutions in order to satisfy the needs of future wireless communication systems.

1.3 5G and Beyond Enabling Technologies

Under the umbrella of the future wireless communication systems, 5G and Beyond, many enabling technologies have emerged recently [17] that offers different improvements.

- The efficient spectrum utilization of the new multi-carrier modulation techniques.
- The high system throughput offered by the Non-Orthogonal Multiple Access.
- The large bandwidths promised by the millimetric waves technology [18].
- The high data rates of the massive MIMO technology [19].
- The unlicensed spectrum utilization and the adaptable capabilities of the Cognitive Radio technology.

Combining these enabling technologies and many others (*e.g.*, wireless software-defined networking, network function virtualization, cloud computing) in the framework of an adaptable communication systems could shape the basis of future railway communication systems.

1.3.1 Radio Access Techniques

Radio access techniques could be seen as the signal processing techniques responsible of transmitting and receiving the desired symbols over the radio air interface through the possible sharing of different resources such as time, frequency, power, and code dimensions. Radio access techniques have access over critical performance metrics such as the time and frequency localization of the transmitted signal, the achieved throughput, and the computational complexity of the transceiver system. At a European level and in the framework of the Information and Communication Technology (ICT) program in FP7, several research projects have investigated the Radio Access Techniques aspect. Among which, we can mention PHYDYAS [20], METIS [21], 5gNow [22], and the EMPhAtic [23] projects. The

major technological evolution that occurred in this domain can be represented by the proposals of many MCM techniques, the non-orthogonal multiple-access technology, and the introduction of the full duplex communications mode.

Multi-Carrier Modulation

The concept of the MCM technique has been first proposed in the 1950s [24] with the aim of combating the frequency selectivity of the wireless channel. This happens by dividing the available bandwidth into many sub-channels with much smaller bandwidths each. Hence, the channel could be considered somehow flat in the frequency domain. This has helped the implementation of low complex transceiver systems and was first represented by the so-called Orthogonal Frequency Division Multiplexing (OFDM) technique. Recently, the interest of MCM technique has been shifted to provide better frequency localization characteristics and which would lead to better exploitation of the available spectrum resources. In addition, the MCM technique could provide waveforms that have short tails in the time domain and hence being efficient to use in short control signals. However, these advantages come normally with additional interference components and/or increased computational complexity. This has led to the proposals and analysis of many MCM schemes.

Non-Orthogonal Multiple Access

In multiple users scenarios, the users access the radio network by sharing the available time and frequency resources. Conventionally, users will be allocated different time and frequency resources in an orthogonal manner such as in the Time Division Multiple Access (TDMA) and the Frequency Division Multiple Access (FDMA) techniques. Recently, NOMA technology [25] has gained a widespread interest due to its accompanied gains in the overall system throughput. NOMA technique allows users to share the same time and frequency resources by adopting a superposition coding schemes at the transmitter and a successive interference cancellation schemes at the receiver. This proved to bring critical improvements in terms of the achieved sumrate of the corresponding users at the cost of additional interference components that needs to be considered within the transceiver design process.

Full Duplex Communications

Conventionally, half duplex communications modes are employed by the use of Time Division Duplex (TDD) or Frequency Division Duplex (FDD) modes. Contrarily to half duplex modes that suffer from a loss in spectral efficiency and an outdated Channel State Information (CSI), full duplex based systems permit the

use of the same time and frequency resources for both transmission and reception. However, this comes with high self interference component where special interference cancellation techniques need to be developed [26].

1.3.2 Millimetric Waves

A straightforward way to increase the channel capacity is to enlarge the deployed bandwidth. This becomes possible by moving toward high frequency ranges, namely, the millimetric waves as suggested by the Federal Communications Commission (FCC) [27]. Millimetric waves normally ranges from the 20 to the 300 GHz which gives the possibility of achieving high throughput in the level of gigabit per second. However, the characteristics of the propagation channel in such frequencies become challenging. The atmosphere absorbs much of the transmitted energy which limits the transmission range [28]. In addition, Non Line of Sight (NLOS) scenarios has shown to cause much more losses in the signal power [29]. In millimetric waves, the NLOS scenario is very common due the blockage that could be caused by small objects such as pedestrians and tree branches [30]. Nevertheless, these bands are very promising for specific applications for 5G and beyond systems [31–33].

1.3.3 Massive MIMO

Another way of increasing the system throughput is through the use of the Massive MIMO (MaMIMO) technology. MaMIMO deploys hundreds of antennas at the base station while using the spatial multiplexing and the Time-Division Duplexing (TDD) modes. In addition to the high spectral efficiency, this results in a reduced latency where the channel will become frequency independent and multipaths propagation will not affect the signal strength anymore. Many studies have been conducted to explore and handle the MaMIMO accompanied challenges such as the pilot contamination [34], the antenna array design [35], and the proposal of appropriate channel models [36].

1.3.4 Cognitive Radio

Cognitive Radio (CR) concept was introduced by Mitola [37] in 1999 and is considered nowadays as a key enabler for efficient spectrum reuse and adaptable wireless communication systems. The CR technology is defined as an *intelligent wireless communication system that is aware of its surrounding environment, and uses the methodology of understanding-by-building to learn from the environment and adapt its internal states to statistical variations in the incoming RF stimuli by making corresponding changes in certain operating parameters in real time, with two pri-*

mary objectives in mind: highly reliable communication whenever and wherever need; efficient utilization of the radio spectrum. [38] The intelligence and awareness capabilities of the CR technology allows it to combine many enabling technologies within an adaptive framework, hence allowing the support of different radio access technologies and the efficient exploitation of the available resources.

Several research works have focused on different aspects of the Cognitive Radio for railways. One of the first CR applications was presented in [39]. Then, the national project *Urbanisme des Radio Communications* (URC) was one of the first projects in France and in Europe to raise the problem of spectral resources optimization in the Paris region while taking into account the transport field and particularly the urban guided systems [40]. Recently, the French national project COgnitive Radio for RaIlway through Dynamic and Opportunistic spectrum Reuse (CORRIDOR) aimed to design, develop and evaluate, in real high-speed railway conditions, CR-based solutions for train-to-ground communications [41]. Several contributions on spectrum sensing and modulation recognition were published also [42–44].

1.4 Focus of the Thesis

Among the many enabling technologies, radio access techniques have a huge impact over different aspects of the wireless communication systems. The rare spectrum resources that are available for the railway sector urges its efficient utilization. To this end, the MCM technique block can provide a highly localized waveform that assures the efficient exploitation of the available resources. However, this efficient spectrum utilization advantage comes normally with additional interference components. This could affect the computational complexity of the transceiver system where special signal processing techniques will be needed. Assuring a higher spectrum efficiency could be done by sharing the same time and frequency resources among different users. This become possible with the NOMA technique where users channel conditions will be used as a degree of freedom to assure achieving an overall higher data rate. In this Ph.D, we consider both the MCM and the NOMA techniques in high speed railway environment where we build our work by the use of MATLAB and some MATLAB classes developed by Vienna University [45].

We start with presenting the MCM technique in **Chapter 2** while considering high mobility environment in addition to the impulsive nature of the noise. The performance of different MCM schemes is evaluated where the aim is to understand the way different MCM schemes react to the challenges of the High Speed Railway (HSR) environment. Based on that, different MCM schemes are highlighted in different scenarios, namely, the Filtered Bank Multi-Carrier (FBMC) waveform will show high robustness to high mobility. This shape the motivation beyond

Chapter 3 and **Chapter 4** where we analyze the estimation and equalization aspects of the FBMC waveform, respectively. In fact, the spectrally efficient version of the FBMC waveform suffers from built-in interference components which urges the need for special signal processing techniques within the design of its transceiver system. Based on this, we propose different contributions aiming to provide an efficient estimation and equalization techniques for the FBMC-OQAM waveform while maintaining a low complexity level.

In the last part of the Ph.D thesis, we included the emerging NOMA technique which brings outstanding data rate gains in multiple access systems. In **Chapter 5**, we study the overall NOMA based MCM system and we compare it to the OMA based MCM system. This study presents the NOMA based MCM advantages and shows that different MCM techniques act with the NOMA system. The fact that NOMA based MCM has two main interference components coming from both NOMA and MCM, motivated us to propose a joint iterative interference cancellation scheme that deals with both interference components. The contribution is analyzed in different channel scenarios.

Further developments and analysis are still needed and envisioned for future studies as we will clarify in the conclusions and perspectives.

Chapter 2

Multi-Carrier Modulation in High Speed Railway Environment

2.1 Introduction

In the previous chapter, we explored the needs for new wireless communication systems that could support the railway services and applications requirements. Many enabling technologies have been proposed as potential answers to the accompanied voracious requirements *e.g.,* high data rate, low latency, large bandwidth. Among the enabling technologies, the multi-carrier modulation technique is considered as a key player in assuring an efficient exploitation of the limited time and frequency resources. In this chapter, we study the MCM technique in details while surfing around its proposed MCM techniques. Besides, we evaluate the MCM performance under different HSR aspects. Low and high mobility cases are adopted along with multipaths scenario. Furthermore, we analyze the effects of the Impulsive Noise (IN) which exists due to the non-perfect contact between the catenary and the pantograph of the railway system.

This chapter is organized as follows. In Section 2.2, we start by presenting a literature study of the MCM technology. A brief historical record of MCM development and the motivations beyond the different proposed MCM schemes are provided. In Section 2.3, we detail the general work principles of the MCM technology. Furthermore, a generalized matrix model is adopted and explained. The model will allow later developments and evaluations to be conducted on different MCM schemes within a unified framework. In Section 2.4, we explore the different types of the MCM technique while explaining their work principles. In addition, we go through their advantages and disadvantages in terms of spectral efficiency, complex orthogonality and time and frequency localization. In Section 2.5, we introduce the wireless propagation environment and the impulsive noise of the HSR. This environment will be used in Section 2.6 to conduct a performance evaluation study where certain MCM techniques will be highlighted in certain conditions.

Finally, we conclude the chapter and we present some perspectives in Section 2.7.

2.2 MCM History and Motivations

The emergence of the MCM technique could be tracked back to the late 1950s [24]. The idea was to send data by dividing it into several bit streams and modulating each stream with a different subcarrier. These subcarriers are totally separated with different steep bandpass filters. This resulted in the so-called Frequency Division Multiplexing (FDM) technology. In 1970, a US patent [46] proposed a high data rate FDM version that uses densely spaced subcarriers with overlapped spectrum. That was possible by designing the overlapped spectrums to be orthogonal, hence the name Orthogonal Frequency Division Multiplexing (OFDM). Although OFDM waveforms allowed full spectral efficiency while handling frequency selective challenges, it was the single carrier technologies that gained control over early communication systems. In fact, it was only with the full digitalization of the implemented IFFT/FFT modem [47, 48] that MCM in general, and OFDM in particular, have sparked a widespread interest.

The OFDM technology came to counter the sensitivity of single carrier techniques to frequency selective channels [49]. This is due to the fact that to send high data rates in a given bandwidth, the symbol duration in single carrier techniques has to be shortened as much as possible. However, in frequency selective channel environments, the symbol duration will become much smaller than channel coherence time, hence, creating high level of inter symbol interference. This implies the need for complex non-linear receivers. OFDM provided a critical solution to achieve the desirable high data rate within a frequency selective channel while assuring the simplicity of the receiver. This happens by dividing the assigned bandwidth into several sub-channel (subcarriers) with narrow bandwidth for each. Hence, the frequency selective channel can be seen as approximately flat within each sub-channel.

In order to prevent the Inter-Symbol Interference (ISI), a Cyclic-Prefix (CP) extension was appended to OFDM, resulting in the CP-OFDM waveform. CP-OFDM has witnessed a wide scale adoption in different wireless and wireline standards, *e.g.*, VDSL, IEEE 802.11a/g, IEEE 802.16, 4G, and lately in 5G also. However, CP-OFDM suffers from two main problematics. First, it has a bad spectral containment due to its rectangular pulse shape. Second, the redundant CP part represents a direct loss in spectral efficiency. Consequently, the crucial need for new MCM technique was risen recently [50]. An interesting amount of research has been carried out where many MCM techniques were proposed while offering various tradeoffs [51–58]. Different approaches have tried to apply tiny modifications on the (CP)-OFDM waveform. This aimed to assure a high backward compatibility with 4G based OFDM systems while enhancing other aspects. Zero-Tail (ZT) Discrete Fourier Transform (DFT)-spread-OFDM, (ZT-DFT-s-OFDM) [51] tech-

nique proposed to zero the edges of the DFT input. This resuls in DFT-s-OFDM symbols with low power tails, thus assuring smoother transition and hence better Out Of Band (OOB) emission. In [52], Unique Word DFT-s-OFDM has been presented to design the DFT tail inputs in such a way that lessen the power of the IFFT output tail. That has shown to enhance performance alongside the spectral containment. In order to take advantage of the existing heads and tails, a generalized version of the ZT DFT-s-OFDM has proposed to use recognized sequences at the head & tail of the DFT input, setting them to be identical at successive symbols [53]. This could be used for synchronization purposes as opposite to the low power head and tail case. Another MCM approach applied windowing on the OFDM based waveform. In other words, the edges of each OFDM symbol are smoothed with a specific window, thus enhancing its spectral containment [54, 59].

To better decrease the OOB emission, another perspective adopted the filtering view point. Filtering based MCM techniques can be divided into subband and subcarrier based filtering methods. In subband filtering, the system bandwidth is divided into several subbands, while a classic OFDM operation is applied in each subband. That allows different settings to be adopted in different subbands, in accordance with the requirements of various applications. For example, a subband with small subcarriers spacing can support massive connections while another with big subcarrier spacing to support low delay applications [55]. Different subband based filtering MCM techniques have been proposed in the literature such as the Universal Filtered Multicarrier (UFMC) [56] and the Filtered OFDM (F-OFDM) [57]. The subband in F-OFDM is normally larger than that in UFMC since F-OFDM subband represents a specific use case. Subband based filtering schemes offer a good tradeoff between time and frequency localization. This is because filtering is not applied on the whole bandwidth, as in OFDM, nor on each subcarrier, but on a flexible group of subcarriers. On the other hand, Filter-Bank MultiCarrier (FBMC) based waveforms adopt the extreme case of filtering each subcarrier on its own. This results in the best frequency localization while loosing other properties [58]. For example, Quadrature Amplitude Modulation (QAM) based FBMC systems sacrifice their spectral efficiency while Offset-QAM (OQAM) based FBMC systems suffer from a new built-in interference.

Different studies have been conducted in the literature to compare many aspects of different MCM techniques [17, 60, 61]. FBMC based waveforms have proven to offer the best spectral containment, hence being mostly suitable for efficient spectrum reuse and asynchronous communications. However, and in addition to the FBMC-OQAM built-in interference induced challenges [62, 63], a main disadvantage is its long filter tails that caused it to be inefficient for the short packet scenarios [64]. Using a rectangular window would be a straightforward answer to this problem, which will remove the tails completely. However that comes at the cost of highly increased OOB [65]. A smoother window has been used in [66] hence enhancing the OOB while resulting in high ISI and Inter-Carrier Interference (ICI). In [67, 68], virtual symbols have been placed at the edges of each packet, while designing them in order to remove the tails. This has helped to avoid increased

ICI/ISI while having a good OOB. On the other hand, subband filtering based waveforms offered a high degree of flexibility while offering a balanced tradeoff between time and frequency localization. OFDM based waveforms enjoy the small complexity feature while having the high backward compatibility. In this chapter, and after analyzing the MCM technique and its proposed schemes, we compare their performance from a high speed railway environment perspective.

2.3 MCM Principles

In multi-carrier modulation techniques, the messages to be transmitted are first mapped into a 2-dimensional space *e.g.*, a time-frequency space. Then, they are transformed into the signal space via the synthesis function $g_{m,k}(t)$ of the m^{th} subcarrier and the k^{th} time symbol. Hence, the time domain transmitted signal $s(t)$ could be written as follows

$$s(t) = \sum_{k=0}^{K-1} \sum_{m=0}^{M-1} g_{m,k}(t) x_{m,k} \tag{2.1}$$

where $x_{m,k} \in \mathbb{C}$ is the transmitted symbol at the m^{th} subcarrier and the k^{th} time symbol, with M denoting the number of sub-carriers and K the number of time domain symbols of the whole transmission block. $x_{m,k} \in \mathbb{R}$ is a possible special case *e.g.*, Pulse Amplitude Modulation (PAM) symbols. The synthesis function $g_{m,k}(t)$ that maps $x_{m,k}$ into the signal space can be written on the following form

$$g_{m,k}(t) = p_{tx}(t - kT) e^{j2\pi mF(t-kT)} \tag{2.2}$$

where $p_{tx}(t)$ is the transmitter prototype filter, also known as the pulse shape or Gabor atom. This pulse shape will determine the energy distribution (in time and frequency domains) of the transmitted symbol. T is the symbol duration while F is the subcarrier spacing. Now, we can read Equation 2.2 as follows: $g_{m,k}(t)$ *is considered as the prototype filter* $p_{tx}(t)$ *with translation of* kT *and modulation of* mF. The family of $g_{m,k}(t)$ functions is called a Gabor system.

In the receiver, and after passing through the channel, we decode the received symbols $y_{m,k}$ by the projection of the received signal $r(t)$ on the analysis function $q_{m,k}(t)$

$$y_{m,k} = \langle r(t), q_{m,k}(t) \rangle = \int_{t=-\infty}^{\infty} r(t) q^*_{m,k}(t) dt \tag{2.3}$$

where

$$q_{m,k}(t) = p_{rx}(t - kT) e^{j2\pi mF(t-kT)} \tag{2.4}$$

Similar to $g_{m,k}(t)$, the analysis function $q_{m,k}(t)$ is expressed as the receiver prototype filter $p_{rx}(t)$ after translation in time and modulation in frequency. This will result in another Gabor system at the receiver. The overall aim of the receiver pulse shape will be to better combine the dispersed energy of the transmitted

symbol. Hence, the performance of a multi-carrier modulation technique could be determined by the joint effects of the analysis and synthesis filters. Three main characteristics can be extracted to determine the overall performance of the MCM system:

1. Orthogonality:
   If the analysis and synthesis filters are designed so that $\langle g_{m1,k1}(t), q_{m2,k2}(t)\rangle = \delta(m_2 - m_1)\delta(k_2 - k_1)$, then the concerned MCM scheme is called to be orthogonal or bi-orthogonal. $\delta(.)$ is the Kronecker delta function given as:

$$\delta(n) = \begin{cases} 1, & n = 0 \\ 0, & n \neq 0 \end{cases} \tag{2.5}$$

   While orthogonality requires the transmitter and the receiver to use the same prototype filters *i.e.*, $p_{tx}(t) = p_{rx}(t)$, bi-orthogonality is more loose and allow the use of different prototype filters.

2. Time Frequency Localization (TFL):
   The time and frequency localization (σ_t and σ_f) of a pulse shape characterizes the time and frequency variance of its energy, respectively. This can be expressed as follows:

$$\sigma_t = \sqrt{\int_{-\infty}^{\infty} (t - \bar{t})|p(t)|^2 dt} \tag{2.6}$$

$$\sigma_f = \sqrt{\int_{-\infty}^{\infty} (f - \bar{f})|P(f)|^2 df} \tag{2.7}$$

   where $P(f)$ is the Fourier transformation of $p(t)$ while $\bar{t}$ and $\bar{f}$ express the mean time and the mean frequency, respectively, of the pulse $p(t)$. In case $\sigma_t\sigma_f < \infty$, the MCM scheme is referred to have TFL localized filters, otherwise, they are non-localized.

3. Symbol density:
   The symbol density of an MCM technique expresses its spectral efficiency. In other words, how much the MCM technique is efficient in exploiting the time and frequency available resources. The maximal spectral efficiency is achieved by designing the MCM technique so that $F = 1/T$, which means a symbol density of $TF = 1$.

Based on the Balian Low Theorem (BLT) [69], the design of any MCM technique cannot achieve the aforementioned three properties simultaneously. Trade-offs have to be made depending on the desired characteristics.

Before presenting different schemes of the MCM technology, we write the overall system model in a matrix form. Hence, the demodulated vector $\boldsymbol{y}$ of the

transmitted block of symbols is given as [58]:

$$\boldsymbol{y} = \underbrace{\boldsymbol{Q}^H \boldsymbol{H} \boldsymbol{G}}_{\mathcal{D}} \boldsymbol{x} + \boldsymbol{Q}^H \boldsymbol{\eta} \tag{2.8}$$

where

$$\boldsymbol{G} = [\boldsymbol{g}_{1,1}\boldsymbol{g}_{2,1}...\boldsymbol{g}_{M,1}\boldsymbol{g}_{1,2}...\boldsymbol{g}_{M,K}] \tag{2.9}$$

$$\boldsymbol{Q} = [\boldsymbol{q}_{1,1}\boldsymbol{q}_{2,1}...\boldsymbol{q}_{M,1}\boldsymbol{q}_{1,2}...\boldsymbol{q}_{M,K}] \tag{2.10}$$

$$\boldsymbol{x} = [x_{1,1}x_{2,1}...x_{M,1}x_{1,2}...x_{M,K}]^T \tag{2.11}$$

$\boldsymbol{\eta} \in \boldsymbol{C}^{N\times 1}$ is the additive noise component. By sampling $g_{m,k}(t)$ and $q_{m,k}(t)$, the samples are grouped in one vector $\boldsymbol{g}_{m,k}, \boldsymbol{q}_{m,k} \in \mathbb{C}^{N\times 1}$, respectively, where $\boldsymbol{g}_{m,k} = \boldsymbol{G}(:, mk)$ and $\boldsymbol{q}_{m,k} = \boldsymbol{Q}(:, mk)$. We denote by N to the number of samples of the whole transmission block while $\boldsymbol{H}$ is the channel convolution matrix which is given as follows:

$$\boldsymbol{H} = \begin{bmatrix} h_0(1) & 0 & \cdots & \cdots & \cdots & \cdots & 0 \\ h_1(1) & h_0(2) & \cdots & \cdots & \cdots & \cdots & 0 \\ \vdots & \vdots & \ddots & & & & \vdots \\ h_{L-1}(1) & h_{L-2}(2) & & \ddots & & & \vdots \\ 0 & h_{L-1} & & & & & \vdots \\ \vdots & \vdots & & & & \ddots & \vdots \\ 0 & 0 & \cdots & h_{L-1}(N-L-1) & \cdots & \cdots & h_0(N) \end{bmatrix} \tag{2.12}$$

where $h_l(n)$ is the channel impulse response of the l^{th} path and the n^{th} time domain sample. The System Transmission Matrix (STM) $\mathcal{D} = \boldsymbol{Q}^H \boldsymbol{H} \boldsymbol{G}$ reflects the complex orthogonality property of the MCM technique and the doubly selectivity of the channel.

By assuming an ideal channel scenario, the STM of complex orthogonal MCM techniques will become diagonal. Being diagonal means that simple single tap equalizer, *i.e.*, $\boldsymbol{A}^H = diag\,(\mathcal{D})^{-1}$, is sufficient to recover the transmitted data.

$$\hat{\boldsymbol{x}} = \boldsymbol{A}^H \boldsymbol{y} = \boldsymbol{x} + diag(\mathcal{D})^{-1}\boldsymbol{\eta} \tag{2.13}$$

However, in non-orthogonal MCM techniques or with the doubly selective nature of the radio propagation channel, as we will see later, the STM will lose its diagonality. This will cause ICI and ISI that will need special treatment in the transceiver design.

$$\boldsymbol{y} = diag(\mathcal{D})\boldsymbol{x} + \underbrace{ndiag(\mathcal{D})\boldsymbol{x}}_{\text{ISI / ICI}} + \boldsymbol{Q}^H\boldsymbol{\eta} \tag{2.14}$$

where applying the one tap equalizer will give

$$\hat{\boldsymbol{x}} = \boldsymbol{x} + diag(\mathcal{D})^{-1}\left(\underbrace{ndiag(\mathcal{D})\boldsymbol{x}}_{\text{ISI/ICI}} + \boldsymbol{Q}^H\boldsymbol{\eta}\right) \tag{2.15}$$

2.4 MCM Techniques

Based on the BLT, different waveforms have been proposed. In this section, we present the well known (CP)-OFDM waveform, an enhanced waveform with high backward compatibility, the Windowed-OFDM, a subband filtering based waveform, the F-OFDM, and a subcarrier filtering based waveform, the FBMC-(O)QAM.

2.4.1 (CP)-OFDM

The OFDM waveform adopts a rectangular pulse shape for the analysis and synthesis filters

$$p_{tx}(t) = p_{rx}(t) = \begin{cases} \frac{1}{T_0}, & -\frac{T_0}{2} \leq t \leq \frac{T_0}{2} \\ 0, & otherwise \end{cases} \tag{2.16}$$

Using this pulse shapes with a symbol duration of $T = T_0$ and subcarrier spacing of $F = 1/T_0$ will allow the OFDM waveform to maintain two main advantages. First, the complex orthogonality condition. Second, the full symbol density (TF=1). However, the complex orthogonality at the receiver is conditioned with the frequency selectivity of the channel. In other words, the channel has to be flat within each subcarrier where the channel maximum delay spread (τ_{max}) has to be much smaller than the symbol duration $\tau_{max} \ll T$. However, this is not usually the case. To handle that, an extended version of the OFDM waveform is used, the so called CP-OFDM.

In CP-OFDM, the last T_{CP} portion of each OFDM symbol is copied and appended to the beginning of the same symbol. By designing the cyclic prefix $T_{CP} > \tau_{max}$, we assure that the frequency selective induced inter-symbol interference will reside the T_{CP} part only. At the receiver, the CP, which is redundant and polluted with ISI, is dropped before the demodulation process. Hence, it guarantees the complex orthogonality condition once again. In 4G systems, two CP versions could be used depending on the channel frequency selectivity, the normal CP with $T_{CP} = 4.7[\mu s]$ and the extended CP version with $T_{CP} = 16.7[\mu s]$.

The main advantage of the CP-OFDM waveform is presented in the low complexity implementation of its modem (IFFT/FFT). Besides, simple one tap equalizers perform well due to CP-OFDM complex orthogonality condition. One the other hand, CP-OFDM suffers from a loss in spectral efficiency due to the use of the Cyclic-Prefix where $TF = 1 + T_{CP}/T_0$. In addition, the rectangular pulse shape of the CP-OFDM is translated into bad frequency localization *i.e.*, $\sigma_f = \infty$, with high OOB emission.

2.4.2 Windowed OFDM

Windowed OFDM aims to decrease the OOB emission of the CP-OFDM waveform by smoothing the edges of each CP-OFDM symbol. This assures a smooth transition from one CP-OFDM symbol to the other, hence getting a better spectral containment.

In Figure 2.1, we illustrate how the Windowed-OFDM, or the so-called Weighted OverLapp and Add (WOLA), is constructed from the OFDM waveform through the following steps:

1. Adding a cyclic prefix: The last $T_{CP} + T_W$ portion of the OFDM symbol is copied and appended to its beginning. T_W expresses the transition area.
2. Adding a cyclic suffix: The first T_W portion of the OFDM symbol is copied and appended to its end.
3. Windowing: The extended symbol of length $T_{W-OFDM} = T_{OFDM} + T_{CP} + 2T_W$ is multiplied with a specific smoothing window.
4. Overlapping: Adjacent symbols are overlapped in the T_W edges of each symbol, hence assuring the same spectral efficiency as that of CP-OFDM.

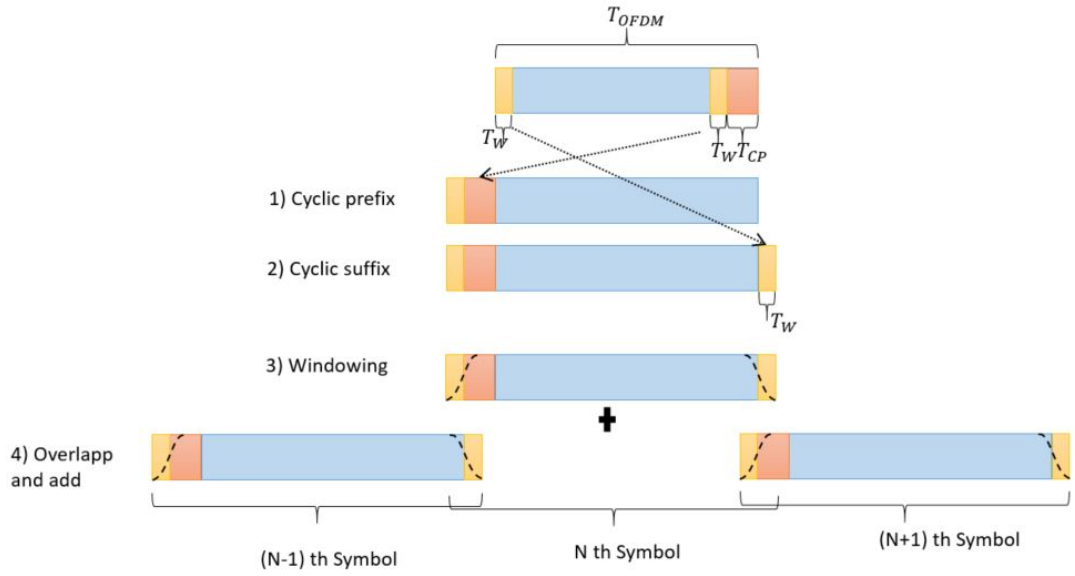

Figure 2.1: WOLA process

Different windowing functions can be used while offering a tradeoff between the main lobe width and side lobes suppression [70]. In our work, we consider the Raised Cosine (RC) window, or the so called Hanning window, since it offers a fair tradeoff as shown in [59]. At the receiver, the windowing principle could be also applied since it helps handling the ISI problem of asynchronous users.

2.4.3 Filtered OFDM

In order to better enhance the frequency localization property, filtering should be included. In Filtered-OFDM, each group of subcarriers (subband) are filtered to assure better frequency localization. A F-OFDM signal is constructed as follows:

1. The assigned bandwidth is divided into several subbands, a subband for each user/use case.
2. Subbands are separated using small guard bands to avoid inter-subband interference.
3. In each subband, a conventional CP-OFDM system is constructed with different design parameters, *e.g.*, CP length, subcarrier spacing, *etc.*
4. On each (sub) CP-OFDM system, a subband filter is applied to achieve lower OOB emission and to suppress the inter-subband interference.

The subband filter design is considered as a tradeoff between time and frequency localization. While the filter should enjoy good time localization to avoid inter-symbol interference, its frequency localization should be well considered also. In this Ph.D, we adopt a soft-truncated sinc filter which is based on using a fully rectangular filter multiplied with Hann window.

One main advantage of the F-OFDM, besides its enhanced OOB emission, is the high degree of flexibility. F-OFDM allows each subband to be designed in a specific way that could satisfy the requirements of the application at hand while considering the accompanied channel conditions.

2.4.4 FBMC

Filter bank multi-carrier based waveforms offer the best spectral containment characteristics due to filtering each subcarrier on its own. Two main versions of FBMC waveforms exist: QAM based FBMC (FBMC-QAM) and Offset QAM (OQAM) based FBMC (FBMC-OQAM).

FBMC-QAM

In FBMC-QAM, the prototype filter $p(t)$ is designed to achieve the TFL property and the complex orthogonality condition at the cost of a big loss in the symbol density.

In Figure 2.2, we illustrate the time and frequency spacing between FBMC-QAM symbols. This mapping results in a symbol density of $TF = 2$ where the loss

is due to the large frequency spacing $F = 2/T_0$. Different TFL prototype filters

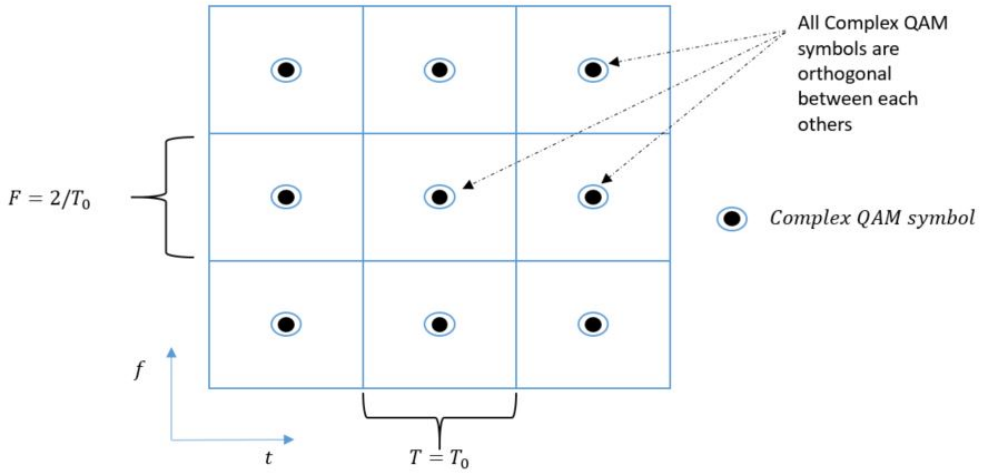

Figure 2.2: Resource grid structure of FBMC-QAM .

exists and are used for the complex orthogonal FBMC-QAM waveform, *e.g.,* PHYDYAS [71], Hermite and the Root Raised Cosine (RRC) prototype filters. The PHYDYAS prototype filter has been given in PHYDYAS project [20] as follows:

$$p(t) = \begin{cases} \frac{1+2\sum_{i=1}^{O-1} a_i cos\left(\frac{2\pi t}{OT_0}\right)}{O\sqrt{T_0}}, & -\frac{OT}{2} < t \leq \frac{OT_0}{2} \\ 0, & \text{Otherwise} \end{cases} \tag{2.17}$$

PHYDYAS coefficients a_i depends on the overlapping factor O.

The Hermite prototype filter is given as:

$$p(t) = \frac{1}{\sqrt{T_0}} e^{-2\pi\left(\frac{t}{T_0}\right)^2} \sum_{i\in\Omega} a_i H_i\left(2\sqrt{\pi}\frac{t}{T_0}\right) \tag{2.18}$$

with

$$\begin{array}{lll} a_0 = 1.412692577 & a_4 = -3.0145e^{-3} & a_8 = -8.8041e^{-6} \\ a_{12} = -2.2611e^{-9} & a_{15} = -4.4570e^{-14} & a_{20} = 1.8633e^{-16} \end{array} \tag{2.19}$$

The RRC filter is given as:

$$p(t) = \begin{cases} \frac{1}{\sqrt{T_0}}\left(1-\alpha+4\frac{\alpha}{\pi}\right), & t = 0 \\ \frac{\alpha}{\sqrt{2T_0}}\left[\left(1+\frac{2}{\pi}\right) sin\left(\frac{\pi}{4\alpha}\right) + \left(1-\frac{2}{\pi}\right) cos\left(\frac{\pi}{4\alpha}\right)\right], & t = \pm\frac{T_0}{4\alpha} \\ \frac{1}{\sqrt{T_0}} \frac{sin\left((1-\alpha)\pi\frac{t}{T_0}\right)+4\alpha\frac{t}{T_0}cos\left((1+\alpha)\pi\frac{t}{T_0}\right)}{\pi\frac{t}{T_0}\left(1-\frac{16\alpha^2t^2}{T_0^2}\right)}, & otherwise \end{cases} \tag{2.20}$$

where α is the roll-off factor. When $\alpha = 1$, the RRC is named as Half-Cosine Function (HCF). This results in good compromise between time and frequency localization and hence it is used in this Ph.D. With $\alpha = 0$, RRC becomes a sinc function.

FBMC-OQAM

In FBMC-OQAM, the aim is to maintain the full symbol density *i.e.,* $TF = 1$, as well as the time frequency localization property *i.e.* $\sigma_t \sigma_f < \infty$. This happens by replacing the complex orthogonality condition with an orthogonality that stands in the real domain only. To do that, FBMC-OQAM is built from the FBMC-QAM waveform as follows:

1. The prototype filter is designed the same as FBMC-QAM where complex orthogonality is guaranteed for $T = T_0$ and $F = 2/T_0$.

2. To achieve the desired symbol density $TF = 1$, the time and frequency spacings are reduced where $F_{FBMC-OQAM} = \frac{F_{FBMC-QAM}}{2} = 1/T_0$ and $T_{FBMC-OQAM} = \frac{T_{FBMC-QAM}}{2} = T_0/2$. This gives $TF = 1/2$ and a new built-in interference component.

3. To eliminate the new built-in interference component, two steps are conducted:

   (a) Complex QAM symbols are replaced with the real PAM symbols.

   (b) The interference induced by the new time and frequency spacings of the Step 2 is shifted to the imaginary part. This happens by introducing a new phase shift component $\theta_{m,k} = \frac{\pi}{2}(k + m)$ to the synthesis and analysis filter design in Equations (2.2,2.4) . Hence, FBMC-OQAM synthesis and analysis function are written as follows:

$$g_{m,k}(t) = p_{tx}(t - kT)e^{j2\pi mF(t-kT)}e^{j\theta_{m,k}} \tag{2.21}$$

$$q_{m,k}(t) = p_{rx}(t - kT)e^{j2\pi mF(t-kT)}e^{j\theta_{m,k}} \tag{2.22}$$

This process is called QAM staggering or the Offset (O)-QAM process, hence the name FBMC-OQAM.

In Figure 2.3, we draw the structure of the FBMC-OQAM resource grid. Compared to Figure 2.2, we observe that time and frequency spacing in FBMC-OQAM are half those of the FBMC-QAM case. As a consequence, FBMC-OQAM spectral density is equal to $TF = 1/2$. However, by keeping in mind that FBMC-OQAM send real symbols, then its corresponding complex symbol density is equal to 1, as in the OFDM case.

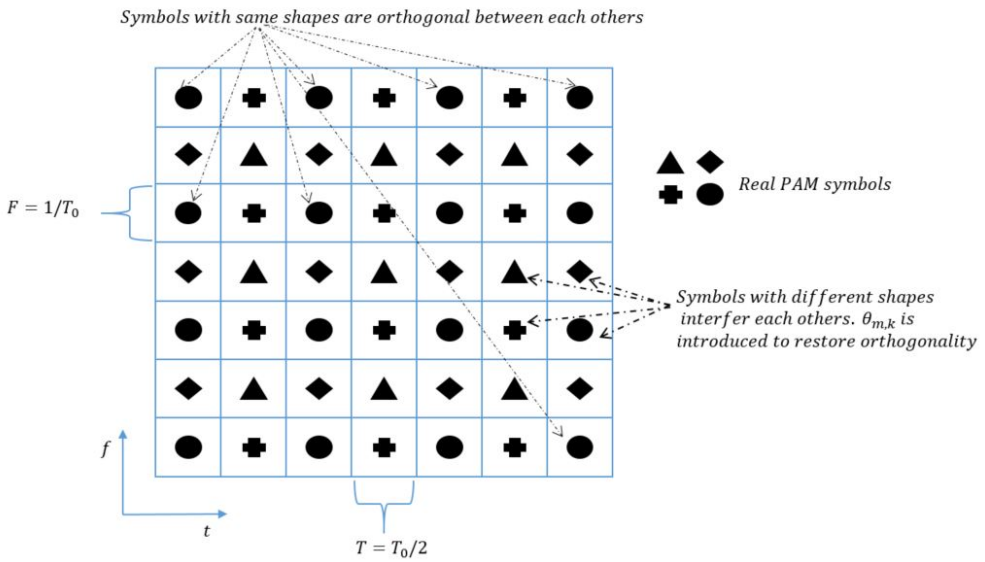

Figure 2.3: Resource grid structure of FBMC-OQAM .

2.5 The Radio Propagation Wireless Environment

2.5.1 Introduction

After constructing the MCM signal, it will be transmitted to the receiver by passing through a specific radio propagation environment. Different propagation environments could be identified such as urban, suburban, rural, indoor, *etc.* Each environment has its own characteristics that will affect differently the transmitted signal. This will impact the quality of the received signal and hence the performance of the overall communication system. For example, depending on the surrounding environment, the signal could reach the desired terminal through a Line Of Sight (LOS) path or it could be critically obstructed by mountains, buildings, *etc.*

The multipaths propagation phenomenon is another aspect that electromagnetic waveforms suffer from through their journey to the receiver. Multipaths means that transmitted signal will take different paths to reach the receiver due to reflection, refraction, diffraction and scattering. At the receiver, these paths will be superpositioned in a constructive or destructive manner with different delays, thus, leading to inter-symbol interference. Furthermore, the surrounding environment is not necessarily static where different objects will be moving, such as cars, humans, *etc.* In addition, the communication terminals could exhibit high movement speeds, such as the case of high speed trains. These facts will cause fast fluctuation in the received signal and they will introduce a Doppler Shift component in each arriving path at the receiver. The different angles of arrivals of the

different paths with Doppler shift will create a Doppler spectrum at the receiver, thus, leading to inter-carrier interference.

Besides the channel induced ICI and ISI interference, communication systems suffer from a corrupting noise nature. While the Gaussian noise model is widely adopted in the literature, the non-Gaussian nature is more dominant in some scenarios such as in the railway context. In fact, the sliding contact between the catenary and the pantograph produces transient electromagnetic emissions that covers a wide range of frequencies and that are received by the train antennas [72]. This electromagnetic interference has been modeled in [73] as symmetric alpha stable distribution.

In this Ph.D work, we consider both channel induced interference sources where we adopt a doubly selective radio environment. Doubly selectivity means the channel will experience fast fluctuations in both time and frequency domains. This will cause the channel to be varying within the time and frequency dimensions of each MCM symbol. As a consequence, the MCM techniques will lose their orthogonality properties, thus introducing both inter-symbol and inter-carrier interference. In addition, we consider both the white Gaussian and the impulsive noise natures.

2.5.2 The Doubly Selective Wireless Channel

The time variant multipaths channel impulse response $h(t,\tau)$ could be written as follows:

$$h(t,\tau) = \sum_{l=0}^{L-1} h_l(t)\delta\left(\tau - \tau_l^{'}(t)\right) \tag{2.23}$$

where $h_l(t)$ and $\tau_l^{'}(t)$ are the channel complex gain and the accompanied delay of the l^{th} macro-path while L is the total number of macro-paths. In fact, the channel gain $h_l(t)$ of the l^{th} macro-path corresponds to the super-positioned gain of all N_l channel micro-paths that have almost the same delay $\tau_l^{'}$

$$h_l(t) = \alpha_l(t)e^{j\theta_l(t)} = \sum_{n=0}^{N_l-1} \alpha_{l,n}e^{j\theta_{l,n}(t)} \tag{2.24}$$

where $\alpha_{l,n}$ and $\theta_{l,n}$ are the amplitude and phase of the n^{th} micro-path within the l^{th} marco-path. Using the Central Limit Theorem (CLT), and with N_l being large enough, $h_l(t)$ is considered as a complex Gaussian random variable with variance $\sigma^2_{h_l}$. Its amplitude $\alpha_l(t)$ follows a Rayleigh distribution, which is given as follows:

$$P(\alpha_l) = \begin{cases} \frac{\alpha_l}{\sigma^2_{h_l}} e^{-\frac{\alpha_l^2}{2\sigma^2_{h_l}}}, & \alpha_l \geq 0 \\ 0, & \alpha_l < 0 \end{cases} \tag{2.25}$$

while the phase component $\theta_l(t)$ is uniformly distributed between 0 and 2π. The dynamic characteristics of each path are measured using time domain auto-correlation

function

$$R_{h_l}(\Delta t) = E\left[h_l(t)h_l^*(t-\Delta t)\right] \tag{2.26}$$

The Fourier transform of the auto-correlation function $R_{h_l}(\Delta t)$ with respect to Δt yields the Doppler spectrum of the l^{th} path:

$$\Gamma_{h_l}(\nu) = \tau\mathcal{F}_{\Delta t}\left\{R_{h_l}(\Delta t)\right\} \tag{2.27}$$

The so called Doppler Bandwidth B_d is the frequency range over which the Doppler spectrum is almost non zero. This helps us in determining the time span over which the channel is considered constant. This is called the channel coherence time and given as follows:

$$T_c \approx \frac{1}{B_d} \tag{2.28}$$

On the other hand, the frequency range over which the channel is nearly constant is called the coherence bandwidth B_c.

$$B_c = \frac{1}{\tau_{max}} \tag{2.29}$$

where τ_{max} is the maximum delay spread that the channel suffers from. If the coherence time and coherence bandwidth are much smaller than the MCM symbol duration T and the subcarrier spacing F, then the channel will be considered as time and frequency selective, respectively. This creates the so-called doubly selective channel where both channel induced ICI and ISI will be introduced.

Wide Sense Stationary Uncorrelated Scattering

In Wide Sense Stationary Uncorrelated Scattering (WSSUS) assumption, channel gains of different taps are considered as statistically independent while the gains of particular tap are correlated over time. Hence, the channel auto-correlation function for each path could be written by using Jakes' formula, as follows:

$$R_{h_l}(\Delta t) = \sigma_{h_l}^2 J_0\left(2\pi\Delta t f_m\right) \tag{2.30}$$

where $\sigma_{h_l}^2$ depends on the channel power delay profile while $\boldsymbol{J}_0()$ is the Bessel function of the first kind with zero order. $f_m = (v/c)f_c$ represents the maximal Doppler spread with v being the mobile terminal speed while c represents the speed of light. f_c is the adopted carrier frequency.

The Fourier transform of this auto-correlation function $R_{h_l}(\Delta t)$ will result in the Doppler spectrum of the lth path, the so known Jakes Doppler spectrum model.

$$\Gamma_{h_l}(\nu) = \begin{cases} \frac{\sigma_{h_l}^2}{\pi f_m\sqrt{1-(\frac{\nu}{f_m})^2}}, & \text{if } |\nu| \leq f_m \\ 0, & otherwise \end{cases} \tag{2.31}$$

2.5.3 Additive Noise

Gaussian Model

The White Gaussian Noise (WGN) case is one of the most adopted models in the wireless communications literature. WGN is justified by the central limit theorem. CLT states that the normalized superposition of ($N \to \infty$) Independent and Identically Distributed (IID) random variables with zero mean and finite variance σ^2, converges to a zero mean Gaussian random variable with variance equal to σ^2. The closed form expression for its Probability Density Function (PDF) is given as follows:

$$P(x) = \frac{1}{\sqrt{2\pi}\sigma} e^{-\frac{x^2}{2\sigma^2}} \tag{2.32}$$

Non-Gaussian Model

Non-Gaussian noise assumption claims that, in some cases, the noise might exhibits an impulsive behavior for short time duration due to either man-made or natural sources. This fact could be represented in the railway environment due to the electromagnetic interference induced by the imperfect contact between the catenary and the pantograph as shown in Figure 2.4.

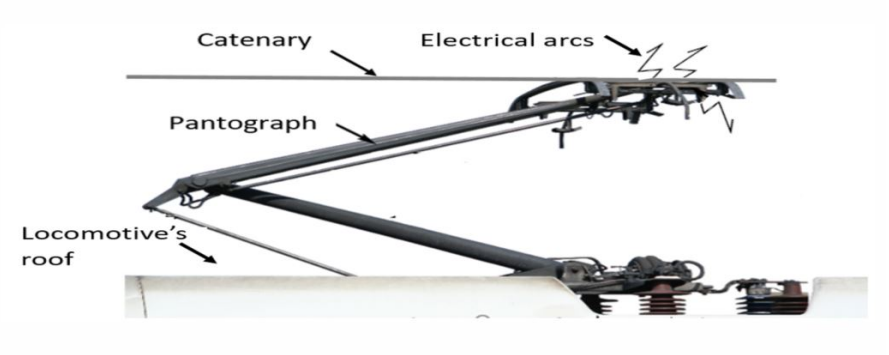

Figure 2.4: Imperfect contact between the catenary and the pantograph

Although different studies have been proposed in the literature to model the impulsive noise nature, *e.g.*, the Gaussian mixture and the Middleton class A models [74], the α-stable distribution provides a suitable non-Gaussian model for different wireless communication scenarios. Contrarily to the Gaussian model, the α-stable distribution inherits its legitimacy from the generalized central limit theorem which states that the superposition of ($N \to \infty$) IID random variables that do not necessarily have finite variance converges to an α-stable distribution.

The α-stable distribution does not have a closed form PDF. Hence, it is described by its characteristic function:

$$\phi_w(t) = exp\left\{j\delta t - \gamma|t|^\alpha \left[1 + j\beta sign(t)k(t,\alpha)\right]\right\} \tag{2.33}$$

where

$$k(t,\alpha) = \begin{cases} tan\left(\frac{\pi\alpha}{2}\right), & \text{if } \alpha \neq 1 \\ \frac{2}{\pi}log|t|, & \text{if } \alpha = 1 \end{cases} \tag{2.34}$$

As we can see, the α-stable distribution is identified using four parameters. The parameter $\alpha \in]0, 2]$ expresses the impulsiveness of the respective random process. The smaller α the more aggressive the impulsivity will be. δ represents the location parameter while γ expresses the spread factor of the distribution. Last, β is considered as the symmetry parameter.

Different studies in the literature have adopted and claimed that the impulsive noise encountered in the railway environment could be well expressed by the the Symmetric α-Stable (SαS) distribution *i.e.*, $\beta = 0$, with $\delta = 0$. [73, 75]. Hence, the characteristic Equation could be re-written as follows:

$$\phi(t) = exp\left\{-\gamma|t|^\alpha\right\} \tag{2.35}$$

Impulsive Noise Pre-Processor

While the literature of IN cancellation schemes is rich, ranging from many iterative interference cancellation schemes as in [76] to whitening the IN nature by using Myriad [77], we adopt in our study the simple memoryless non-linearity pre-processing techniques, such as the blanking and clipping schemes [78, 79]. This choice is made since they do not totally destroy the diagonality property of the STM matrix, as apposite to Myriad case. This allows us to maintain a low complexity level at the receiver side while using the simple one tap equalizer.

The blanking and clipping schemes are applied on the received signal in time domain, before the demodulation process, on a sample by sample basis. The blanking scheme zeros the received signal samples with amplitudes above a defined threshold, as follows

$$\tilde{r}(n) = \begin{cases} r(n), & |r(n)| \leq \lambda \\ 0, & |r(n)| > \lambda \end{cases} \tag{2.36}$$

while the clipping scheme will cut the head of the samples that cross a predefined threshold. We write:

$$\tilde{r}(n) = \begin{cases} r(n), & |r(n)| \leq \lambda \\ \lambda e^{j\arg(r(n))}, & |r(n)| > \lambda \end{cases} \tag{2.37}$$

where λ is a predefined threshold.

2.6 Performance Evaluation

In this section, we evaluate the performance of the studied MCM techniques, namely, the CP-OFDM, WOLA, F-OFDM, and the FBMC-OQAM waveforms. We start by comparing their power spectral density where we note the superiority of the subcarrier filtering based waveforms, FBMC. The power distribution of the STM matrix is illustrated for ideal and non-ideal channel cases. This is important since STM diagonality implies a low complex receiver. In the end, we study the Bit Error Rate (BER) performance of the one tap equalizer while considering the doubly selectivity nature of the channel and the impulse noise case.

2.6.1 Power Spectral Density

One of the main motivations beyond the recently proposed MCM schemes, is the efficient spectrum utilization aspect. For a given bandwidth, how many subcarriers an MCM scheme has to use as a guard band to avoid having an OOB emission above a given threshold. To this end, we consider a 5 MHz channel bandwidth, and we draw the Power Spectral Density (PSD) of the studied MCM schemes within this given bandwidth. We require that the OOB emission is less than -25 dB. Based on that, we draw the PSD in Figure 2.5. The MCM design parameters are given in Table 2.1 with a subcarrier spacing of 15 kHz.

	CP-OFDM	WOLA	F-OFDM	FBMC
Nr. Subcarriers	300	318	324	331
Nr. Symbols	14	14	14	30
TF	1.07	1.07	1.07	1
Constellation	16-QAM	16-QAM	16-QAM	4-PAM
Filtering / Windowing	sinc	Raised Cosine [59]	Soft-truncated sinc [57]	Hermite [58]

Table 2.1: MCM simulation parameters

We note that out of the available 333 subcarriers of the 5 MHz bandwidth, CP-OFDM can use 300 data subcarriers only, while FBMC offers the highest efficiency by using 2 guard subcarriers only. F-OFDM and WOLA schemes has close utilization efficiency by using about 324 and 318 data subcarriers, respectively.

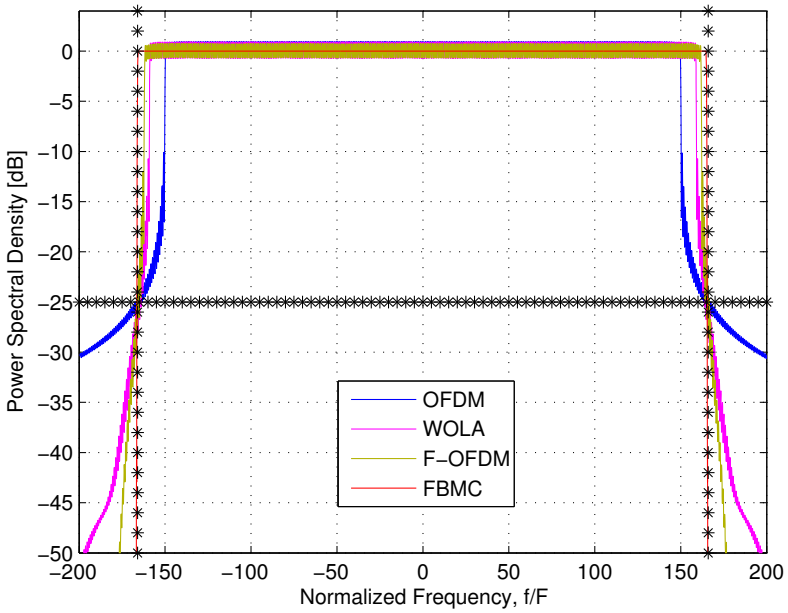

Figure 2.5: PSD of different MCM within 5MHz channel bandwidth

2.6.2 STM diagonality

Another interesting aspect of the MCM technology, is the diagonality of its system transmission matrix. This could be translated into an overall low complexity degree of the corresponding MCM-based transceiver system. The power distribution structure of the STM is directly related to the adopted prototype filter properties. In addition, the doubly selectivity of the wireless channel has a power spreading effect that causes the deterioration of the STM diagonality, as explained in Equations (2.13-2.15). In this section, we illustrate the MCM power distribution of the studied MCM schemes in both ideal and doubly selective channel scenarios.

In Figures 2.6 and 2.7, we present the STM matrix of the CP-OFDM and the WOLA waveforms. In the ideal channel case, we note that complex orthogonality of both waveforms is directly translated into diagonal STM matrix. This fact, is the main reason beyond the widespread adoption of CP-OFDM scheme in different communication standards, where Equation (2.13) could be simply used. In the doubly selective channel case, we consider a Vehicular-A power delay profile and a Jakes Doppler spectrum model. The terminal speed is set to 300 [km/h] for a 2.5 GHz carrier frequency. We can note from Figures 2.6 and 2.7 that both CP-OFDM and WOLA schemes lose their diagonality while having different power spread STM structures.

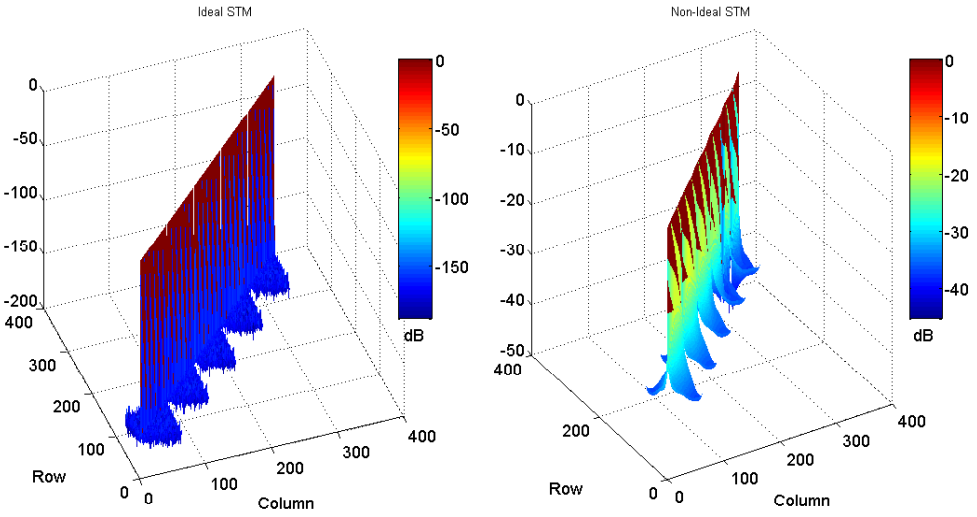

Figure 2.6: STM for CP-OFDM .

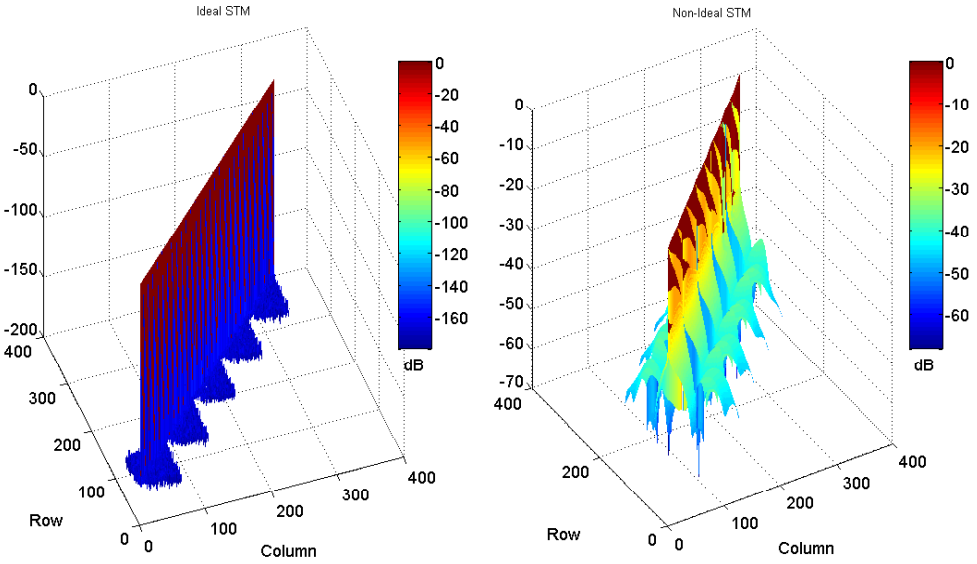

Figure 2.7: STM for WOLA

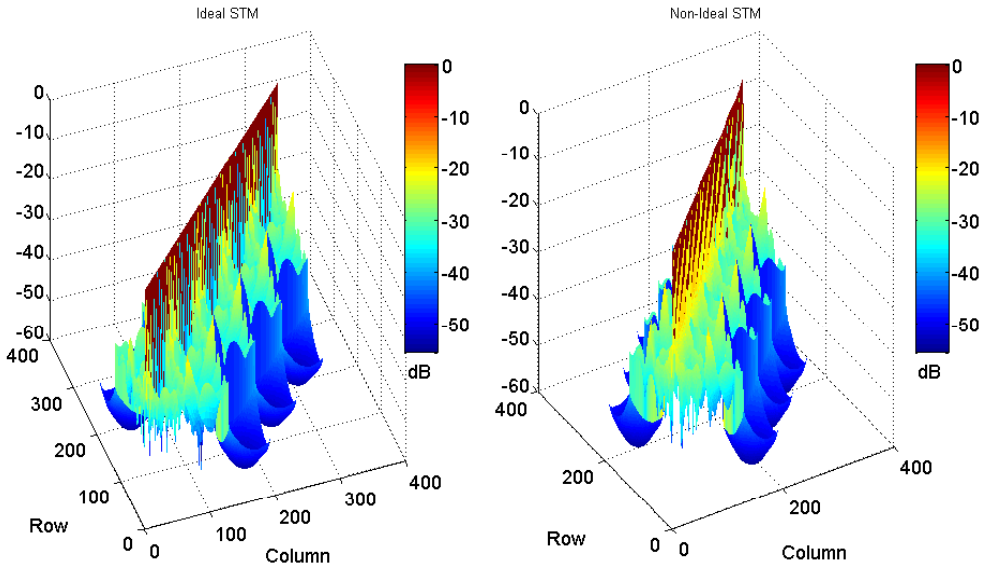

Figure 2.8: STM for F-OFDM

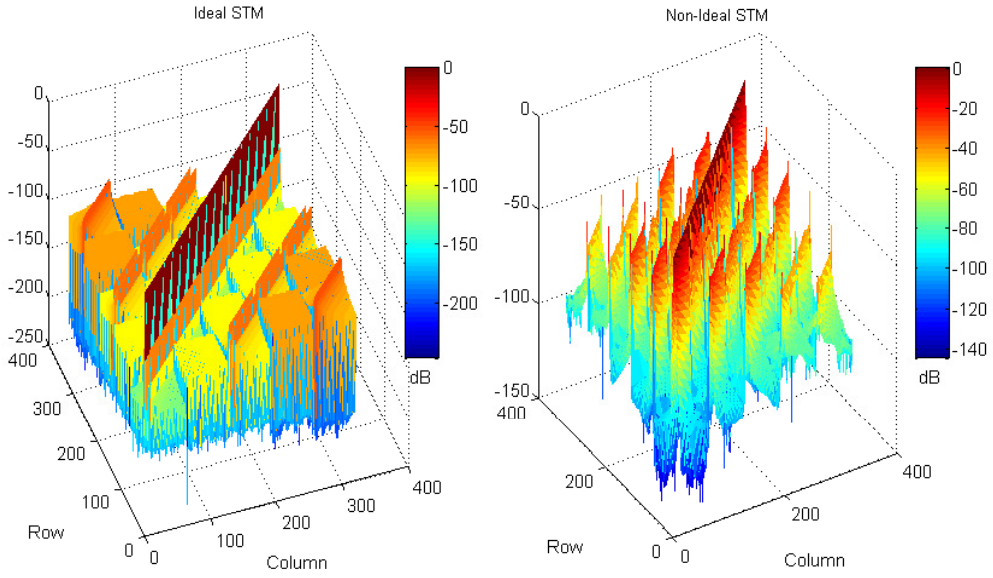

Figure 2.9: STM for FBMC-OQAM with Hermite

Figure 2.8 presents the case of the filtered-OFDM waveform. We can see the lost of orthogonality accompanied with the filtering process. The STM has lost its diagonality even in the ideal channel case. This implies that F-OFDM is expected to perform poorly compared to CP-OFDM in the ideal channel scenario. However, if we look at the doubly selective channel case, we can note that the F-OFDM STM is merely affected. Also, the overall power of the non-diagonal elements could be seen as almost equivalent to that of the CP-OFDM scheme.

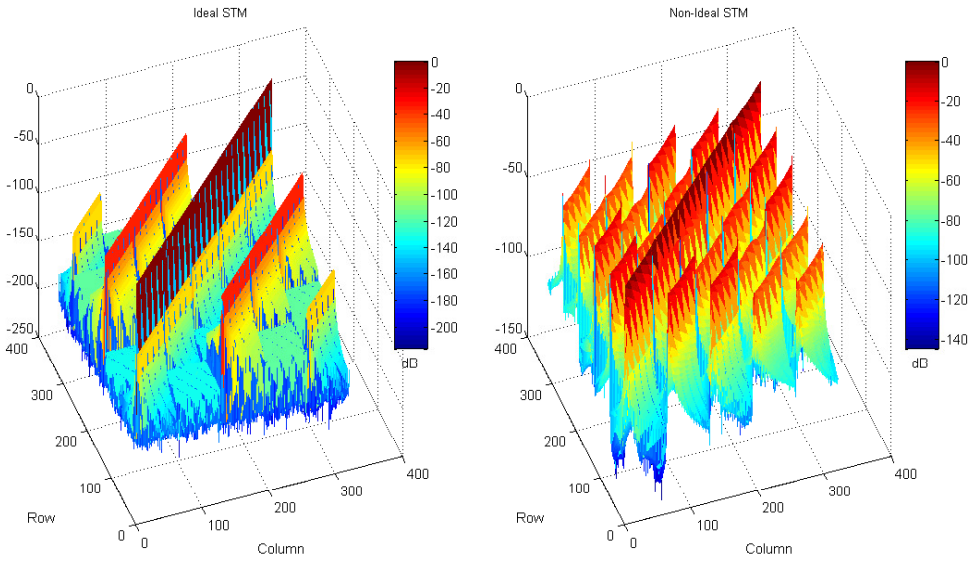

Figure 2.10: STM for FBMC-OQAM with PHYDYAS

In Figures 2.9 and 2.10, we consider the PHYDYAS and Hermite cases of the FBMC-OQAM waveform, respectively. We should remember that only the real part of the demodulated signal is used for the detection process where the imaginary part is dropped. Hence, we draw the power spread structure of the STM real components only. In the ideal channel case, we note that the STM is not totally diagonal as in the CP-OFDM and WOLA case. This predicts less accurate performance than that of CP-OFDM as will be verified in the next section. However, in the doubly selective channel case, we see again that the STM does not change much its overall structure. Also, the overall power of the non-diagonal components could be seen as less than that of other MCM waveform. This will be translated in superior performance of the FBMC-OQAM waveform compared to other MCMs. This robustness to doubly selectivity could be rendered to the outstanding frequency localization the FBMC-OQAM enjoys.

2.6.3 Bit Error Rate in Different Scenarios

In this section, we evaluate the performance of the studied MCM techniques in terms of BER while taking into account different aspects of the radio propagation wireless environment. To this end, we consider the one-tap equalizer of Equation (2.13) while conducting Monte Carlo simulations with 1000 repetitions. Jakes Doppler spectrum model is adopted with a Vehicular-A power delay profile. We set the subcarrier spacing to 15 kHz and the carrier frequency to 2.5 GHz. The same MCM settings of Table 2.1 are taken into account in this section also. However, and for simulations simplicity, we consider only 24 subcarriers for all studied MCM techniques. We use both the Symmetric α Stable and the White Gaussian noise

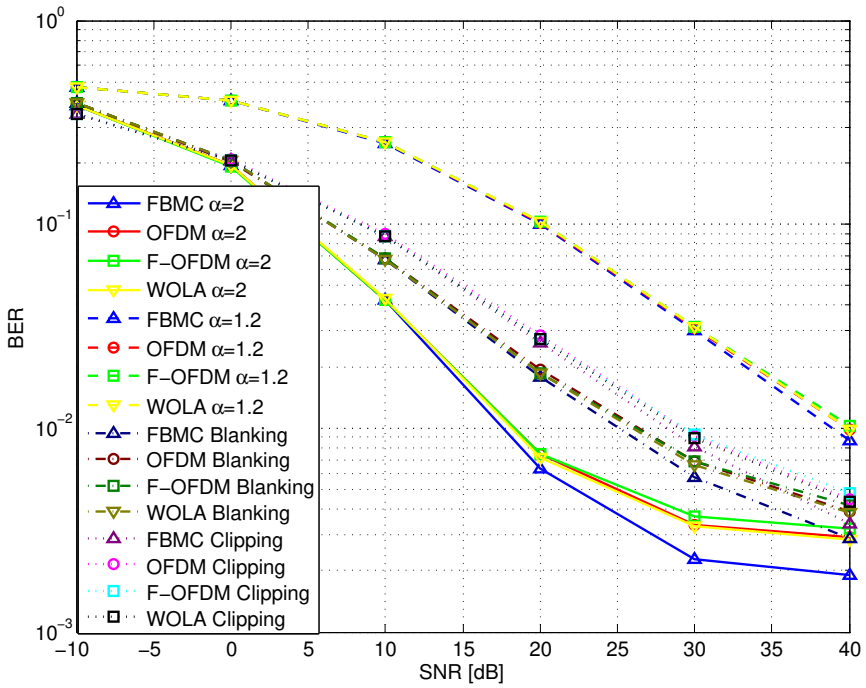

Figure 2.11: BER performance versus GSNR for different impulsive noise settings and under a terminal speed of 200 [km/h]

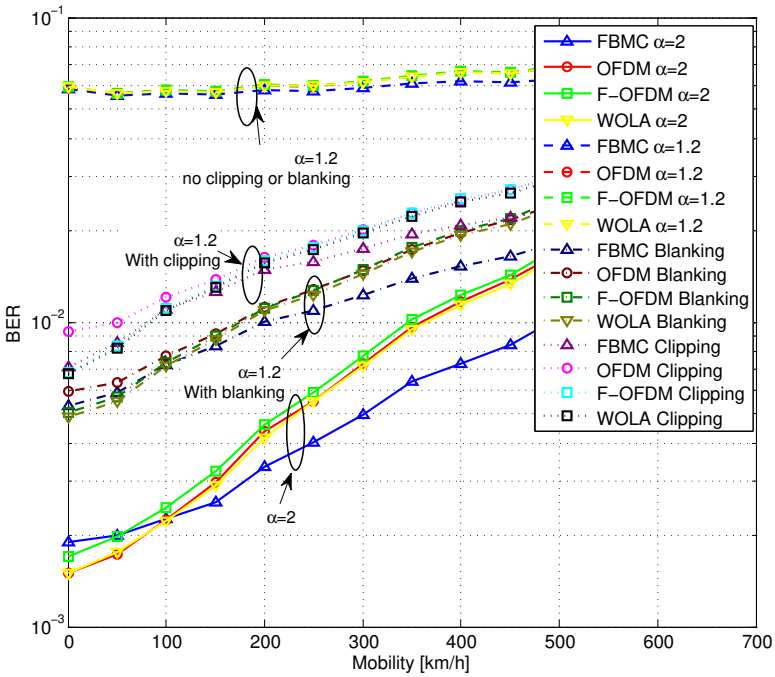

Figure 2.12: BER versus speed for different impulsive noise settings and a fixed GSNR value of 25 dB

cases. As explained in Section 2.5.2, the WGN could be considered as a special case of the SαS case by setting $\alpha = 2$. Unless stated otherwise, we set $\alpha = 1.2$ and $\gamma = 0.4$ where [73] has proven that these settings fits well the high speed railway environment. To handle the impulsive noise induced impairments, we study also the performance of the clipping and blanking schemes of Equations (2.36-2.37). We choose the threshold (λ) to be equal to the maximal value of the noiseless received signal. Unless stated otherwise, the user terminal has a speed value of 200 [km/h].

Conventional Signal to Noise Ratio (SNR) definition cannot be used when dealing with the SαS distribution since its variance is infinity. Hence, we consider here the Generalized SNR (GSNR) definition [80], which is defined as the ratio between the average signal power (P_t) and the noise dispersion parameter (γ).

$$GSNR = \frac{P_t}{\gamma} \tag{2.38}$$

We start in Figure 2.11 by drawing the BER performance versus GSNR for the

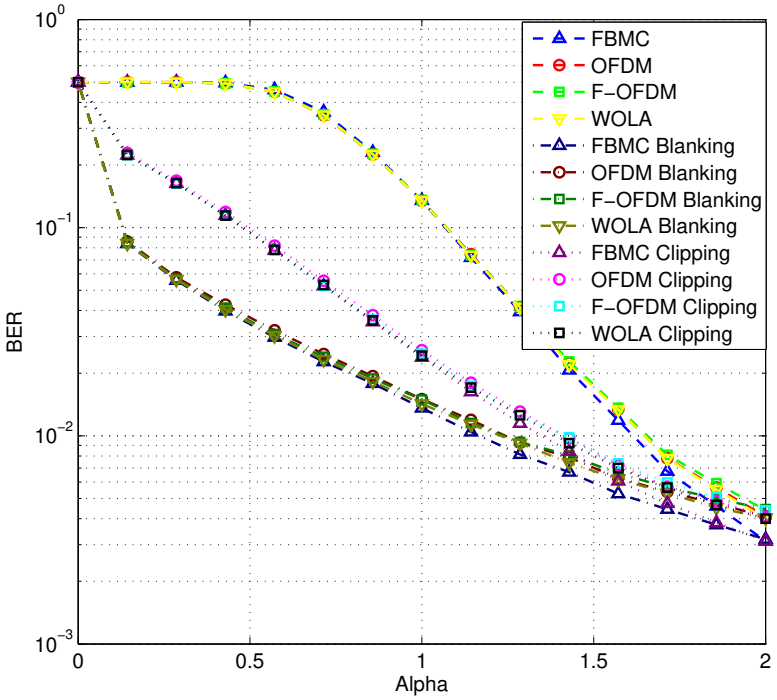

Figure 2.13: BER performance versus α with $\gamma = 0.4$ and a speed of 200 [km/h]

studied MCM waveforms and for a fixed terminal speed of 200 [km/h]. Different conclusions could be made from this figure. In the case of WGN ($\alpha = 2$), the FBMC-OQAM waveform has a superior BER performance, followed by the WOLA and the CP-OFDM waveforms, while ending up with the F-OFDM scheme. Although this order is preserved in all other cases of Figure 2.11, the performance gap of the different MCM schemes is decreasing when treating the IN with clipping

and blanking schemes to almost disappear in the non-treatment case. Also, we note that adopting clipping and blanking techniques enhances the BER performance of all studied MCM schemes. In addition, we see that the blanking scheme performs better than the clipping scheme within the adopted parameters and the corresponding scenario.

In Figure 2.12, we evaluate the BER versus different terminal speeds, ranging from 0 to 500 [km/h] while fixing the GSNR value to 25 dB. FBMC-OQAM performs the worst in low speed scenarios while CP-OFDM and WOLA have almost the best performance. This could be explained due to the fact that in low speed scenarios, the power spread of the STM matrix in the CP-OFDM and WOLA cases could be seen as almost diagonal as previously explained for ideal channel cases in Figures 2.6 and 2.7. On the other hand, STM is highly non-diagonal in the ideal channel case of FBMC-OQAM waveform, as previously illustrated in Figures 2.9 and 2.10. This explains its bad performance accuracy in low mobility scenarios.

In Figure 2.13, we present the BER performance versus the parameter γ while fixing the GSNR value to 25 dB and the terminal speed to 200 [km/h]. We consider the cases of IN with no preprocessing, IN with blanking, and IN with clipping cases. We note that for low values of α, the different MCM schemes will be performing the same. Starting from around $\alpha = 1$, we note that a performance gap will start appearing between the different MCM schemes with FBMC-OQAM having a superior performance.

2.7 Conclusion

In this chapter, we have studied the Multi-Carrier Modulation technique as a key enabling technology for future railway communication systems. In fact, MCM technique is considered as a major player in assuring an efficient utilization of the rare spectrum and in enabling high-data rate communications. Besides, MCM affects the complexity degree of the overall communication system. Based on that, we adopted different MCM schemes from different families, namely, the conventional (CP)-OFDM waveform, the windowed OFDM, a subband filtered OFDM, and a subcarrier filtering based waveform, the FBMC.

To better understand how these waveforms perform, we conducted a performance evaluation study while taking different aspects of HSR environment into considerations. In fact, the high speed of the trains and the different surroundings that trains could pass through, render their communications systems susceptible of suffering from the doubly selectivity of the channel. In other words, channel coherence time and coherence bandwidth become much smaller than MCM symbol duration and subcarrier spacing, respectively. Thus, they suffer from channel induced ISI and ICI. In addition, we consider the impulsive noise nature of the HSR

environment and which exists due to the sliding contact between the catenary and the pantograph.

The sub-carrier filtering based waveforms have shown to have an outstanding frequency localization properties. This renders FBMC as highly suitable for efficient spectrum utilization. Furthermore, a BER performance comparison study was conducted in a doubly selective wireless channel versus different parameters. The FBMC outperforms other MCM schemes in high mobility scenarios. CP-OFDM and WOLA schemes enjoy superior performance in low mobility scenarios which could be accorded to their complex orthogonality condition, and hence their diagonal STM matrix.

We considered also the impulsive noise case. We noted that MCM schemes in general performed poorly. In fact, the performance gap between them almost disappear if we do not deploy a suitable IN cancellation scheme. Hence, we analyzed the enhancement of the blanking and clipping schemes where performance gaps are re-established. In future works, we aim to consider more practical cases of the blanking and clipping schemes where we include the selection process of the corresponding threshold. The performance of other impulsive noise filters *e.g.*, the Myriad filter, should be evaluated also for the different MCM schemes.

The conclusions made in this chapter highlight the FBMC waveform, as a promising technique for high speed scenarios, high data-rates, and for efficient spectrum reuse. Based on that, we conduct in next chapters (Chapters 3 and 4) deeper studies on the FBMC waveform where we consider both the channel estimation and equalization aspects, respectively.

Chapter 3

Doubly Selective Channel Estimation with Different MCMs

3.1 Introduction

In the previous chapter, we conducted a performance evaluation study of different MCM techniques and under various wireless channel conditions. The FBMC-OQAM waveform offered superior performance over other MCM techniques. This superiority was manifested in better frequency localization, spectral efficiency, and bit error rate performance. However, these results were obtained under the inaccurate assumption of full channel knowledge at the receiver. In practice, channel estimation has to be conducted. Under high speed scenarios and/or the non orthogonal MCM waveforms case, the system transmission matrix loses its diagonality. This implies that traditional Least Square (LS) based channel estimation techniques will lose their advantages. Hence, in this chapter, we present two contributions that deal with high speed channel estimation for different MCM techniques.

This chapter is organized as follows. In Section 3.2 is devoted to a literature study regarding the high speed channel estimation aspect in MCM in general where we end up dealing with the FBMC-OQAM case where special built-in interference cancellation schemes are needed. The first contribution of the chapter is detailed in Section 3.3. It could be summarized as the generalization of the sliding-window TD-LMMSE channel estimation technique so that it might be implemented on different MCM techniques (Section 3.3.1). Besides, we extend it to exploit multi-paths (Section 3.3.2) and multi-antennas (Section 3.3.3) correlation as well. We also show that in special scenarios *e.g.*, HSR, very low computational complexity could be achieved (Section 3.3.4). We also conduct numerical simulations (Section 3.3.5) to verify the analytical model while presenting achieved performance gains. In Section 3.4, we investigate the channel estimation of the FBMC-OQAM waveform taking into account its built-in interference (Section 3.4.1). The sec-

ond contribution of this chapter includes the proposal of a pattern based LMMSE channel estimator (Section 3.4.2), that exploits the power spread pattern of different prototype filters. We provide the Mean Square Error (MSE) relation (Section 3.4.3) that is verified in the simulation part (Section 3.4.4). In the end, we give our conclusions and perspectives (Section 3.5).

3.2 Estimation Techniques and MCM

Although many studies have dealt with the channel estimation aspect in the history of wireless communication systems, the majority of them holds at least the slow time varying channel [63] or the orthogonal MCM [81,82] assumptions. Nowadays, both cases are not valid. This is due to the increasing need to support high mobility wireless communication systems, e.g., HSR [83], and the fact that the majority of the newly proposed MCM techniques are non-orthogonal [84]. As previously explained in Section 2.2, both, the doubly selectivity of the radio environment and the possible non-orthogonality of the MCM technology, contribute to the non-diagonality of the STM matrix. In pilot based channel estimation, this non-diagonality interferes the pilots by creating inter-pilot and data interference components. This could be noted by writing the demodulated vector $\boldsymbol{y}$ at the set of pilot positions, Ω_p, as follows:

$$\boldsymbol{y}(\Omega_p) = \underbrace{diag\big(\mathcal{D}(\Omega_p,\Omega_p)\big)\boldsymbol{x}_p}_{\text{Useful part}} + \underbrace{ndiag\big(\mathcal{D}(\Omega_p,\Omega_p)\big)\boldsymbol{x}_p}_{\text{Inter-pilot interference}} + \underbrace{\mathcal{D}(\Omega_p,\Omega_d)\boldsymbol{x}_d}_{\text{Data interference}} + \boldsymbol{Q}^H\boldsymbol{\eta} \quad (3.1)$$

where Ω_d is the set of data symbols positions. N_d and N_p are the number of data and pilots symbols, respectively. Conventionally, simple LS is applied to estimate the channel at pilots positions

$$\hat{\mathfrak{h}}(i_p) = \boldsymbol{y}(i_p)/\boldsymbol{x}(i_p) \quad (3.2)$$

where $\hat{\mathfrak{h}}$ is the $MK \times 1$ diagonal vector of the STM matrix ($\mathcal{D}$) and $i_p \in \Omega_p$. LS is followed with an interpolation technique that estimates the channel at data positions

$$\hat{\mathfrak{h}}(\Omega_d) = \mathcal{W}^H\hat{\mathfrak{h}}(\Omega_p) \quad (3.3)$$

with $\mathcal{W} \in \mathbb{C}^{N_d \times N_p}$ being the interpolation filter This traditional perspective loses its advantages due to the loss of diagonality that STM suffers from and which introduces the ICI and ISI interference. Consequently, it necessitates the estimation of the whole STM matrix in order to cancel the non-diagonal induced interference. Estimating the whole STM matrix can be done directly in the frequency domain. However, this could require the estimation of $MK \times MK$ elements, where MK denotes the total number of transmitted symbols. Based on that, estimating the Channel Impulse Response (CIR) is usually preferred where only $N \times L$ channel taps need to be estimated. To estimate the i^{th} path of the CIR, interference

components could be seen by writing the received signal $\boldsymbol{r}$ as follows:

$$\boldsymbol{r} = \underbrace{\boldsymbol{S}_p^{(i)}\boldsymbol{h}_i}_{\text{Useful part}} + \underbrace{\sum_{\substack{l=0 \\ l\neq i}}^{L-1} \boldsymbol{S}_p^{(l)}\boldsymbol{h}_l}_{\text{Inter-pilot interference}} + \underbrace{\sum_{l=0}^{L-1} \boldsymbol{S}_d^{(l)}\boldsymbol{h}_l}_{\text{Data interference}} + \boldsymbol{\eta} \tag{3.4}$$

where

$$\boldsymbol{s}_d^{(l)} = \boldsymbol{G}^{(l)}\boldsymbol{x}_d \tag{3.5}$$

$$\boldsymbol{S}_p^{(l)} = diag\left(\boldsymbol{s}_p^{(l)}\right) = diag\left(\boldsymbol{G}^{(l)}\boldsymbol{x}_p\right) \tag{3.6}$$

$$\boldsymbol{S}_d^{(l)} = diag\left(\boldsymbol{s}_d^{(l)}\right) = diag\left(\boldsymbol{G}^{(l)}\boldsymbol{x}_d\right) \tag{3.7}$$

$\boldsymbol{G}^{(l)}$ is a row shifted version of $\boldsymbol{G}$

$$\boldsymbol{G}^{(l)}(n,:) = \begin{cases} \boldsymbol{G}(n-l,:), & 0 \leq n-l < N \\ 0, & otherwise \end{cases} \tag{3.8}$$

Basis Expansion Model (BEM) [85] has been widely studied in the literature in order to reduce the number of channel elements that need to be estimated even further. This happens by modeling the time varying channel as a linear combination of deterministic basis functions where the problem is reduced to estimate the basis function coefficients $\boldsymbol{\zeta}_l \in \mathbb{C}^{Q\times 1}$ of each path.

$$\boldsymbol{h}_l = \boldsymbol{B}_l\boldsymbol{\zeta}_l + \boldsymbol{\epsilon}_l \tag{3.9}$$

$\boldsymbol{B}_l \in \mathbb{C}^{N\times Q}$ and $\epsilon_l \in \mathbb{C}^{N\times 1}$ are the matrix of basis functions and the BEM modelization error vector of the lth path, respectively. Hence, we have $Q \times L$ elements to be estimated only with $Q << N$. Many basis functions have been used in the literature such as the generalized complex exponential BEM [86], the polynomial BEM [87], the doubly polynomial BEM [88], *etc.* Although BEM based estimation has much less variables to estimate, they could suffer from a significant modelling error. In addition, and since they are based on estimating the CIR on the whole MCM symbol, they have low estimation accuracy at the edges of each symbol. This is compared to the channel estimate of the centralized samples. This could be explained by the fact that channel estimate at centralized samples could exploit channel correlations with surrounding samples, while it is not the case for edge samples. Hence, channel estimation techniques that do well exploit this property are needed.

The Linear Minimum Mean Square (LMMSE) filter is extensively investigated in the literature due to its capability of exploiting the correlated nature of the wireless channel while being optimal in additive white noise and the wide sense stationary channel assumptions [89]. It has been largely applied as an interpolator such as in [90, 91] for the OFDM based waveforms, while in [92] for FBMC based waveforms. LMMSE based BEM has been examined as well [86, 93]. Different studies investigated the adaptive version of the LMMSE filter, the so-called

Kalman filter, in order to estimate the BEM coefficients as in [94] for OFDM, and [95] for FBMC. In a recent work done by our team [96], the LMMSE filter has been applied in a sliding window form. This allowed exploiting the correlation of the OFDM pre-demodulated received signal while estimating the channel in the middle of the window, hence giving superior performance. The exploitation of channel correlation has been conducted on post-demodulated signals also, while exploiting the correlation between adjacent time and frequency domain symbols. In [97, 98], the non diagonal elements of the STM matrix are estimated using the LMMSE filter to be used afterward in iterative interference cancellation schemes.

In this chapter, we first propose to generalize the sliding window approach so that it exploits the multipaths and multi-antennas correlation, once they exist *e.g.*, tunnels [99], high speed railway [100] and Vehicle to Vehicle (V2V) [101] environments. In addition, the SW TD-LMMSE technique is extended to cover other MCM techniques. The performance of the generalized technique and the accompanied improvements are evaluated for the CP-OFDM, FBMC-QAM and FBMC-OQAM waveforms. While SW TD-LMMSE performs well in FBMC-QAM and CP-OFDM waveforms, a high error floor exists in FBMC-OQAM due to its built-in interference. In fact, FBMC-OQAM needs special interference cancellation schemes prior to the channel estimation process. [102, 103] proposed to use an Auxiliary Pilot (AP) besides each pilot, designed in a way to cancel the built in interference coming from surrounding symbols. However, that means APs will have high power offset compared to data symbols. Hence, a better perspective was to use two APs for each pilot [104], which distributes the needed power among two APs. This leads to a lower power offset at the cost of a loss in spectral efficiency. Other studies have adopted a precoding scheme [105], thus alleviating the power offset at the cost of increased complexity and sensitivity to doubly selective channels. In the second contribution of this chapter, we use the AP built-in interference cancellation scheme while proposing an efficient LMMSE estimator that exploits the power spread pattern of different FBMC-OQAM prototype filters to give a better estimate of the centralized symbol.

3.3 Generalized Sliding Window Time Domain LMMSE Channel Estimation

The sliding window time domain LMMSE channel estimator aims to estimate the channel impulse response at the receiver. This happens by gathering a window of N_w successive received samples in the time domain and estimating the channel impulse response at the middle of this window by using the LMMSE technique. Hence, a better channel estimate is expected by exploiting the correlation between received samples, at both sides of the desired sample [96]. Then, we slide the window one sample, generate the new LMMSE filter, estimate the new mid sample, and so on. In high mobility scenarios, adopting the comb type pilot pattern has

shown in our previous work to be preferred than the block type [96], hence it is adopted in our study also.

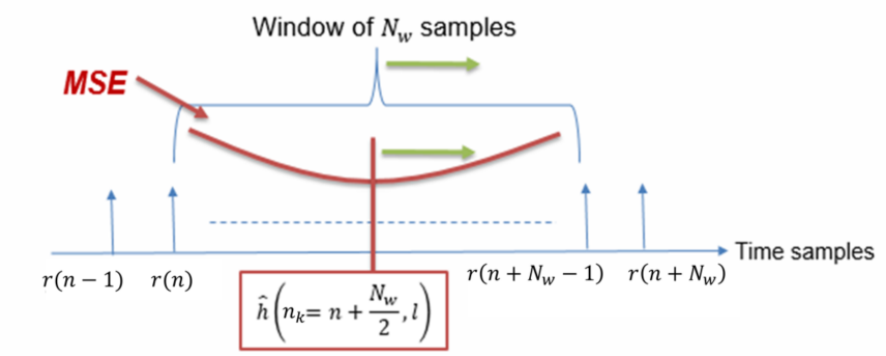

Figure 3.1: SW TD-LMMSE work principle

3.3.1 Mathematical Model

In Figure 3.1, we illustrate that in order to estimate the channel sample $h_l(n_k)$, we have first to collect the $(N_w - 1)$ surrounding samples of the ${n_k}^{th}$ received sample *i.e.* $\boldsymbol{r}_{n_k} = [r(n_k - N_w/2)...r(n_k + N_w/2 - 1)]^T$. For simplicity, we omit the subscript n_k when it is possible. Hence, we write $\boldsymbol{r}_{n_k}$ as follows:

$$\boldsymbol{r} = \boldsymbol{A}\Big(\sum_{l=0}^{L-1}\Big(\boldsymbol{S}_p^{(l)} + \boldsymbol{S}_d^{(l)}\Big)\boldsymbol{h}_l + \boldsymbol{\eta}\Big) \tag{3.10}$$

where $\boldsymbol{h}_l = [h_l(n_k - N_w/2)...h_l(n_k + N_w/2 - 1)]^T$, $\boldsymbol{\eta} = [\eta(n_k - N_w/2)...\eta(n_k + N_w/2 - 1)]^T$.

$$\boldsymbol{G}^{(l)}(n,:) = \begin{cases} \boldsymbol{G}(n_k - N_w/2 - l : n_k + N_w/2 - 1 - l, :), & 0 \leq n - l < N \\ 0, & otherwise \end{cases} \tag{3.11}$$

$\boldsymbol{A}$ is a mapping matrix used in the CP-OFDM waveform to remove the cyclic prefix. Using (3.10), the TD-LMMSE estimates the channel sample $h_l(n_k)$ using the following equation:

$$\hat{h}_l(n_k) = \underbrace{\Big(\mathbb{E}\left[\boldsymbol{r}\boldsymbol{r}^H\right]^{-1}\mathbb{E}\left[\boldsymbol{r}h_l(n_k)^*\right]\Big)^H}_{\text{TD-LMMSE}}\boldsymbol{r} \tag{3.12}$$

$\mathbb{E}\left[\boldsymbol{r}\boldsymbol{r}^H\right] \in \mathbb{C}^{N_w \times N_w}$ is the covariance matrix of the received window $\boldsymbol{r}$. $\mathbb{E}\left[\boldsymbol{r}h_l(n_k)^*\right] \in \mathbb{C}^{N_w \times 1}$ is the correlation matrix between the received window $\boldsymbol{r}$ and the channel sample $h_l(n_k)$. Assuming a Wide Sense Stationary Uncorrelated Scattering (WSSUS) channel, we can write:

$$\mathbb{E}\left[\boldsymbol{r}\boldsymbol{r}^H\right] = \boldsymbol{A}\Big(\sum_{l=0}^{L-1}\left[\boldsymbol{R}p_{l,l} + \boldsymbol{R}d_{l,l}\right] \odot \boldsymbol{R}_{\boldsymbol{h}_l\boldsymbol{h}_l} + \boldsymbol{R}_\eta\Big)\boldsymbol{A}^H \tag{3.13}$$

$$\mathbb{E}\left[\boldsymbol{r}h_l(n_k)^*\right] = \boldsymbol{A}\boldsymbol{S}_p^{(l)}\boldsymbol{R}_{\boldsymbol{h}_l\boldsymbol{h}_l}(:,n_k) \tag{3.14}$$

Equation (3.38) has been written by noting that

$$diag(\boldsymbol{a})\boldsymbol{B}diag(\boldsymbol{a}^H) = \boldsymbol{a}\boldsymbol{a}^H \odot \boldsymbol{B} \tag{3.15}$$

$$\boldsymbol{R}p_{l_1,l_2} = \boldsymbol{G}^{(l_1)}\boldsymbol{x}_p\boldsymbol{x}_p^H\left(\boldsymbol{G}^{(l_2)}\right)^H \tag{3.16}$$

$$\boldsymbol{R}d_{l_1,l_2} = \boldsymbol{G}^{(l_1)}\mathbb{E}\left[\boldsymbol{x}_d\boldsymbol{x}_d^H\right]\left(\boldsymbol{G}^{(l_2)}\right)^H \tag{3.17}$$

$\mathbb{E}\left[\boldsymbol{x}_d\boldsymbol{x}_d^H\right] = \sigma_d^2\boldsymbol{I}_{MK}$ where σ_d^2 is the data symbols allocated power which is equal to one unless stated otherwise. $\boldsymbol{R}_\eta = E[\boldsymbol{\eta}\boldsymbol{\eta}^H] = \sigma_w^2\boldsymbol{I}_N$ with σ_η^2 being the noise variance. The $N_w \times N_w$ channel covariance matrix $\boldsymbol{R}_{\boldsymbol{h}_l\boldsymbol{h}_l} = E\left[\boldsymbol{h}_l\boldsymbol{h}_l^H\right]$ is a Toeplitz matrix with its first row elements given from Jakes Doppler spectrum model for different time samples (n_1, n_2):

$$\boldsymbol{R}_{\boldsymbol{h}_l\boldsymbol{h}_l}(1,|n_2-n_1|) = \alpha_l J_0(2\pi(|n_2-n_1|)T_s f_m) \tag{3.18}$$

where α_l depends on the channel power delay profile. $J_0()$ is the Bessel function of the first kind with zero order, T_s is the sampling period and f_m is the maximum Doppler spread.

3.3.2 Multipaths Correlation

The assumption of uncorrelated multipaths is not suitable for all scenarios. Recent studies have shown a good amount of correlation among multipaths in mobile scenarios such as the HSR [100] environment. Hence, TD-LMMSE performance could be enhanced by exploiting the channel correlated samples within different multipaths.

By adopting a correlated multipaths scenario, Equations (3.38) and (3.14) could be reformulated as follows:

$$\mathbb{E}\left[\boldsymbol{r}\boldsymbol{r}^H\right] = \boldsymbol{A}\Big(\sum_{l_1=0}^{L-1}\sum_{l_2=0}^{L-1}\left[\boldsymbol{R}p_{l_1,l_2} + \boldsymbol{R}d_{l_1,l_2}\right] \odot \boldsymbol{R}_{\boldsymbol{h}_{l_1}\boldsymbol{h}_{l_2}} + \boldsymbol{R}_\eta\Big)\boldsymbol{A}^H \tag{3.19}$$

$$\mathbb{E}\left[\boldsymbol{r}h_{l_1}(n_k)^*\right] = \boldsymbol{A}\sum_{l_2=0}^{L-1} diag\left(\boldsymbol{G}^{(j)}\boldsymbol{x}_p\right)\boldsymbol{R}_{\boldsymbol{h}_{l_1}\boldsymbol{h}_{l_2}}(:,n_k) \tag{3.20}$$

For simplicity, we guard Jake's formula of Equation (3.18) while adding multipaths correlation as follows:

$$\boldsymbol{R}_{\boldsymbol{h}_{l_1}\boldsymbol{h}_{l_2}}(1,|n_2-n_1|) = \rho_{l_1,l_2}\alpha_{l_1}\alpha_{l_2}J_0(2\pi(|n_2-n_1|)T_s f_m) \tag{3.21}$$

where ρ_{l_1,l_2} is the multipaths correlation coefficient between the paths l_1 and l_2. The channel estimate $\hat{h}_l(n_k)$ is given by Equation (3.12).

3.3.3 Multi Antenna Correlation

In a similar way, by assuming a Single Input Multiple Output (SIMO) system with M antennas at the receiver, the correlation between the received signals of different antennas, which exists in different scenarios such as in tunnels [99], could be exploited thus enhancing the TD-LMMSE performance. The overall received window could be written as:

$$\tilde{\boldsymbol{r}} = \tilde{\boldsymbol{A}}\Big(\sum_{l=0}^{L-1}(\tilde{\boldsymbol{S}}_p^{(l)} + \tilde{\boldsymbol{S}}_d^{(l)})\tilde{\boldsymbol{h}}_l + \tilde{\boldsymbol{\eta}}\Big) \tag{3.22}$$

where $\tilde{\boldsymbol{r}} = [\boldsymbol{r}_1^T \boldsymbol{r}_2^T ... \boldsymbol{r}_M^T]^T$ and $\boldsymbol{r}_m$ is the received window $\boldsymbol{r}$ from the m^{th} antenna. $\tilde{\boldsymbol{S}}_x^{(l)} = diag(\tilde{\boldsymbol{s}}_x^{(l)})$ where $\tilde{\boldsymbol{s}}_x^{(l)} = [\underbrace{\boldsymbol{s}_x^{(l)^T}}_{1}\underbrace{\boldsymbol{s}_x^{(l)^T}}_{2} ... \underbrace{\boldsymbol{s}_x^{(l)^T}}_{\mathrm{M}}]^T$. $\tilde{\boldsymbol{h}}_l = [\boldsymbol{h}_{l,1}^T \boldsymbol{h}_{l,2}^T ... \boldsymbol{h}_{l,M}^T]^T$ where $\boldsymbol{h}_{l,m}$ is the channel vector $\boldsymbol{h}_l$ of the m^{th} antenna. The covariance matrices of the overall received window in (3.22) could be written as:

$$\mathbb{E}\left[\tilde{\boldsymbol{r}}\tilde{\boldsymbol{r}}^H\right] = \tilde{\boldsymbol{A}}\Big(\sum_{l_1=0}^{L-1}\sum_{l_2=0}^{L-1}\left[\boldsymbol{R}\tilde{p}_{l_1,l_2} + \boldsymbol{R}\tilde{d}_{l_1,l_2}\right] \odot \boldsymbol{R}_{\tilde{\boldsymbol{h}}_{l_1}\tilde{\boldsymbol{h}}_{l_2}} + \boldsymbol{R}_{\tilde{\boldsymbol{\eta}}}\Big)\tilde{\boldsymbol{A}}^H \tag{3.23}$$

$$E\left[\tilde{\boldsymbol{r}}h_{l_2}(n_k,m)^*\right] = \tilde{\boldsymbol{A}}\Big(\sum_{l_1=0}^{L-1}\tilde{\boldsymbol{S}}_p^{(l_1)}\boldsymbol{R}_{\tilde{\boldsymbol{h}}_{l_1}\tilde{\boldsymbol{h}}_{l_2}}(:,n_k m)\Big) \tag{3.24}$$

where $h_l(n_k,m)$ is the ${n_k}^{th}$ channel sample of the l^{th} path and the m^{th} antenna. $\boldsymbol{R}\tilde{p}_{l_1,l_2} = \tilde{\boldsymbol{s}}_p^{(l_1)}\tilde{\boldsymbol{s}}_p^{(l_2)H}$. $\boldsymbol{R}\tilde{d}_{l_1,l_2} = E[\tilde{\boldsymbol{s}}_{d_{l_1}}\tilde{\boldsymbol{s}}_{d_{l_2}}^H]$. $\boldsymbol{R}_{\tilde{\boldsymbol{\eta}}} = E[\tilde{\boldsymbol{\eta}}\tilde{\boldsymbol{\eta}}^H]$. $\boldsymbol{R}_{\tilde{\boldsymbol{h}}_{l_1}\tilde{\boldsymbol{h}}_{l_2}} = E[\tilde{\boldsymbol{h}}_{l_1}\tilde{\boldsymbol{h}}_{l_2}^H]$ is the $MN_w \times MN_w$ channel covariance matrix which is a combination of M^2 Toeplitz matrix where the first row elements of each are given for different n_2, n_1 values by:

$$\boldsymbol{R}_{\tilde{\boldsymbol{h}}_{l_1}\tilde{\boldsymbol{h}}_{l_2}}(m_1,m_2|n_2-n_1|) = \beta_{l_1 l_2 m_1 m_2} J_0\left(2\pi(|n_2-n_1|)T_s f_m\right) \tag{3.25}$$

where

$$\beta_{l_1 l_2 m_1 m_2} = \gamma_{m_1,m_2}\rho_{l_1,l_2}\alpha_{l_1}\alpha_{l_2} \tag{3.26}$$

γ_{m_1,m_2} is the correlation coefficient between the antennas m_1 and m_2.

The estimated channel sample could be written as:

$$\hat{h}_l(n_k,m) = \left(\mathbb{E}^{-1}\left[\tilde{\boldsymbol{r}}\tilde{\boldsymbol{r}}^H\right]\mathbb{E}\left[\tilde{\boldsymbol{r}}h_l(n_k,m)^*\right]\right)^H\tilde{\boldsymbol{r}} \tag{3.27}$$

3.3.4 Complexity Analysis

From Equation (3.27) we can see that the calculation of $\hat{h}_l(n_k,m)$ comes with a complexity of $\left((MN_w)^2 + LMN_w\right)$ where $(MN_w)^2$ corresponds to the calculation

of $\mathbb{E}\left[\tilde{\boldsymbol{r}}\tilde{\boldsymbol{r}}^H\right]^{-1}\tilde{\boldsymbol{r}}$ while LMN_w corresponds to $E\left[\tilde{\boldsymbol{r}}h_l(n_k,m)^*\right]^H(\mathbb{E}\left[\tilde{\boldsymbol{r}}\tilde{\boldsymbol{r}}^H\right]^{-1}\tilde{\boldsymbol{r}})$. In the special cases of a SISO system and/or $\rho = 0$, complexity could be calculated by substituting with $M = 1$ and/or $L = 1$, respectively.

To reduce complexity, which is mainly due to the matrix inversion, we have suggested in [96] to fix our window during each MC symbol. That means we calculate $\mathbb{E}\left[\tilde{\boldsymbol{r}}\tilde{\boldsymbol{r}}^H\right]^{-1}$ once for each symbol while $E\left[\tilde{\boldsymbol{r}}h_l(n_k,m)^*\right]$ is calculated on a sample basis. In addition, the use of a periodic pilot sequence means that $\boldsymbol{R}_{\tilde{p}_{l_1,l_2}}$ is the same among symbols. Adding this to the fact that in some communication environments we have a fixed trajectory, *e.g.* trains, means that the channel statistics and SNR values would be similar each time the train passes by the same location. Hence, $\mathbb{E}\left[\tilde{\boldsymbol{r}}\tilde{\boldsymbol{r}}^H\right]^{-1}$ could be calculated offline for different channel statistics and SNR values and stored in a database.

3.3.5 Mean Square Error (MSE)

In order to evaluate the performance of the propose channel estimation technique, we derive the mean square error metric. The MSE could be written as [89]

$$MSE_{n_k,l,m} = \frac{\sigma^2_{h_l(n_k,m)} - \sigma^2_{\hat{h}_l(n_k,m)}}{\sigma^2_{h_l(n_k,m)}} \tag{3.28}$$

where $\sigma^2_{h_l(n_k,m)}$ is the variance of $h_l(n_k,m)$ and

$$\sigma^2_{\hat{h}_l(n_k,m)} = E\left[\tilde{\boldsymbol{r}}h_l(n_k,m)^*\right]^H E\left[\tilde{\boldsymbol{r}}\tilde{\boldsymbol{r}}^H\right]^{-1} E\left[\tilde{\boldsymbol{r}}h_l(n_k,m)^*\right] \tag{3.29}$$

The average MSE over one MC symbol is:

$$MSE = \frac{1}{NLM}\sum_{n_k,l,m} MSE_{n_k,l,m} \tag{3.30}$$

In next section, we verify the MSE relation by conducting numerical simulations with Monte-Carlo repetitions.

3.3.6 Numerical simulations

In this section, we demonstrate the simulation part where we report the numerical results. We adopt Jakes Doppler spectrum model to demonstrate the time varying nature of the channel with a normalized square power delay profile where $L = 7$. We adopt a subcarrier spacing of 15 kHz, carrier frequency $f_c = 2.5$ GHz, pilot spacing of $S_p = 6$, a window size of 3 OFDM symbols, a mobile speed of 400 [km/h], and a (1×4) SIMO system are adopted. Z=256 and K is chosen in a way to include all significant interferers. FBMC prototype filters are designed with

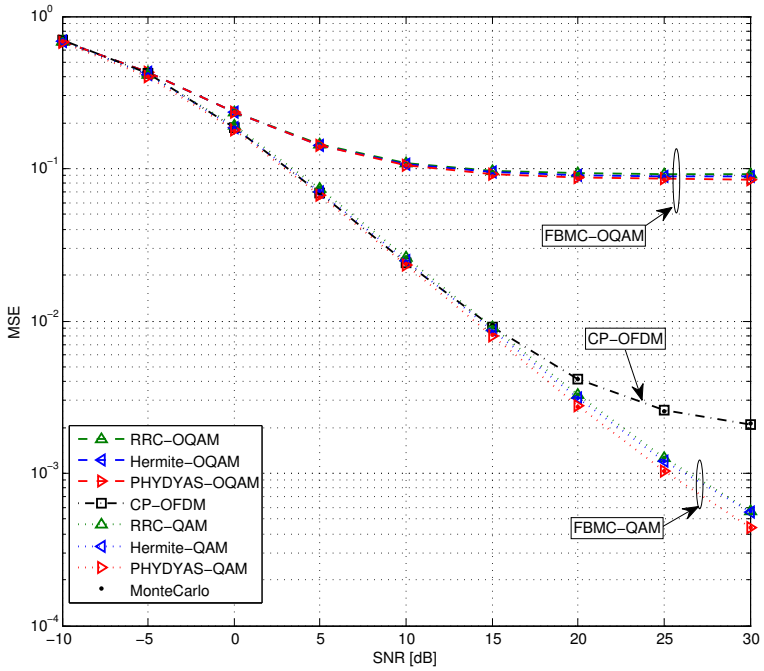

Figure 3.2: MSE vs SNR for CP-OFDM and FBMC-(O)QAM with different prototype filters and $\rho = 0, \gamma = 0$

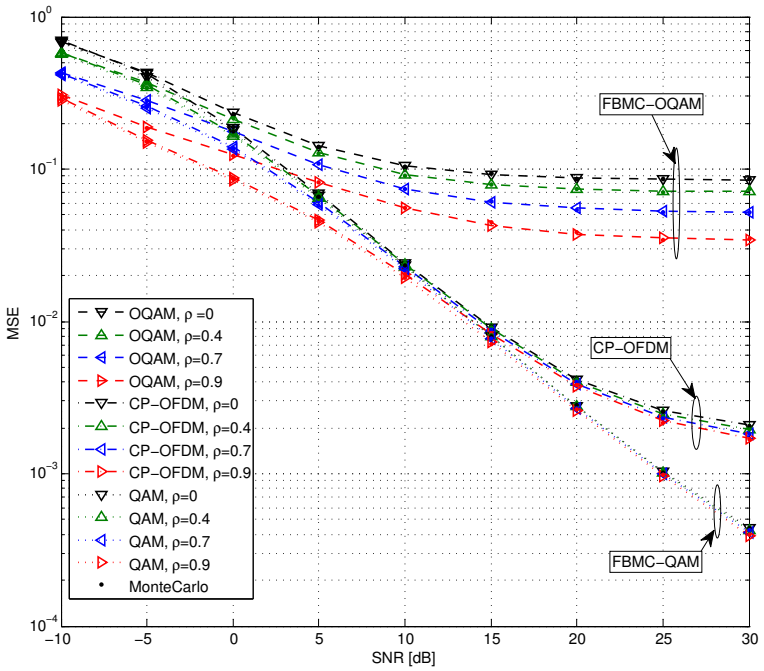

Figure 3.3: CP-OFDM and FBMC-(O)QAM performance with PHYDYAS and $\rho = 0.4, 0.7, 0.9, \gamma = 0$

an overlapping factor value of 4. A cyclic prefix of six samples length and 3000 repetitions for Montecarlo simulations are used.

In Figure 3.2, we show the theoretical and numerical performance of the TD-LMMSE technique for CP-OFDM and FBMC-(O)QAM with uncorrelated antennas and multipaths where different prototype filters are adopted *i.e.*, PHYDYAS, Hermite, RRC. We note that PHYDYAS prototype filter offers better performance than Hermite and RRC due to the fact that it is more localized in the frequency domain. Hence, we adopt the PHYDYAS filter in what follows.

Figure3.3 shows the enhancements in performance by the adoption of the multipaths correlation assumption. We assumed for simplicity that multipaths are correlated with each others by the same correlation coefficient ρ and pictured the performance for different values of $\rho = 0.4, 0.7, 0.9$.

In Figure 3.4, we draw the results for the multi antennas correlation case. For clarity, we depict the performance of the FBMC-QAM only. We assume once again that antennas are correlated with each others with the same value γ and we simulate the performance for different correlation values of $(\rho = 0, \gamma = 0.4, 0.7, 0.9)$. We note that the enhancement in performance falls in the low SNR region only. To sum up, we consider both the SIMO correlation and multipaths

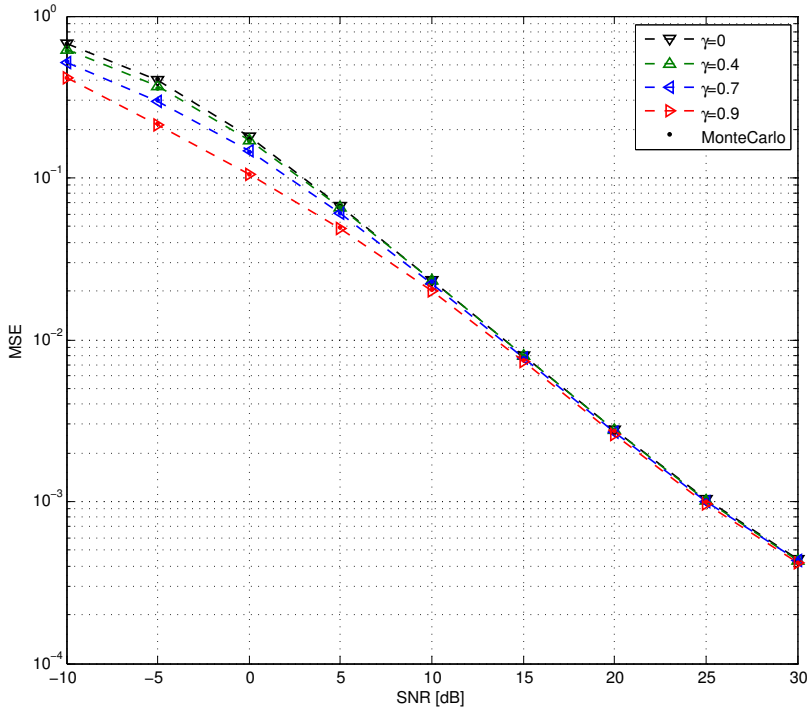

Figure 3.4: FBMC-QAM performance with PHYDYAS prototype filter and $\rho = 0, \gamma = 0.4, 0.7, 0.9$

correlation assumptions altogether. For clarity, we adopt a correlation coefficient

of 0.7 and simulate the performance of FBMC-OQAM only.

Figure 3.5 depicts the cases of no correlation at all ($\gamma = 0, \rho = 0$), only SIMO's correlation ($\gamma = 0.7, \rho = 0$), only multipaths correlation ($\gamma = 0, \rho = 0.7$), and the case where both SIMO and multipaths correlations exist ($\gamma = 0.7, \rho = 0.7$).

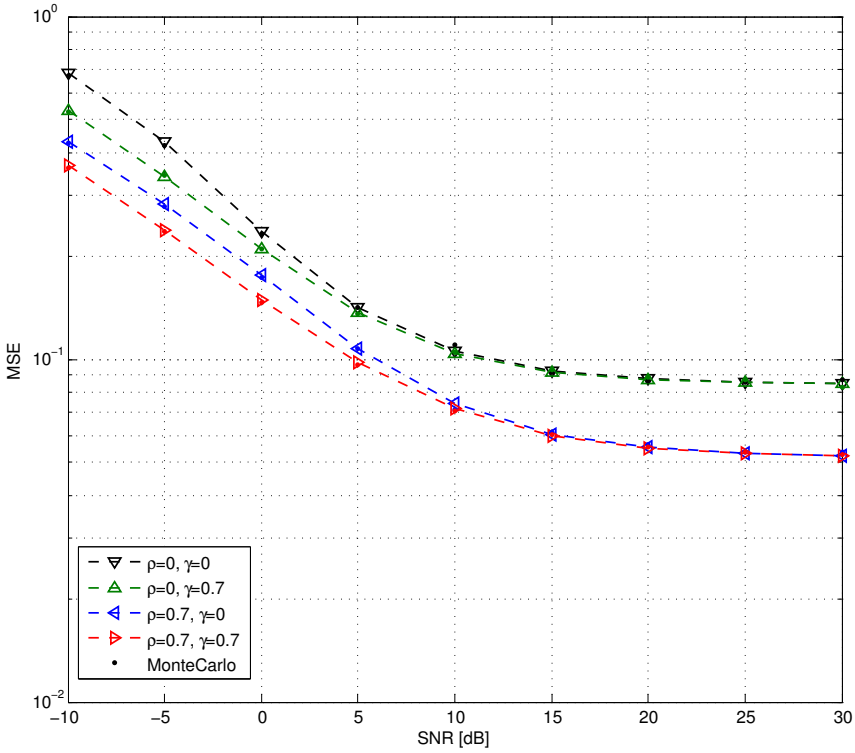

Figure 3.5: FBMC-OQAM performance with PHYDYAS prototype filter and different ρ and γ values

3.4 Pattern Based LMMSE for FBMC-OQAM

In the previous section, we proposed a time domain channel estimator that could exploit the time domain correlation, the multi-paths correlation, and the multi-antennas correlation of the received signal. Although the channel estimation performance was improved for all studied waveforms, FBMC-OQAM has shown in general a bad channel estimation accuracy due to its built-in interference. To this end, auxiliary pilots could be applied at the transmitter to cancel the built-in interference at the demodulated pilot symbols. This could render traditional LS based channel estimation techniques to be applicable. However, the doubly selectivity of the wireless channel and the non-orthogonality of the FBMC-OQAM waveform imply high power spread of each pilot symbol.

In this section, we propose a pattern based LMMSE channel estimator that could exploit the power spread pattern of the corresponding FBMC-OQAM waveform. This LMMSE filtering will not only depend on received pilot symbols, but it includes surrounding symbols within the filtering process, those who have highest pilots leaked power. Hence, performance accuracy will be enhanced with the increase of adopted adjacent symbols at the cost of slightly increased computational complexity. An analytical analysis of the aforementioned study is proposed and verified by Monte Carlo simulations.

3.4.1 Auxiliary Pilots Design

Estimating the channel in FBMC-OQAM systems is quite problematic due the loss of orthogonality which leads to built-in inter carrier and inter symbol interference. This means that surrounding symbols will interfere the pilots in a manner related to the adopted prototype filter. That can be expressed in ideal channel case as follows:

$$\boldsymbol{y}_p = \boldsymbol{Q}(:,\Omega_p)^H \boldsymbol{G}(:,\Omega_p)\boldsymbol{x}_p + \boldsymbol{Q}(:,\Omega_p)^H \boldsymbol{G}(:,\Omega_d)\boldsymbol{x}_d \tag{3.31}$$

One way to counter this interference is to sacrifice some data symbols that are close to the pilots, one or two symbols for each pilots for example as in Figure 3.6. Then, we design these sacrificed symbols in a way that helps the pilots getting

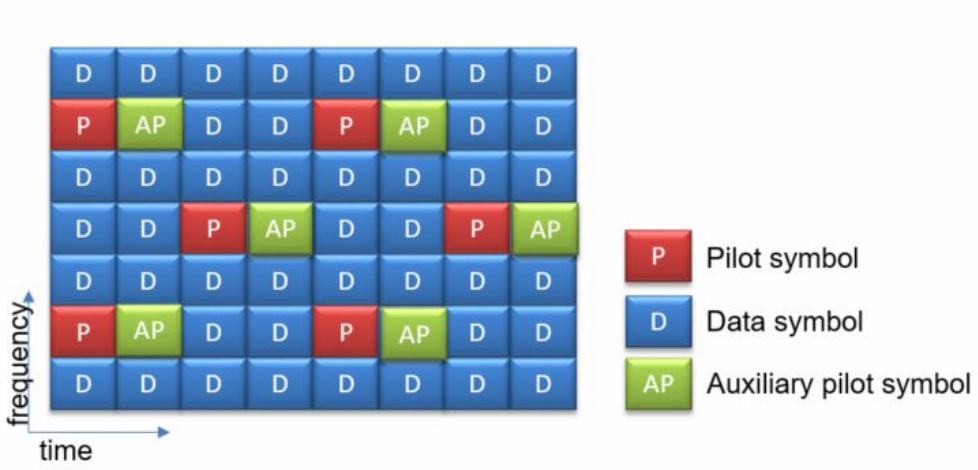

Figure 3.6: Auxiliary pilots in a 7×8 resource grid with scattered pilots pattern

rid from surrounding interference, hence the name auxiliary pilots. We denote by Ω_a to their set of indices with N_a AP symbols. Hence, we add auxiliary pilots to Equation (3.31), and we rewrite it as follows:

$$\boldsymbol{y}_p = \boldsymbol{Q}(:,\Omega_p)^H \boldsymbol{G}(:,\Omega_p)\boldsymbol{x}_p + \boldsymbol{Q}(:,\Omega_p)^H \boldsymbol{G}(:,\Omega_d)\boldsymbol{x}_d + \boldsymbol{Q}(:,\Omega_p)^H \boldsymbol{G}(:,\Omega_a)\boldsymbol{x}_a \tag{3.32}$$

The AP is designed as in [104]:

$$\boldsymbol{x}_a = \big(\boldsymbol{Q}(:\,\Omega_p)^H \boldsymbol{G}(:,\Omega_a)\big)^{\dagger} \left[\big(\boldsymbol{I} - \boldsymbol{Q}(:,\Omega_p)^H \boldsymbol{G}(:,\Omega_p)\big)\boldsymbol{x}_p - \boldsymbol{Q}(:,\Omega_p)^H \boldsymbol{G}(:,\Omega_d)\boldsymbol{x}_d\right] \tag{3.33}$$

This represents the general AP design equation, which takes both data interference and inter pilots interference into account. This is useful in case we use LS channel estimation at pilot positions followed with an interpolation technique at data positions. However, this represents also inefficiency in exploiting the transmitted pilots energy in the case of small pilots spacing in time or frequency. To handle that, we first need to design an estimator that could exploit the overall pilot transmitted energy, which will be done in the following section. Secondly, we need to consider cancelling the data interference part only, which means:

$$\boldsymbol{x}_a = -\left(\boldsymbol{Q}(:,\Omega_p)^H \boldsymbol{G}(:,\Omega_a)\right)^{\dagger} \boldsymbol{Q}(:,\Omega_p)^H \boldsymbol{G}(:,\Omega_d)\boldsymbol{x}_d \tag{3.34}$$

This will result in better performance, and less power offset at auxiliary pilots positions in the case of relatively small pilots spacing. The less power offset side is explained by the fact that APs do not cancel the inter pilots interference anymore but only data interference. This means APs will need less allocated power and hence decreasing the power offset issue. On the other hand, avoiding the removal of inter pilots interference will allow our developed direct LMMSE estimator to exploit pilots spread energy and hence getting the performance enhancements. This become clearer in next section. We should mention that in the AP design equation, we do not practically consider all data symbols in the transmission block, but only those adjacent ones which cause highest interference, we denote to their set of indices by Ω_{adj}. The more symbols we consider in Ω_{adj}, the lower the built in interference, however at the cost of higher power offset at AP positions, and vice versa. In what follows, and in order to maintain the simplified mathematical development, we denote by $\mathcal{C} \in \mathbb{C}^{N_d N_p N_a \times N_p N_d}$ to the precoding matrix. Where its sub-matrix $\mathcal{C}(\Omega_d \cup \Omega_p; \Omega_d \cup \Omega_p)$ is an identity matrix. The rows of $\mathcal{C}(\Omega_a; \Omega_d)$ are designed from Equation (3.34) while taking into consideration the adopted set Ω_{adj}. The sub-matrix $\mathcal{C}(\Omega_a; \Omega_p)$ is a zero matrix.

3.4.2 Direct LMMSE Channel Estimation

Exploiting Pilots Spread Energy

Interpolation methods are normally adopted to estimate the channel at data positions after applying an LS filter that estimate the channel at pilot positions [92] [106]. However, with non orthogonal waveforms, such as the FBMC-OQAM in our case, the symbol energy is spread across adjacent time and frequency subcarriers in a way related to the adapted prototype filter, and the spreading nature of the doubly selective channel. That is better explained in Figures 3.7 and 3.8, where we plot the received power of a single transmitted symbol using Hermite and PHYDYAS prototype filters, respectively, with an overlapping factor of $O = 4$. Section (a) of Figures 3.7 and 3.8 show an ideal channel case while section (b) present the doubly selective channel case. A VehicularA power delay profile with Jakes Doppler spectrum model at speed: 400 [km/h] are considered.

Applying an LS filter at pilot positions will suffer from power loss since it can only use the pilots' energy available at pilot positions. Hence, a better idea would be to consider an LMMSE filter to estimate the channel at pilot positions to exploit this wasted power. The best way to do that is to apply the LMMSE filter on the whole received vector *i.e.* $\Omega_{adj} = \{1, 2, ..., MK\}$, full block LMMSE filtering, which will guarantee perfect exploitation of pilots energy. However, this implies high computational complexity to invert a matrix of $MK \times MK$ size. On the other hand, if we apply the LMMSE filter on pilot positions only, Ω_{adj} : {Pilot positions}, the complexity will decrease but without exploiting the pilots spreaded energy, as in the LS case. Hence, tradeoffs could be achieved by including the adjacent symbols, that have the highest pilots leaked energy, within the LMMSE estimation process *i.e.* $\Omega_{adj} = \{\{\text{Pilot Positions}\} \bigcup \{\text{Adjacent Pilot Positions}\}\}$.

In Figure 3.9, we show different patterns of adjacent symbols with highest leaked power. Patterns with size of 8,16 and 28 adjacent symbols are considered for Hermite filter while patterns with size of 8, 12 and 22 adjacent symbols are considered for PHYDYAS filter. It is worth mentioning that with this "small to medium" sized patterns, the pattern shape will not change if we move from an ideal channel case to the aforementioned doubly selective VehicularA channel case. However, by increasing the patterns size, the doubly selective channel will have the ability to modify the patterns shape as we show in Figure 3.10, where we have considered patterns size of 36 adjacent symbols. However, the performance gain of these big patterns will be negligible in our study compared to the one obtained with small patterns as we may note from the simulation section.

Direct LMMSE Estimation

The direct LMMSE estimation of $(i, j)^{th}$ element of the system transmission matrix could be written as follows:

$$\hat{\mathcal{D}}(i, j) = \mathcal{W}_{i,j}^{H} \boldsymbol{y}(\Omega_{adj}) \tag{3.35}$$

where $\boldsymbol{y}(\Omega_{adj})$ is the desired set of demodulated symbols that will be applied to the LMMSE filter and it will differ according to the adopted pattern as illustrated in Figures 3.9 and 3.10.

$$\boldsymbol{y}(\Omega_{adj}) = \boldsymbol{Q}(\Omega_{adj}, :) \sum_{l=0}^{L-1} \boldsymbol{S}_{p}^{(l)} \boldsymbol{h}_l + \boldsymbol{Q}(\Omega_{adj}, :) \sum_{l=0}^{L-1} \boldsymbol{S}_{d,a}^{(l)} \boldsymbol{h}_l + \boldsymbol{Q}(\Omega_{adj}, :)\eta \tag{3.36}$$

where $\boldsymbol{S}_{d,a}^{(l)} = diag(\boldsymbol{s}_{d,a}^{(l)}) = diag\left(\boldsymbol{G}^{(l)} \mathcal{C}(\Omega_d \cup \Omega_a, :) \boldsymbol{x}_d\right)$. $\mathcal{W}_{i,j}$ is the corresponding direct LMMSE filter of the $(i, j)^{th}$ element of the STM matrix.

$$\mathcal{W}_{i,j} = E\left[\boldsymbol{y}(\Omega_{adj}) \boldsymbol{y}(\Omega_{adj})^{H}\right]^{-1} E\left[\boldsymbol{y}(\Omega_{adj}) \mathcal{D}(i, j)^{*}\right] \tag{3.37}$$

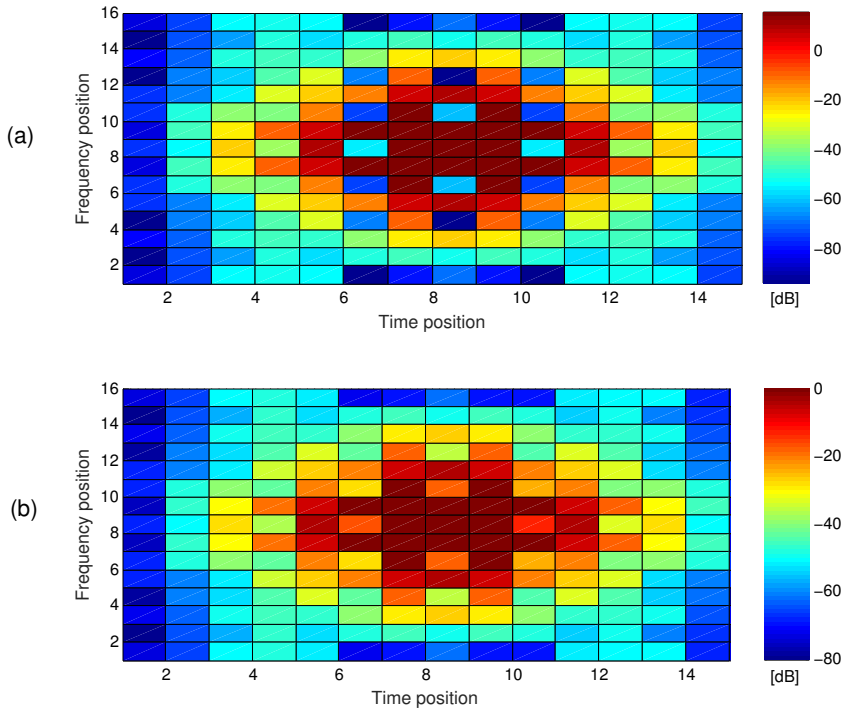

Figure 3.7: The power distribution of one FBMC-OQAM symbol located in the middle of the resource grid using Hermite

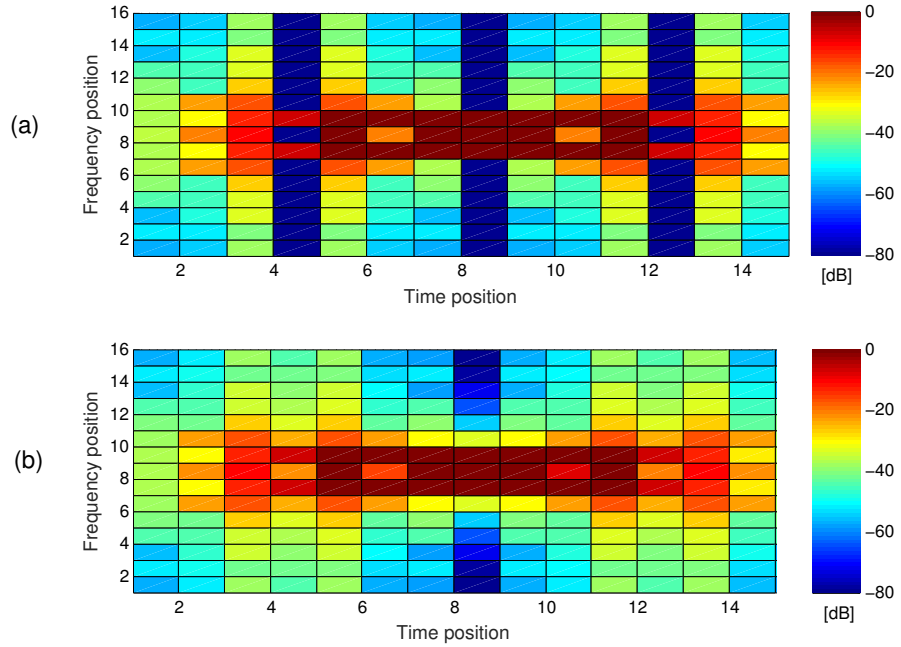

Figure 3.8: The power distribution of one FBMC-OQAM symbol located in the middle of the resource grid using PHYDYAS

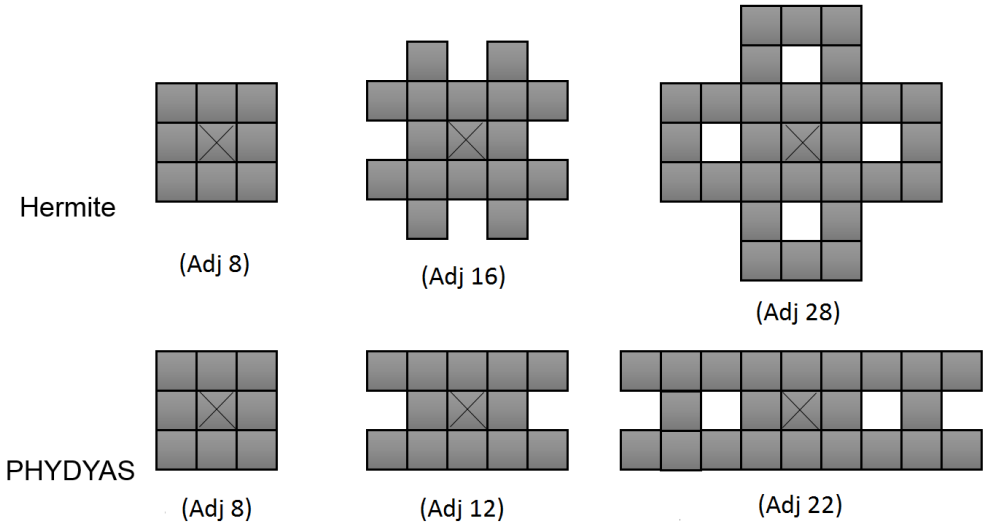

Figure 3.9: Different patterns of sizes 8(8), 16(12) and 28(22) of adjacent symbols with highest pilot leaked energy for Hermite (PHYDYAS) prototype filters

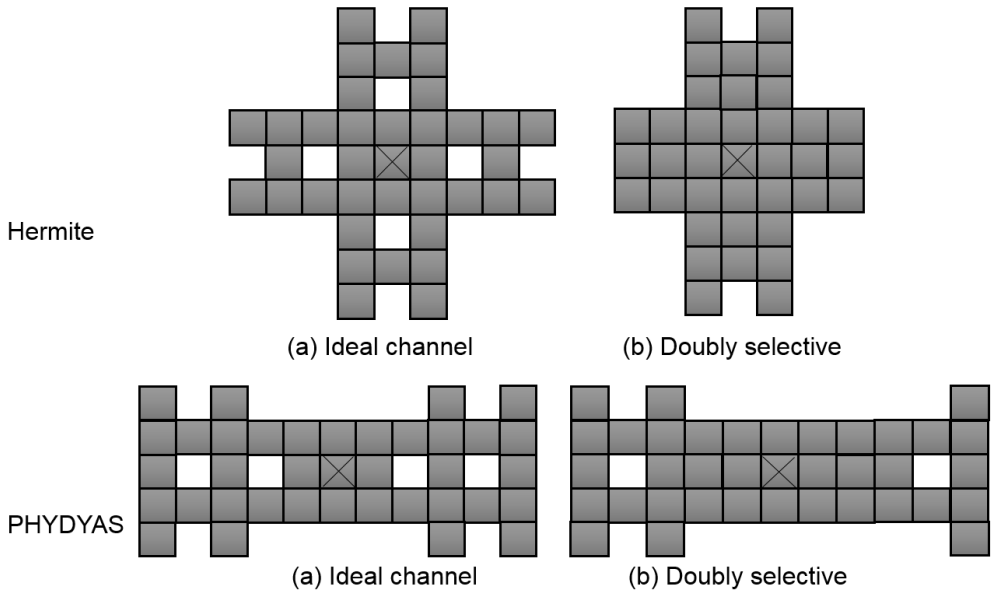

Figure 3.10: Different patterns of size 36 of adjacent symbols with highest pilot leaked energy for both Hermite and PHYDYAS prototype filters. Patterns shape change by moving from an ideal channel case to the aforementioned VehicularA channel case

Under the assumption of the Wide Sense Stationary and Uncorrelated Scatterers (WSSUS), we may write the covariance matrix $E\left[\boldsymbol{y}(\Omega_{adj})\boldsymbol{y}(\Omega_{adj})^H\right]$ as follows:

$$\mathbb{E}\left[\boldsymbol{y}(\Omega_{adj})\boldsymbol{y}(\Omega_{adj})^H\right] = \boldsymbol{Q}(\Omega_{adj},:)\Big(\sum_{l=0}^{L-1}\left[\boldsymbol{R}p_{l,l} + \boldsymbol{R}d_{l,l}\right] \odot \boldsymbol{R}_{\boldsymbol{h}_l\boldsymbol{h}_l} + \boldsymbol{R}_\eta\Big)\boldsymbol{Q}(\Omega_{adj},:)^H \tag{3.38}$$

By writing the (i,j) element of the STM matrix as follows:

$$\mathcal{D}(i,j) = \boldsymbol{Q}(:,i)^H \sum_{l=0}^{L-1} diag\left(\boldsymbol{G}^{(l)}(:,j)\right)\boldsymbol{h}_l \tag{3.39}$$

we can calculate the covariance matrix $E\left[\boldsymbol{y}(\Omega)\mathcal{D}(i,j)^*\right]$ using the following equation:

$$E\left[\boldsymbol{y}(\Omega)\mathcal{D}(i,j)^*\right] = \boldsymbol{Q}(:,\Omega)^H\left(\sum_{l=0}^{L-1}\boldsymbol{S}_p^{(l)}\boldsymbol{R}_{h_l} diag\left(\boldsymbol{G}^{(l)}(:,j)\right)\right)\boldsymbol{Q}(:,i) \tag{3.40}$$

3.4.3 Mean Square Error

In this study, we evaluate the performance of the proposed channel estimator with the sample one tap equalizer. Hence, the MSE of the diagonal vector of the STM matrix is written as follows:

$$MSE = \frac{1}{MK}Tr\left(E\left[\left(\hat{\mathfrak{h}}-\mathfrak{h}\right)\left(\hat{\mathfrak{h}}-\mathfrak{h}\right)^H\right]\right) \tag{3.41}$$

$$= \frac{1}{MK}Tr\left(E\left[\hat{\mathfrak{h}}\hat{\mathfrak{h}}^H\right] - 2\Re\left\{E\left[\hat{\mathfrak{h}}\mathfrak{h}^H\right]\right\} + E\left[\mathfrak{h}\mathfrak{h}^H\right]\right) \tag{3.42}$$

The covariance matrix of the estimated channel vector is written as:

$$E\left[\hat{\mathfrak{h}}\hat{\mathfrak{h}}^H\right] = \mathcal{W}_{LMMSE}^H E\left[\boldsymbol{y}(\Omega_{adj})\boldsymbol{y}(\Omega_{adj})^H\right]\mathcal{W}_{LMMSE} \tag{3.43}$$

and the matrix $\mathbb{E}\left[\hat{\mathfrak{h}}\mathfrak{h}^H\right]$ is calculated by noting that

$$\mathbb{E}\left[\hat{\mathcal{D}}(i,i)\mathcal{D}(i,i)^*\right] = \mathcal{W}_i^H\left[\boldsymbol{y}(\Omega_{adj})\mathcal{D}(i,i)^*\right] \tag{3.44}$$

In next section, we verify the MSE relation by conducting numerical simulations with Monte-Carlo repetitions.

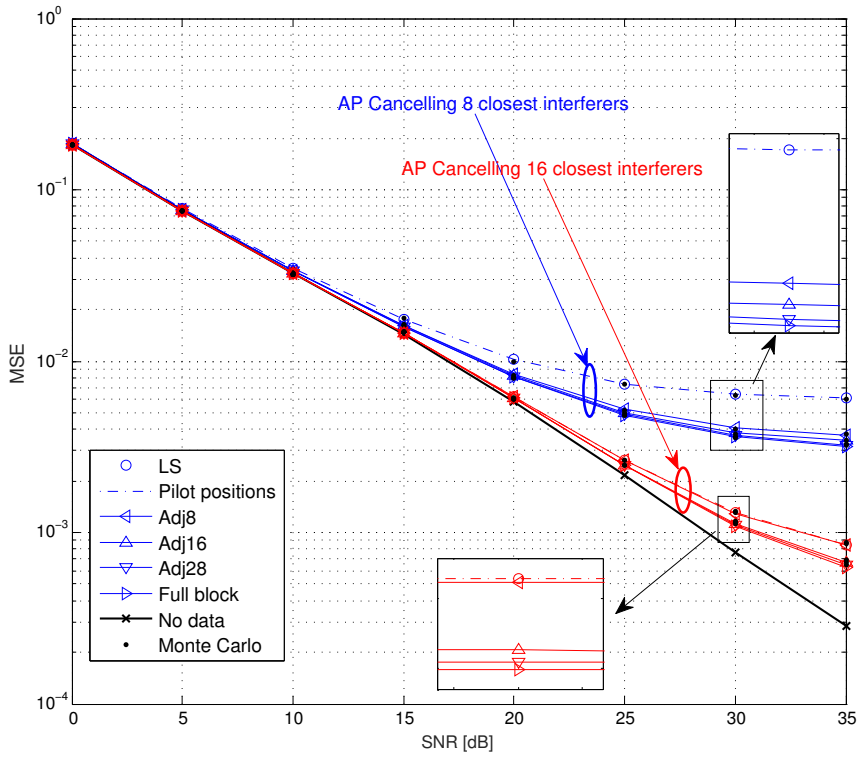

Figure 3.11: Direct LMMSE performance for Hermite filter under speed of 50 [km/h] and over different vectors: Pilot positions, Adj8, Adj16, Adj28

.

3.4.4 Numerical Simulations

In this section, we simulate the performance of the studied LMMSE channel estimator for the FBMC-OQAM waveform with the PHYDYAS and Hermite prototype filters. We compare it with the work of [92] where LS was used at pilot positions while LMMSE interpolator at data positions. This allows us to see the benefits of exploiting the pilots power spread. VehicularA channel model is adopted with Jakes Doppler spectrum model to modulate the time varying nature of the channel. LTE parameters are adopted with subcarriers frequency spacing of

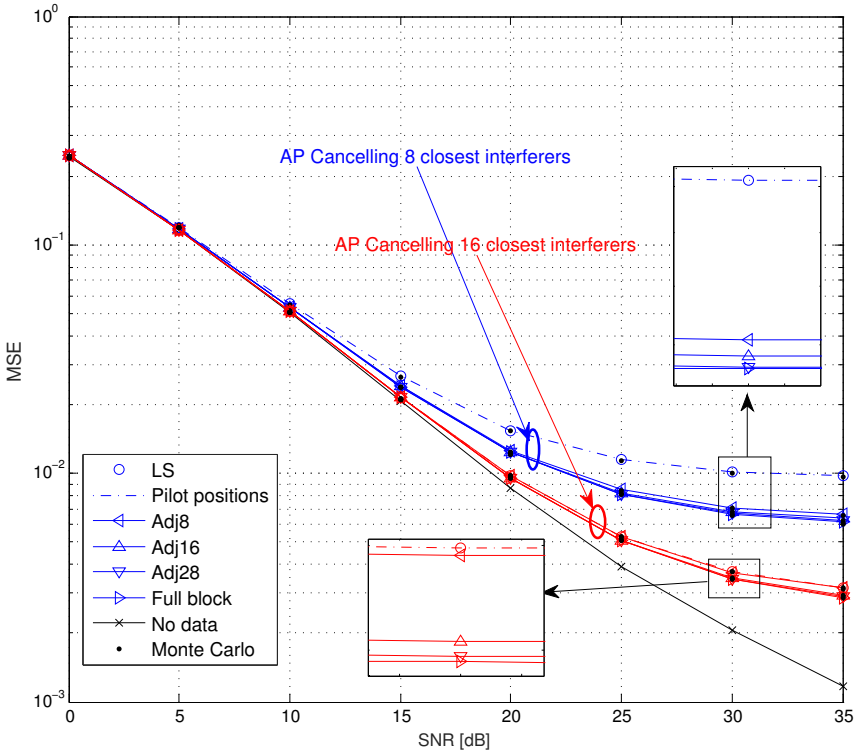

Figure 3.12: Direct LMMSE performance for Hermite filter under speed of 200 [km/h] and over different vectors: Pilot positions, Adj8, Adj16, Adj28.

15 kHz, and a 2.5 GHz carrier frequency. PHYDYAS and Hermite prototype filters are adopted for FBMC-OQAM with an overlapping ratio of 4. FBMC-OQAM is designed with 16 subcarriers and for 30 symbols in the time domain. We consider a scattered Pilot pattern with frequency spacing of 6 subcarriers and time spacing of 8 FBMC-OQAM symbols. Two auxiliary pilots method is used to counter the intrinsic interference at pilot positions of either the 8^{th} or 16^{th} closest interferers. Monte Carlo simulations with 3000 repetitions is performed. In Figures 3.11 and 3.12, we show the MSE performance versus the SNR of the Hermite prototype filter and for two mobile speed values of 50 [km/h] and 200 [km/h], respectively. We note that the (LS/LMMSE) estimator has similar performance as our LMMSE estimator when applied at data positions only. On the other hand, we can see the

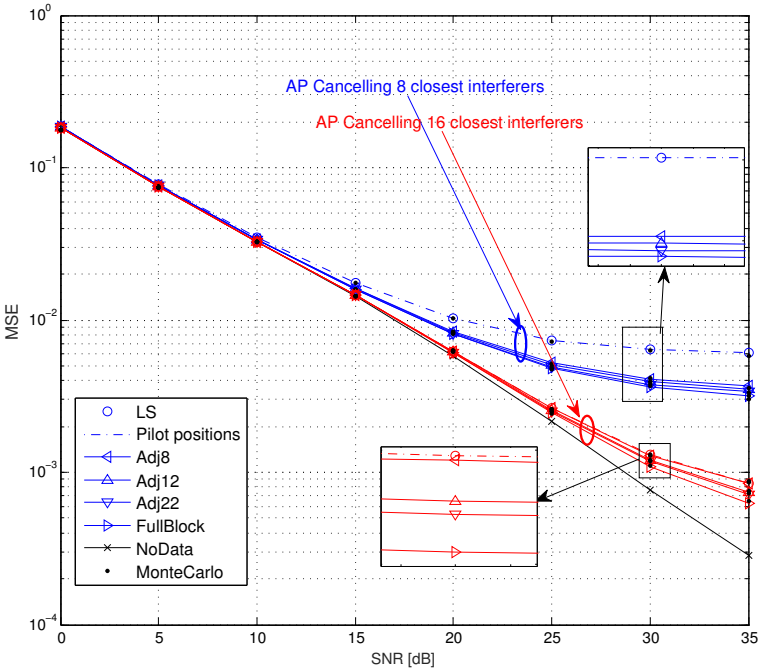

Figure 3.13: Direct LMMSE performance for PHYDYAS filter under speed of 50 [km/h] and over different vectors: Pilot positions, Adj8, Adj12, Adj22.

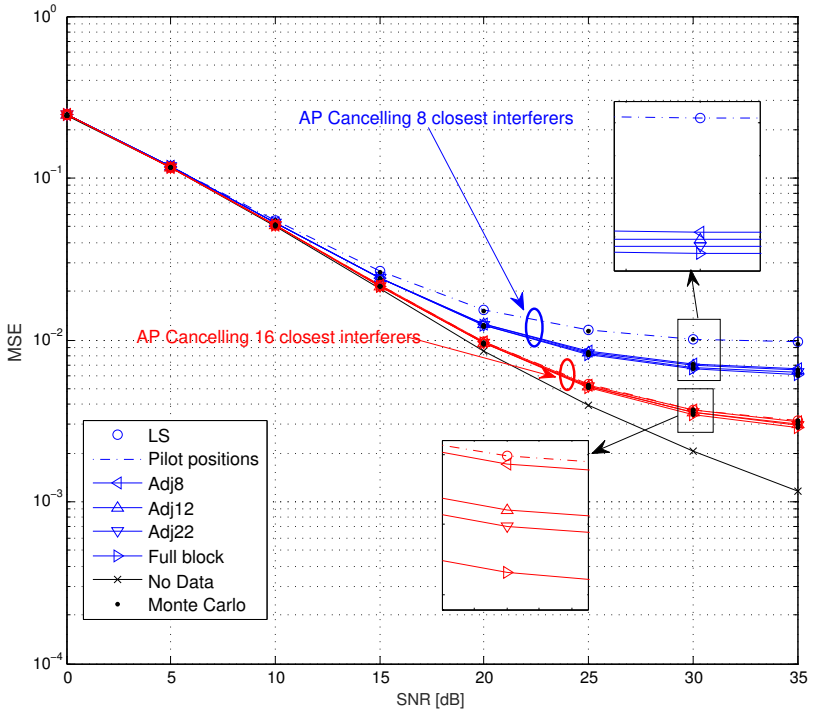

Figure 3.14: Direct LMMSE performance for PHYDYAS filter under speed of 200 [km/h] and over different vectors: Pilot positions, Adj8, Adj12, Adj22

performance gap between the two cases when we apply our LMMSE filter on the Full block of received symbols. We observe that with filtering adjacent pilot positions as in Figure 3.9, the performance will be approaching the Full block case. Also, we note that with designing the auxiliary pilots to cancel larger amount of interferers, the performance gap between the two cases will be decreasing at the cost of increasing the power offset at auxiliary pilots' positions.

In Figures 3.13 and 3.14, we show the MSE performance versus the SNR of the PHYDYAS prototype filter and for the same two mobile speed values of 50 [km/h] and 200 [km/h], respectively. Again, we can note the efficiency of our proposed LMMSE estimator where filtering on adjacent pilot positions gives performance close to the full block case. We note also that the conducted Monte Carlo simulation has similar performance with the analytical results.

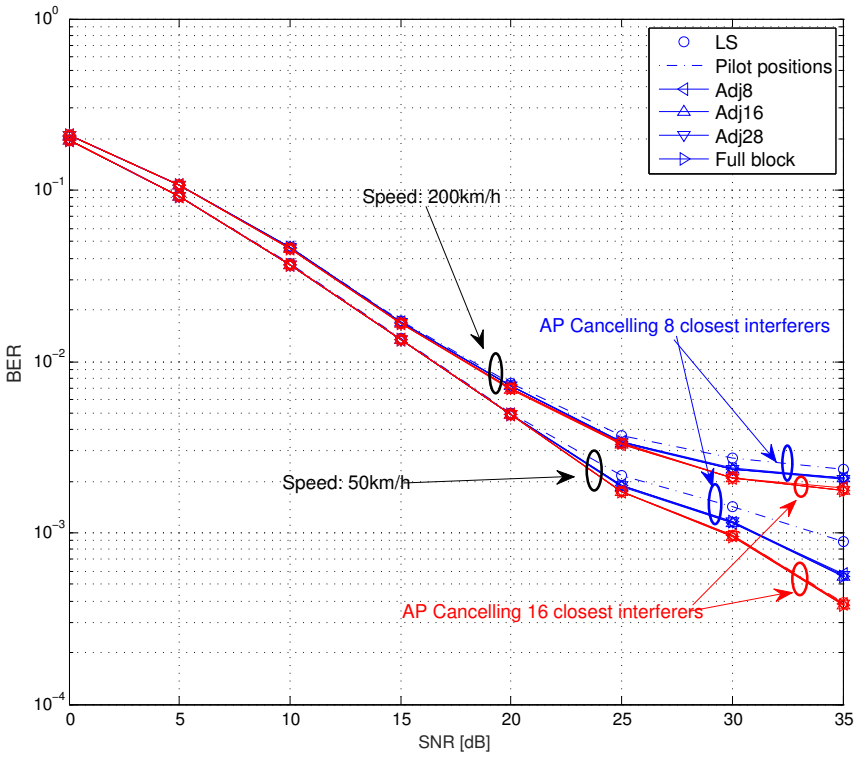

Figure 3.15: BER performance of the direct LMMSE estimator and the Hermite filter. Two mobility cases are considered: 50 [km/h] and 200 [km/h]

In Figures 3.15 and 3.16, we present the corresponding BER performance versus SNR for both Hermite and PHYDYAS prototype filters, respectively. In these figures, we adopt a one tap equalizer while considering two speeds values of 50 [km/h] and 200 [km/h]. In the case of AP cancelling 8 closest interferes, we note the accompanied gains of our direct LMMSE estimator. In the case of AP cancelling 16 closest interferers, we note that the direct LMMSE estimator gives the same performance if it is applied either on pilot positions only or on the full block.

This means that applying the direct LMMSE on pilot positions will be preferred in this case to guard a low computational complexity.

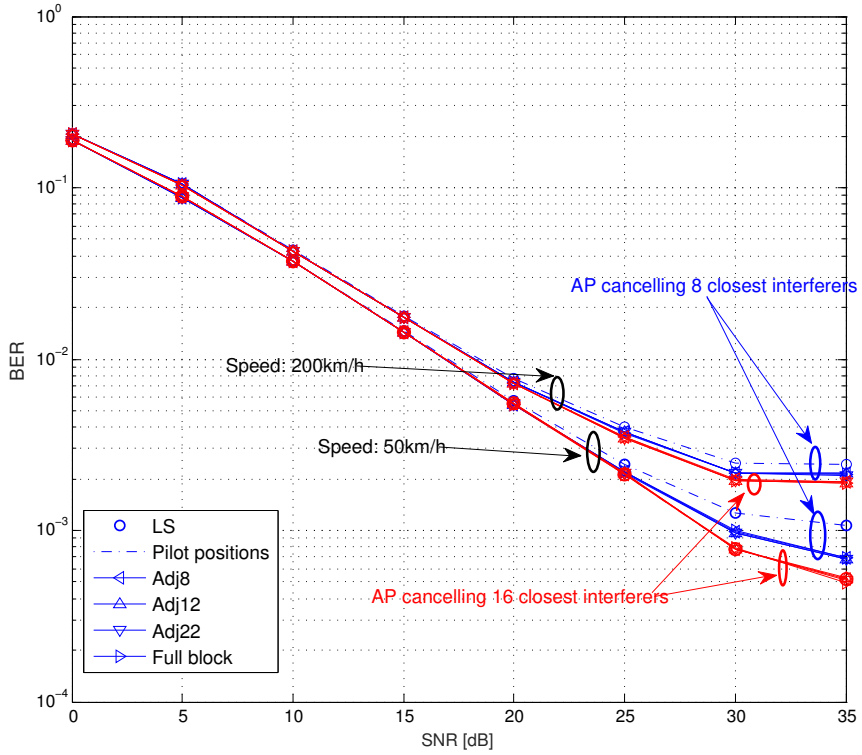

Figure 3.16: BER performance of the direct LMMSE estimator and the PHYDYAS filter. Two mobility cases are considered: 50 [km/h] and 200 [km/h]

3.5 Conclusion

In this chapter, we have considered the doubly selective channel estimation aspects of different multi-carrier modulation techniques. Two main contributions have been presented. In a first place, the Sliding Window Time Domain LMMSE channel estimation technique, which suits high mobility scenarios, has been analyzed for a group of MCM techniques, namely the CP-OFDM, FBMC-QAM, and the FBMC-OQAM waveforms. This has been made by first proposing a generalized analytical development of the SW TD-LMMSE so that it might exploit the multipaths and the multiantennas correlation as well, once they exist. The fact that a comb type pilot pattern was adopted means that the interference is coming only from adjacent subcarriers in the frequency domain and not from the time domain. Hence, in FBMC based waveforms, the PHYDYAS filter has shown better performance than Hermite and RRC filters since it has better frequency localization. It has been also shown that FBMC-QAM offers better performance

in the high speed scenarios due to the fact that the subcarriers spacing is twice that of FBMC-OQAM and OFDM, hence there is less ICI. This was verified by Monte Carlo simulations.

We have seen also that FBMC-OQAM performs poorly due to its built-in interference which necessitates the use of a special interference cancellation schemes. The fact that FBMC-OQAM is a non orthogonal waveform meant that its symbols power will be spread across adjacent symbols, depending on the adopted prototype filter and the doubly selective channel case. Hence, we presented the incapability of the LS based estimator to exploit the spread power.

To handle that, we proposed a direct LMMSE channel estimator that can exploit the power spreading patterns of different prototype filters, in addition to considering the spreading effects of the doubly selective channel. This allowed the developed estimator to present superior performance accuracy with small additional complexity where a tradeoff is made. We have noted also that doubly selective channels will modify big patterns only. However, the LMMSE performance will converge with small to medium patterns, hence, channel effects on adopted patterns could be neglected in our studied case. We also studied the effects of the adopted interference cancellation scheme, the two auxiliary pilots. We noted that when auxiliary pilots consider more surrounding data to remove, the performance will be enhanced and the performance gap between full block LMMSE and pilot positions one, would be smaller. However, that would come with an increase in the power offset at auxiliary pilots' positions. An analytical study for our work is provided and verified by Monte Carlo simulations. Lastly, the BER performance of the one tap equalizer was analyzed for the different channel estimations.

Future works include enhancing the SW-TD LMMSE performance for FBMC-OQAM by proposing suitable time domain interference cancellation schemes. These schemes should be able to exploit the FBMC-OQAM structure. It is worth mentioning also that, thanks to the generalized adopted model, the proposed techniques could be integrated in a more general communication framework where the performance could be evaluated from a system level view point.

Chapter 4

FBMC-OQAM Efficient Equalization Under Doubly Selective Channel Estimation Errors

4.1 Introduction

In the previous chapter, we have considered the channel estimation aspect of the MCM technique while concentrating on the FBMC-OQAM waveform. This is due to the outstanding frequency localization and high mobility robustness that FBMC-OQAM proved to possess. We have seen in Chapter 3 that channel estimation is not a straight forward task in FBMC-OQAM due to its built-in interference. In this chapter, we present the effects of FBMC-OQAM non-orthogonality on its equalization block. While many equalization techniques have been proposed in its literature, we propose an efficient equalizer that considers the imperfect channel estimation aspect and tries to exploit it while causing no additional complexity.

In Section 4.2, we conduct a literature study regarding the FBMC-OQAM equalization process while formulating the problematic of the study. In Section 4.3, we present a direct LMMSE estimator that will be used in Section 4.4 to propose the efficient equalizer scheme. In Section 4.5, we conduct the numerical study that presents the performance enhancements of our proposed scheme. Finally, we conclude the chapter and give perspectives in Section 4.6.

4.2 Problem Formulation and Literature Study

In ideal channel scenarios and orthogonal MCM techniques, the STM matrix $\mathcal{D}$ becomes diagonal. Hence, the demodulated vector $\boldsymbol{y}$ could be written in function of the transmitted symbols $\boldsymbol{x}$ and the additive white Gaussian noise vector $\boldsymbol{\eta}$ as follows:

$$\boldsymbol{y} = diag\left(\mathcal{D}\right)\boldsymbol{x} + \boldsymbol{Q}^H\boldsymbol{\eta} \tag{4.1}$$

In this case, the one tap equalizer *i.e.* $\boldsymbol{A}^H = diag\left(\mathcal{D}\right)^{-1}$ corresponds to the maximum likelihood equalizer [58]. The optimality of this low complexity equalizer could be maintained as long as the subcarrier spacing of the orthogonal MCM technique is capable of handling both the time and frequency selectivity of the wireless channel. However, this is not the case in doubly selective wireless channels and the non-orthogonal MCM techniques.

In FBMC-OQAM, orthogonality holds in the real domain only *i.e.* $\Re\{\boldsymbol{Q}^H\boldsymbol{G} = \boldsymbol{I}\}$ where the demodulated signal could be written as follows:

$$\boldsymbol{y} = \boldsymbol{x} + \Im\{\boldsymbol{Q}^H\boldsymbol{G}\}\boldsymbol{x} + \boldsymbol{Q}^H\boldsymbol{\eta} \tag{4.2}$$

By using the real part of the demodulated signal only, we cancel the imaginary interference component. However, this property is vulnerable due to different facts. First, the prototype filters do not assure perfect reconstruction property *i.e.* $\Re\{\boldsymbol{Q}^H\boldsymbol{G} \neq \boldsymbol{I}\}$. Second, the complex nature of the doubly selective wireless channel destroys the real orthogonality advantages where the imaginary interference components will leak into the real part. This results in a non-diagonal structure of the FBMC-OQAM system transmission matrix, as we have seen in Figures 2.9 and 2.10 for Hermite and PHYDYAS prototype filters, respectively. In addition, the channel is not perfectly known at the receiver where channel estimation errors will lead to worsen the performance accuracy.

In the literature, many equalization studies have assumed a frequency selective nature of the channel while considering it to be time-unvarying [107–111]. Parallel equalization was suggested in [108] where different IFFT blocks were used in parallel. In [110], larger FFT blocks were needed. The LMMSE equalizer has been proposed in [109] to suit the FBMC-OQAM waveform. In fact, traditional LMMSE equalizers cannot be applied directly to the FBMC-OQAM since the interference component will be included within the minimization process. To handle that, [109] proposed to use the real and imaginary parts of the demodulated signal separately. Hence, the full block LMMSE equalization process of the $\boldsymbol{x}(k,m)$ symbol is written as follows:

$$\hat{\boldsymbol{x}}(k,m) = \mathcal{A}_{k,m}^H \begin{bmatrix} \boldsymbol{y}_\Re \\ \boldsymbol{y}_\Im \end{bmatrix} \tag{4.3}$$

where

$$\mathcal{A}_{k,m} = E\begin{bmatrix} \boldsymbol{y}_\Re\boldsymbol{y}_\Re^T & \boldsymbol{y}_\Re\boldsymbol{y}_\Im^T \\ \boldsymbol{y}_\Im\boldsymbol{y}_\Re^T & \boldsymbol{y}_\Im\boldsymbol{y}_\Im^T \end{bmatrix}^{-1} E\left[\begin{bmatrix} \boldsymbol{y}_\Re \\ \boldsymbol{y}_\Im \end{bmatrix}\boldsymbol{x}(k,m)\right] \tag{4.4}$$

$\boldsymbol{y}_{\Re}$ and $\boldsymbol{y}_{\Im}$ represent real and imaginary parts of $\boldsymbol{y}$, respectively. Although using this full block LMMSE equalizer will guarantee high performance accuracy, it has a high computational complexity due to the $MK \times MK$ matrix inversion of Equation 4.4. In addition, it suffers from a high delay since it needs to receive the whole transmitted block of symbols before starting the equalization the process.

As a tradeoff, the LMMSE equalizer of a desired time frequency symbol $\boldsymbol{x}(k,m)$ was applied, in [109], on a group of adjacent symbols $\Omega_{k,m}$ in the time domain.

$$\hat{\boldsymbol{x}}(k,m) = \mathcal{A}_{k,m}^{H} \begin{bmatrix} \boldsymbol{y}_{\Re}(\Omega_{k,m}) \\ \boldsymbol{y}_{\Im}(\Omega_{k,m}) \end{bmatrix} \tag{4.5}$$

This study was extended to cover the MIMO case in [111]. In [112], a 2D LMMSE equalizer was proposed that considers adjacent symbols in time and frequency domains. This offers better performance accuracy and was evaluated in a doubly selective channel scenario. In [113], the adjacent time and frequency symbols of [112] were not chosen arbitrary but based on the power spread pattern of the adopted prototype filter. This presented a tradeoff between complexity and performance accuracy. Its performance was also compared with a one tap equalizer that employs an iterative interference cancellation of the non-diagonal STM elements. This has a shown a close performance to the LMMSE equalizer while having much less computational complexity.

All previous studies have considered a perfect channel knowledge at the receiver. Recently, [98] has developed the work of [113] by adding a channel estimation block to the iterative one tap equalizer. A LS channel estimator with LMMSE interpolator was used. However, and to the best of our knowledge, channel estimation errors have not been considered within the design phase of FBMC-OQAM equalizers, thus leading to sub-optimal performance. In [114], we proposed an efficient LMMSE equalizer that exploits channel estimation errors in FBMC-OQAM waveform. In order to suit the proposed equalizer, we redesigned our direct LMMSE channel estimator in a way to use the same covariance matrices needed for LMMSE equalizer. This study is conducted for high mobility scenarios and evaluated with Monte Carlo simulations.

4.3 The Redesigned Direct Channel Estimator

In this section, we develop the direct LMMSE channel estimator in way that will suit the proposed LMMSE equalizer. The motivations will become clear in next section. To this end, we stack the real and imaginary parts of the demodulated signal in one vector, *i.e.*, $\mathcal{Y} = \begin{bmatrix} \boldsymbol{y}_{\Re} \\ \boldsymbol{y}_{\Im} \end{bmatrix}$. For the channel estimation part, we use the

multipaths model of the demodulated signal

$$\boldsymbol{y} = \boldsymbol{Q}^H \sum_{l=0}^{L-1} \underbrace{diag\left(\boldsymbol{G}^{(l)}\boldsymbol{\mathcal{C}}\boldsymbol{x}\right)}_{\boldsymbol{S}_l} \boldsymbol{h}_l + \boldsymbol{w} \tag{4.6}$$

where $\boldsymbol{w} = \boldsymbol{Q}^H\boldsymbol{\eta}$ and $\boldsymbol{\mathcal{C}} \in (N_d N_p N_a \times N_p N_d)$ is the precoding matrix used to design the N_a auxiliary pilots that will cancel surrounding data interference at pilots positions. We write the estimated real and imaginary parts of the l^{th} CIR path as follows:

$$\hat{\boldsymbol{h}}_{l,\Re} = \boldsymbol{\mathcal{W}}_{l,\Re}^T \boldsymbol{\mathcal{Y}}_{\Omega_{est}} \tag{4.7}$$

$$\hat{\boldsymbol{h}}_{l,\Im} = \boldsymbol{\mathcal{W}}_{l,\Im}^T \boldsymbol{\mathcal{Y}}_{\Omega_{est}} \tag{4.8}$$

where $\boldsymbol{\mathcal{W}}_{l,\Re}$ and $\boldsymbol{\mathcal{W}}_{l,\Im}$ represent the LMMSE filters used to estimate the real and imaginary components of the lth path CIR, respectively. We denote by $\boldsymbol{\mathcal{Y}}_{\Omega_{est}}$ to the vector $\begin{bmatrix}\boldsymbol{y}_\Re(\Omega_{est})\\ \boldsymbol{y}_\Im(\Omega_{est})\end{bmatrix}$, where Ω_{est} refers to the symbols indices in vector $\boldsymbol{y}$ that we use to estimate the channel. This could be the set of pilot positions only or including their surrounding symbols also to enhance performance, as explained in Chapter 3.

$$\boldsymbol{\mathcal{W}}_{l,i} = E\left[\boldsymbol{\mathcal{Y}}_{\Omega_{est}}\boldsymbol{\mathcal{Y}}_{\Omega_{est}}^T\right]^{-1} E\left[\boldsymbol{\mathcal{Y}}_{\Omega_{est}}\boldsymbol{h}_{l,i}^T\right] \tag{4.9}$$

where

$$\begin{aligned} &E\left[\boldsymbol{\mathcal{Y}}_{\Omega_{est}}\boldsymbol{\mathcal{Y}}_{\Omega_{est}}^T\right] = \\ &\begin{bmatrix} E\left[\boldsymbol{y}_\Re(\Omega_{est})\boldsymbol{y}_\Re^T(\Omega_{est})\right] & E\left[\boldsymbol{y}_\Re(\Omega_{est})\boldsymbol{y}_\Im^T(\Omega_{est})\right] \\ E\left[\boldsymbol{y}_\Im(\Omega_{est})\boldsymbol{y}_\Re^T(\Omega_{est})\right] & E\left[\boldsymbol{y}_\Im(\Omega_{est})\boldsymbol{y}_\Im^T(\Omega_{est})\right] \end{bmatrix} \end{aligned} \tag{4.10}$$

$$E\left[\boldsymbol{y}_i\boldsymbol{y}_j^T\right] = E\left[\boldsymbol{z}_i\boldsymbol{z}_j^T\right] + E\left[\boldsymbol{w}_i\boldsymbol{w}_j^T\right] \tag{4.11}$$

$i, j \in \{\Re, \Im\}$ and $E\left[\boldsymbol{z}_i\boldsymbol{z}_j^T\right]$ and $E\left[\boldsymbol{\mathcal{Y}}_{\Omega_{est}}\boldsymbol{h}_{l,i}^T\right]$ are calculated later in Equations (4.24-4.27) and (4.36-4.39), respectively.

4.4 Efficient LMMSE Equalizer

For the equalization process, we use the demodulated signal of the form:

$$\boldsymbol{y} = \underbrace{\boldsymbol{Q}^H\boldsymbol{H}\boldsymbol{G}\boldsymbol{\mathcal{C}}}_{\mathcal{D}}\boldsymbol{x} + \boldsymbol{w} \tag{4.12}$$

where we consider the STM matrix to be equal to $\mathcal{D} = \boldsymbol{Q}^H\boldsymbol{H}\boldsymbol{G}\boldsymbol{\mathcal{C}}$. Applying the conventional LMMSE equalizer is not suitable for FBMC-OQAM waveform due to its built in interference. This has motivated the use of vector $\boldsymbol{\mathcal{Y}}$ to design the LMMSE equalizer $\mathcal{A}$, as in [109]. Hence, we write:

$$\hat{\boldsymbol{x}} = \mathcal{A}^H\boldsymbol{\mathcal{Y}}_{det} \tag{4.13}$$

We should mention that $\boldsymbol{\mathcal{Y}}_{det}$ is the same as $\boldsymbol{\mathcal{Y}}$, however, it has the knowledge of the previously estimated channel. The same applies for $\boldsymbol{y}_{det}$. To start, we write the equalizer input of Equation (4.13) as a function of the estimated STM and the estimation error:

$$\boldsymbol{\mathcal{Y}}_{det} = \hat{\boldsymbol{\mathcal{H}}}\boldsymbol{x} + \boldsymbol{\mathcal{E}}\boldsymbol{x} + \boldsymbol{\beta} \tag{4.14}$$

where $\hat{\mathcal{H}} = \begin{bmatrix}\hat{\mathcal{D}}_{\Re}\\ \hat{\mathcal{D}}_{\Im}\end{bmatrix}$, $\boldsymbol{\mathcal{E}} = \begin{bmatrix}\Delta_{\Re}\\ \Delta_{\Im}\end{bmatrix}$, and $\boldsymbol{\beta} = \begin{bmatrix}\boldsymbol{w}_{\Re}\\ \boldsymbol{w}_{\Im}\end{bmatrix}$. This is done by writing the STM matrix of Equation (4.12) in terms of its estimated part $\hat{\mathcal{D}}$ and the accompanied error matrix $\boldsymbol{\Delta}$

$$\mathcal{D} = \hat{\mathcal{D}} + \Delta \tag{4.15}$$

To design the $2N \times N_d$ LMMSE equalizer filter, $\mathcal{A}$, we write the non zero elements of its i^{th} column as follows:

$$\begin{aligned}&\mathcal{A}(\Omega_{i(\Re\cup\Im)}, i) = \\ &\underbrace{E\left[\boldsymbol{\mathcal{Y}}_{det,\Omega_{i(\Re\cup\Im)}}\left(\boldsymbol{\mathcal{Y}}_{det,\Omega_{i(\Re\cup\Im)}}\right)^T\right]^{-1}}_{\boldsymbol{R}_{\boldsymbol{\mathcal{Y}}}(\Omega_{i(\Re\cup\Im)},\Omega_{i(\Re\cup\Im)})}\underbrace{E\left[\boldsymbol{\mathcal{Y}}_{det,\Omega_{i(\Re\cup\Im)}}\boldsymbol{x}(i)^T\right]}_{\boldsymbol{R}_{\boldsymbol{\mathcal{Y}},\boldsymbol{x}}(\Omega_{i(\Re\cup\Im)},i)}\end{aligned} \tag{4.16}$$

where $\boldsymbol{\mathcal{Y}}_{det,\Omega_{i(\Re\cup\Im)}} = \begin{bmatrix}\boldsymbol{y}_{det,\Re}(\Omega_i)\\ \boldsymbol{y}_{det,\Im}(\Omega_i)\end{bmatrix}$. We denote by $\Omega_{i(\Re\cup\Im)}$ to the set of indices Ω_i of the real and imaginary parts of $\boldsymbol{y}_{det}$ within the vector $\boldsymbol{\mathcal{Y}}_{det}$. While i represents the index of desired symbol that we want to estimate, Ω_i represents the indices of its surrounding symbols in the vector $\boldsymbol{y}_{det}$. Different patterns of Ω_i could be adopted depending on the used prototype filter, where this offers a trade off between performance and complexity, as explained in [113]. Calculating the equalizer covariance matrices could be done as follows:

$$\boldsymbol{R}_{\boldsymbol{\mathcal{Y}}} = \hat{\mathcal{H}}E\left[\boldsymbol{x}\boldsymbol{x}^T\right]\hat{\mathcal{H}}^T + E\left[\boldsymbol{\mathcal{E}}\boldsymbol{x}\boldsymbol{x}^T\boldsymbol{\mathcal{E}}^T\right] + E\left[\boldsymbol{\beta}\boldsymbol{\beta}^T\right] \tag{4.17}$$

$$\boldsymbol{R}_{\boldsymbol{\mathcal{Y}},\boldsymbol{x}} = \hat{\mathcal{H}}E\left[\boldsymbol{x}\boldsymbol{x}^T\right] \tag{4.18}$$

In order to calculate the part including the Error Covariance Matrix (ECM), we write:

$$\begin{aligned}&E\left[\boldsymbol{\mathcal{E}}\boldsymbol{x}\boldsymbol{x}^T\boldsymbol{\mathcal{E}}^T\right] = \\ &\begin{bmatrix}E\left[\Delta_{\Re}\boldsymbol{x}\boldsymbol{x}^T\left(\Delta_{\Re}\right)^T\right] & E\left[\Delta_{\Re}\boldsymbol{x}\boldsymbol{x}^T\left(\Delta_{\Im}\right)^T\right]\\ E\left[\Delta_{\Im}\boldsymbol{x}\boldsymbol{x}^T\left(\Delta_{\Re}\right)^T\right] & E\left[\Delta_{\Im}\boldsymbol{x}\boldsymbol{x}^T\left(\Delta_{\Im}\right)^T\right]\end{bmatrix}\end{aligned} \tag{4.19}$$

Using the system model of Equation (4.6), we represent each sub-matrix of Equation (4.19) as follows:

$$\begin{aligned}&E\left[\Delta_i\boldsymbol{x}\boldsymbol{x}^T\left(\Delta_j\right)^T\right] = \\ &E\left[\boldsymbol{z}_i\boldsymbol{z}_j^T\right] + E\left[\hat{\boldsymbol{z}}_i\left(\hat{\boldsymbol{z}}_j\right)^T\right] - E\left[\hat{\boldsymbol{z}}_i\boldsymbol{z}_j^T\right] - E\left[\hat{\boldsymbol{z}}_i\left(\boldsymbol{z}_j\right)^T\right]\end{aligned} \tag{4.20}$$

where $i, j \in \{\Re, \Im\}$. We denote by $\boldsymbol{z}$ to the noise free demodulated signal of Equation (4.6), while $\hat{\boldsymbol{z}}$ is represented as:

$$\hat{\boldsymbol{z}} = \boldsymbol{Q}^H \sum_{l=0}^{L-1} \boldsymbol{S}_l \hat{\boldsymbol{h}}_l \tag{4.21}$$

To calculate Equation (4.20), we start by writing the real and imaginary parts of the noise free demodulated signal as follows:

$$\begin{aligned} \tilde{\boldsymbol{z}}_\Re = &\left(\boldsymbol{Q}^H\right)_\Re \sum_{l=0}^{L-1} \left(\boldsymbol{S}_{l,\Re} \tilde{\boldsymbol{h}}_{l,\Re} - \boldsymbol{S}_{l,\Im} \tilde{\boldsymbol{h}}_{l,\Im}\right) \\ &- \left(\boldsymbol{Q}^H\right)_\Im \sum_{l=0}^{L-1} \left(\boldsymbol{S}_{l,\Im} \tilde{\boldsymbol{h}}_{l,\Re} + \boldsymbol{S}_{l,\Re} \tilde{\boldsymbol{h}}_{l,\Im}\right) \end{aligned} \tag{4.22}$$

$$\begin{aligned} \tilde{\boldsymbol{z}}_\Im = &\left(\boldsymbol{Q}^H\right)_\Re \sum_{l=0}^{L-1} \left(\boldsymbol{S}_{l,\Im} \tilde{\boldsymbol{h}}_{l,\Re} + \boldsymbol{S}_{l,\Re} \tilde{\boldsymbol{h}}_{l,\Im}\right) \\ &+ \left(\boldsymbol{Q}^H\right)_\Im \sum_{l=0}^{L-1} \left(\boldsymbol{S}_{l,\Re} \tilde{\boldsymbol{h}}_{l,\Re} - \boldsymbol{S}_{l,\Im} \tilde{\boldsymbol{h}}_{l,\Im}\right) \end{aligned} \tag{4.23}$$

We use the notation $\tilde{\boldsymbol{x}}$ to denote that this can represent either the estimated version $\hat{\boldsymbol{x}}$ or the random variable itself $\boldsymbol{x}$. Based on that, and the assumption of WSSUS channel, we can write:

$$\begin{aligned} E\left[\tilde{\boldsymbol{z}}_\Re \left(\tilde{\boldsymbol{z}}_\Re\right)^T\right] = &\left(\boldsymbol{Q}^H\right)_\Re \left(\boldsymbol{V}_{\tilde{\boldsymbol{h}}\tilde{\boldsymbol{h}}} \boldsymbol{Q}_\Re - \boldsymbol{B}_{\tilde{\boldsymbol{h}}\tilde{\boldsymbol{h}}} \boldsymbol{Q}_\Im\right) - \\ &\left(\boldsymbol{Q}^H\right)_\Im \left(\boldsymbol{F}_{\tilde{\boldsymbol{h}}\tilde{\boldsymbol{h}}} \boldsymbol{Q}_\Re - \boldsymbol{T}_{\tilde{\boldsymbol{h}}\tilde{\boldsymbol{h}}} \boldsymbol{Q}_\Im\right) \end{aligned} \tag{4.24}$$

$$\begin{aligned} E\left[\tilde{\boldsymbol{z}}_\Re \left(\tilde{\boldsymbol{z}}_\Im\right)^T\right] = &\left(\boldsymbol{Q}^H\right)_\Re \left(\boldsymbol{B}_{\tilde{\boldsymbol{h}}\tilde{\boldsymbol{h}}} \boldsymbol{Q}_\Re + \boldsymbol{V}_{\tilde{\boldsymbol{h}}\tilde{\boldsymbol{h}}} \boldsymbol{Q}_\Im\right) - \\ &\left(\boldsymbol{Q}^H\right)_\Im \left(\boldsymbol{T}_{\tilde{\boldsymbol{h}}\tilde{\boldsymbol{h}}} \boldsymbol{Q}_\Re + \boldsymbol{F}_{\tilde{\boldsymbol{h}}\tilde{\boldsymbol{h}}} \boldsymbol{Q}_\Im\right) \end{aligned} \tag{4.25}$$

$$\begin{aligned} E\left[\tilde{\boldsymbol{z}}_\Im \left(\tilde{\boldsymbol{z}}_\Re\right)^T\right] = &\left(\boldsymbol{Q}^H\right)_\Re \left(\boldsymbol{F}_{\tilde{\boldsymbol{h}}\tilde{\boldsymbol{h}}} \boldsymbol{Q}_\Re - \boldsymbol{T}_{\tilde{\boldsymbol{h}}\tilde{\boldsymbol{h}}} \boldsymbol{Q}_\Im\right) + \\ &\left(\boldsymbol{Q}^H\right)_\Im \left(\boldsymbol{V}_{\tilde{\boldsymbol{h}}\tilde{\boldsymbol{h}}} \boldsymbol{Q}_\Re - \boldsymbol{B}_{\tilde{\boldsymbol{h}}\tilde{\boldsymbol{h}}} \boldsymbol{Q}_\Im\right) \end{aligned} \tag{4.26}$$

$$\begin{aligned} E\left[\tilde{\boldsymbol{z}}_\Im \left(\tilde{\boldsymbol{z}}_\Im\right)^T\right] = &\left(\boldsymbol{Q}^H\right)_\Re \left(\boldsymbol{T}_{\tilde{\boldsymbol{h}}\tilde{\boldsymbol{h}}} \boldsymbol{Q}_\Re + \boldsymbol{F}_{\tilde{\boldsymbol{h}}\tilde{\boldsymbol{h}}} \boldsymbol{Q}_\Im\right) + \\ &\left(\boldsymbol{Q}^H\right)_\Im \left(\boldsymbol{B}_{\tilde{\boldsymbol{h}}\tilde{\boldsymbol{h}}} \boldsymbol{Q}_\Re + \boldsymbol{V}_{\tilde{\boldsymbol{h}}\tilde{\boldsymbol{h}}} \boldsymbol{Q}_\Im\right) \end{aligned} \tag{4.27}$$

where by noting that $diag(\boldsymbol{a})\boldsymbol{\mathcal{B}} diag(\boldsymbol{a}^H) = \boldsymbol{a}\boldsymbol{a}^H \odot \boldsymbol{\mathcal{B}}$, we can write:

$$\begin{aligned} \boldsymbol{V}_{\tilde{\boldsymbol{h}}\tilde{\boldsymbol{h}}} = \sum_{l=0}^{L-1} \Big[&\boldsymbol{R}_{s_{l,\Re}, s_{l,\Re}} \odot \boldsymbol{R}_{\tilde{h}_{l,\Re} \tilde{h}_{l,\Re}} - \kappa \boldsymbol{R}_{s_{l,\Re}, s_{l,\Im}} \odot \boldsymbol{R}_{\tilde{h}_{l,\Re} \tilde{h}_{l,\Im}} \\ &- \kappa \boldsymbol{R}_{s_{l,\Im}, s_{l,\Re}} \odot \boldsymbol{R}_{\tilde{h}_{l,\Im} \tilde{h}_{l,\Re}} + \boldsymbol{R}_{s_{l,\Im}, s_{l,\Im}} \odot \boldsymbol{R}_{\tilde{h}_{l,\Im} \tilde{h}_{l,\Im}} \Big] \end{aligned} \tag{4.28}$$

$$\begin{aligned}\boldsymbol{B}_{\tilde{\boldsymbol{h}}\tilde{\boldsymbol{h}}} = \sum_{l=0}^{L-1} \Big[& \boldsymbol{R}_{s_{l,\Re},s_{l,\Im}} \odot \boldsymbol{R}_{\tilde{h}_{l,\Re}\tilde{h}_{l,\Re}} + \kappa \boldsymbol{R}_{s_{l,\Re},s_{l,\Re}} \odot \boldsymbol{R}_{\tilde{h}_{l,\Re}\tilde{h}_{l,\Im}} \\ & -\kappa \boldsymbol{R}_{s_{l,\Im},s_{l,\Im}} \odot \boldsymbol{R}_{\tilde{h}_{l,\Im}\tilde{h}_{l,\Re}} - \boldsymbol{R}_{s_{l,\Im},s_{l,\Re}} \odot \boldsymbol{R}_{\tilde{h}_{l,\Im}\tilde{h}_{l,\Im}} \Big]\end{aligned} \tag{4.29}$$

$$\begin{aligned}\boldsymbol{F}_{\tilde{\boldsymbol{h}}\tilde{\boldsymbol{h}}} = \sum_{l=0}^{L-1} \Big[& \boldsymbol{R}_{s_{l,\Im},s_{l,\Re}} \odot \boldsymbol{R}_{\tilde{h}_{l,\Re}\tilde{h}_{l,\Re}} - \kappa \boldsymbol{R}_{s_{l,\Im},s_{l,\Im}} \odot \boldsymbol{R}_{\tilde{h}_{l,\Re}\tilde{h}_{l,\Im}} \\ & +\kappa \boldsymbol{R}_{s_{l,\Re},s_{l,\Re}} \odot \boldsymbol{R}_{\tilde{h}_{l,\Im}\tilde{h}_{l,\Re}} - \boldsymbol{R}_{s_{l,\Re},s_{l,\Im}} \odot \boldsymbol{R}_{\tilde{h}_{l,\Im}\tilde{h}_{l,\Im}} \Big]\end{aligned} \tag{4.30}$$

$$\begin{aligned}\boldsymbol{T}_{\tilde{\boldsymbol{h}}\tilde{\boldsymbol{h}}} = \sum_{l=0}^{L-1} \Big[& \boldsymbol{R}_{s_{l,\Im},s_{l,\Im}} \odot \boldsymbol{R}_{\tilde{h}_{l,\Re}\tilde{h}_{l,\Re}} + \kappa \boldsymbol{R}_{s_{l,\Im},s_{l,\Re}} \odot \boldsymbol{R}_{\tilde{h}_{l,\Re}\tilde{h}_{l,\Im}} \\ & +\kappa \boldsymbol{R}_{s_{l,\Re},s_{l,\Im}} \odot \boldsymbol{R}_{\tilde{h}_{l,\Im}\tilde{h}_{l,\Re}} + \boldsymbol{R}_{s_{l,\Re},s_{l,\Re}} \odot \boldsymbol{R}_{\tilde{h}_{l,\Im}\tilde{h}_{l,\Im}} \Big]\end{aligned} \tag{4.31}$$

$$\boldsymbol{R}_{s_{l,i},s_{l,j}} = \left(\boldsymbol{G}^{(l)}\mathcal{C}\right)_i \left(E\left[\boldsymbol{x}_d\boldsymbol{x}_d^T\right] + \boldsymbol{x}_p\boldsymbol{x}_p^T\right) \left(\boldsymbol{G}^{(l)}\mathcal{C}\right)_j^T \tag{4.32}$$

Again, we have $i, j \in \{\Re, \Im\}$. We set the parameter $\kappa = 0$ for the calculations of $\boldsymbol{V}_{\boldsymbol{h},\boldsymbol{h}}, \boldsymbol{B}_{\boldsymbol{h},\boldsymbol{h}}, \boldsymbol{F}_{\boldsymbol{h},\boldsymbol{h}}, \boldsymbol{T}_{\boldsymbol{h},\boldsymbol{h}}$, while it is set to $\kappa = 1$ otherwise, *e.g.*, $\boldsymbol{V}_{\hat{\boldsymbol{h}},\hat{\boldsymbol{h}}}, \boldsymbol{V}_{\hat{\boldsymbol{h}},\boldsymbol{h}}$, *etc.* Regarding the needed channel correlation matrices, we write:

$$\boldsymbol{R}_{\hat{h}_{l,i}h_{l,j}} = \boldsymbol{\mathcal{W}}_{l,i}^T E\left[\boldsymbol{\mathcal{Y}}_{\Omega_{est}}\boldsymbol{h}_{l,j}^T\right] \tag{4.33}$$

$$\boldsymbol{R}_{\hat{h}_{l,i}\hat{h}_{l,j}} = \boldsymbol{\mathcal{W}}_{l,i}^T E\left[\boldsymbol{\mathcal{Y}}_{\Omega_{est}}\boldsymbol{\mathcal{Y}}_{\Omega_{est}}^T\right] \boldsymbol{\mathcal{W}}_{l,j} \tag{4.34}$$

$$\boldsymbol{R}_{h_{l,i}\hat{h}_{l,j}} = E\left[\boldsymbol{\mathcal{Y}}_{\Omega_{est}}\boldsymbol{h}_{l,i}^T\right]^T \boldsymbol{\mathcal{W}}_{l,j} \tag{4.35}$$

Knowing that $E\left[\boldsymbol{\mathcal{Y}}_{\Omega_{est}}\boldsymbol{h}_{l,j}^T\right] = \begin{bmatrix} E\left[\boldsymbol{y}_\Re(\Omega_{est})\boldsymbol{h}_{l,j}^T\right] \\ E\left[\boldsymbol{y}_\Im(\Omega_{est})\boldsymbol{h}_{l,j}^T\right] \end{bmatrix}$, we calculate these sub-matrices by taking the Ω_{est} rows of:

$$E\left[\boldsymbol{y}_\Re\boldsymbol{h}_{l,\Re}^T\right] = \left(\left(\boldsymbol{Q}^H\right)_\Re \boldsymbol{S}_{l,p,\Re} - \left(\boldsymbol{Q}^H\right)_\Im \boldsymbol{S}_{l,p,\Im}\right) \boldsymbol{R}_{h_l} \tag{4.36}$$

$$E\left[\boldsymbol{y}_\Re\boldsymbol{h}_{l,\Im}^T\right] = \left(-\left(\boldsymbol{Q}^H\right)_\Re \boldsymbol{S}_{l,p,\Im} - \left(\boldsymbol{Q}^H\right)_\Im \boldsymbol{S}_{l,p,\Re}\right) \boldsymbol{R}_{h_l} \tag{4.37}$$

$$E\left[\boldsymbol{y}_\Im\boldsymbol{h}_{l,\Re}^T\right] = \left(\left(\boldsymbol{Q}^H\right)_\Re \boldsymbol{S}_{l,p,\Im} + \left(\boldsymbol{Q}^H\right)_\Im \boldsymbol{S}_{l,p,\Re}\right) \boldsymbol{R}_{h_l} \tag{4.38}$$

$$E\left[\boldsymbol{y}_\Im\boldsymbol{h}_{l,\Im}^T\right] = \left(\left(\boldsymbol{Q}^H\right)_\Re \boldsymbol{S}_{l,p,\Re} - \left(\boldsymbol{Q}^H\right)_\Im \boldsymbol{S}_{l,p,\Im}\right) \boldsymbol{R}_{h_l} \tag{4.39}$$

where $\boldsymbol{S}_{l,p} = diag\left(\boldsymbol{G}^{(l)}\boldsymbol{\mathcal{C}}\boldsymbol{x}_p\right)$.

The additional complexity that our equalizer has compared to the LMMSE equalizers that do not exploit ECM, *e.g.*, [113], is represented in calculating the error matrix $E\left[\boldsymbol{\mathcal{E}}\boldsymbol{x}\boldsymbol{x}^T\boldsymbol{\mathcal{E}}^T\right]$, which comes from Equation (4.17). The computation of this matrix is explained in details in Equations (4.19-4.39). However, some high mobility environments have specified trajectories, such as in the high speed railways case. This fact means that channel statistics could be similar each time the train passes through the same location. As a result, the ECM matrix of Equation (4.19) could be calculated offline for different channel statistics and stored in a database. Hence, our proposed equalizer will not add any additional online complexity compared with the work of [113].

4.5 Simulations

In this section, we simulate the numerical performance of the proposed LMMSE equalizer by conducting 2000 Monte Carlo repetitions, and we present achieved improvements in terms of bit error rate. The performance improvements of our proposed technique are compared with other techniques that do not consider channel estimation errors. We compare also with the one tap equalizer and its iterative scheme of [113] where we consider 4 iterations in addition to considering the case of perfect channel knowledge at the receiver. We adopt Jakes Doppler spectrum model and a VehicularA [115] power delay profile with a carrier frequency of 5 GHz and a subcarrier spacing of 15 kHz. An FBMC-OQAM system with PHYDYAS prototype filter of an overlapping factor of 4 is adopted. We transmit 16 symbols in time domain with 16 subcarriers each and we consider a 4QAM constellation scheme, *i.e.*, 2PAM for FBMC-OQAM systems. Regarding channel estimation, we adopt a scattered pilot pattern with pilot spacing of 4 symbols in frequency domain and 4 symbols in time domain, and we use 1 auxiliary pilot for each pilot to cancel interference coming from surrounding 8 data symbols. We consider Ω_{est} to refer to all data and pilot symbols.

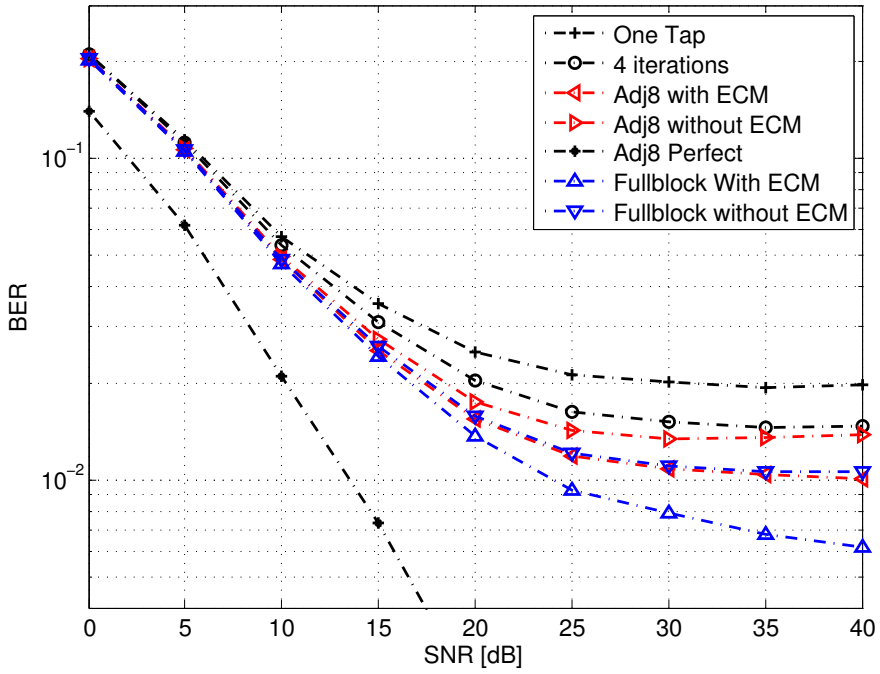

Figure 4.1: BER performance of the efficient equalizer versus SNR and under speed of 350 [km/h].

In Figure 4.1, we present the BER performance versus SNR for a fixed mobile speed of 350 [km/h]. We consider different sets of Ω_i *i.e.* the closest 8 symbols and the full block case. In addition, we consider the perfect channel scenario. We can see the attained improvements accompanied with each case. *e.g.*, the performance

of our technique that considers Ω_i with adjacent 8 symbols *i.e.*, 8-tap equalizer, is similar to that which does not use the ECM and considers the full block case.

In Figure 4.2, we present the BER performance versus different terminal speed values ranging from 0 to 500 [km/h]. We consider a fixed SNR value of 25 dB. Again, we can note the accompanied improvements of our proposed technique that considers the ECM within the design of the LMMSE equalizer. We note that as the speed increases, the performance gap increases between our efficient LMMSE equalizer and the one that does not use consider the channel estimation errors within its design.

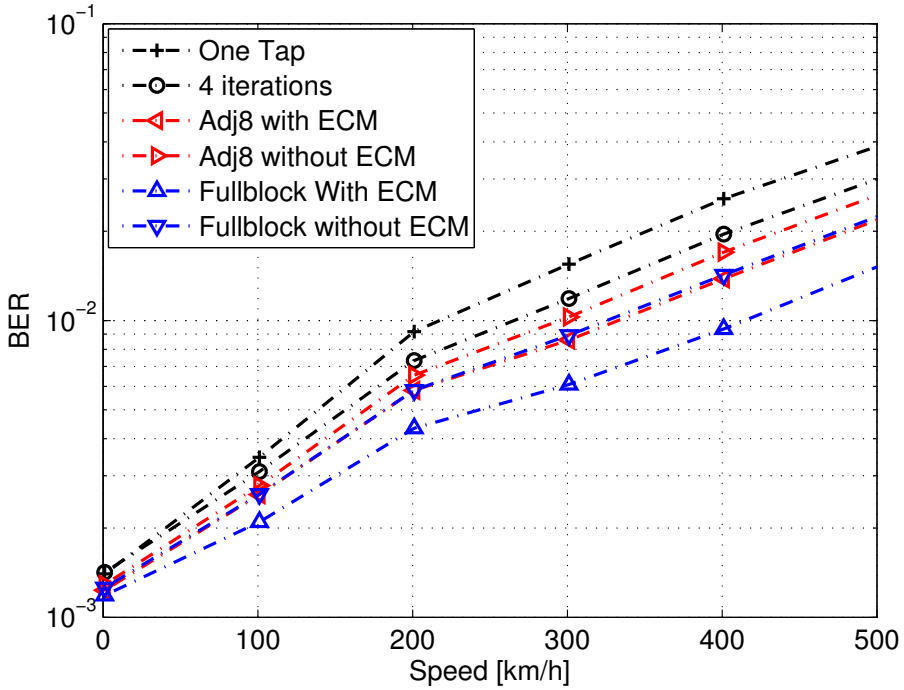

Figure 4.2: BER performance of the efficient equalizer versus speed under SNR value of 25 dB.

4.6 Conclusion

In this chapter, we have proposed an efficient LMMSE equalizer for FBMC-OQAM while considering the channel estimation errors. The proposed equalizer uses the covariance matrices developed for the LMMSE estimator, thus avoiding unnecessary additional complexity. The achieved efficiency could be viewed in terms of superior performance accuracy for same allocated power or in terms of power efficiency and less power offset at auxiliary pilots for the same performance accuracy. In addition, we have shown that in special scenarios, such as in trains, exploiting channel estimation errors in our technique will not add additional online complexity while having superior performance. We have presented a mathemat-

ical analysis for the aforementioned study and conducted a numerical analysis via Monte Carlo simulations. The achieved enhancements have been compared with state of art LMMSE equalizers that do not use the channel estimation errors within their design. In future works, we plan to exploit the developed technique within the design of joint iterative channel estimation and detection schemes for the FBMC-OQAM waveform.

Chapter 5

MCM based NOMA

5.1 Introduction

Till now, we have handled the Multi-Carrier Modulation enabling technology. We have analyzed the performance of different MCM schemes in different scenarios. The FBMC-OQAM waveform has gained a major portion of our study due to its outstanding frequency localization and high spectral efficiency. In this chapter, we consider another major player of future wireless communication systems, the non-orthogonal multiple access technology. Unlike the conventional Orthogonal Multiple Access (OMA) schemes, NOMA serves multiple users at the same time and frequency resources. This yields higher overall data rate at the cost of additional interference components. The main contributions of this chapter could be summarized as the study of different MCM-based NOMA combinations where we end up highlighting the FBMC based NOMA scheme. In addition, we handle the interference issue by proposing an efficient inter-user and intra-user iterative interference cancellation scheme.

This chapter is organized as follows. In Section 5.2, we start by presenting the NOMA technique and we go through its work principles. We then conduct a literature study where the NOMA advantages over the conventional OMA technology are emphasized. In Section 5.3, we give a general mathematical model while taking the MCM technique into consideration. This will allow for later development and analysis of different MCM-based NOMA technologies. Section 5.4 is devoted to the first contribution of the chapter which could be summarized as the comparison of the MCM-based NOMA technique with the corresponding MCM-based OMA technology. This is done in doubly selective channel scenario. The study shows the MCM-based NOMA accompanied advantages in terms of the overall sum-rate metric. In Section 5.5, we present the second main contribution of this chapter where we propose a joint iterative inter-user and intra-user interference cancellation scheme. In other words, we handle both NOMA induced interference (inter-user interference), which is caused by the imperfect Successive Interference

Cancellation (SIC) scheme, and the non-diagonality of the STM induced interference (intra-user interference). Numerical simulations show the effectiveness of the proposal compared with the perfect SIC case. In Section 5.5, we conclude the chapter and we propose some perspectives.

5.2 Multi-Carrier Modulation Based Non-Orthogonal Multiple Access technology

The NOMA technique has been recognized as the potential multiple access scheme for future communication systems [116]. By virtue of exploiting the power domain, NOMA can serve multiple users at the same time, frequency, and code resources, yielding higher spectral efficiency. The implementation of NOMA communications system involves two major processes, namely, Superposition Coding (SC) and Successive Interference Cancellation (SIC) at the base station and users terminals [117], respectively. NOMA users are distinguished according to their channel status, wherein users are allocated with portion of power inversely proportional to their channel condition. To decode their own messages, NOMA users suppress the information messages of all weaker users, while considering the information of the stronger users as interference.

In the literature, different studies have been conducted to present the advantages carried out by the NOMA technique over the traditional OMA one. This has been proven in terms of user fairness [118], multi-user capacity [119], and cell-edge user rate [120]. Furthermore, it has been shown that combining NOMA with MIMO technology could provide even higher diversity order [121], better sum rate [122] and enhanced outage behaviour [123] when compared to MIMO based OMA systems.

Most of the aforementioned studies have considered the Perfect SIC (PSIC) assumption. PSIC means that an accurate knowledge of all weaker users information messages is available at the each user's terminal. However, this assumption is not practical as it implies that the user should perfectly estimate the amplitude of all weaker users waveform [124]. Few literature studies have evaluated the overall performance of the imperfect SIC combined with the MCM technology. In [125], the architecture of imperfect SIC receiver for NOMA system combined with Orthogonal Frequency Division Multiple Access (OFDMA) waveform is investigated. Sum rate maximization problem in MCM-Based NOMA is tackled in [126], by proposing a three-step joint allocation strategy. Whereas, the authors in [127] propose an efficient power allocation scheme for an uplink MCM-Based NOMA system.

In this chapter, we consider a general MCM-based NOMA model based on which we propose two main contributions. First, we evaluate the achieved advantages of different MCM-based NOMA techniques in terms of the sumrate metric.

This is done while taking the MCM and the doubly selective channel induced interference into considerations. Second, we present a joint iterative interference cancellation scheme that will cancel both the Imperfect SIC induced interference and the one caused by the different MCM techniques and the doubly selectivity nature of the wireless channel.

5.3 System Model

We consider a downlink NOMA cellular system, wherein a base station is communicating with two users at the center (strong user) and the edge (weak user) of the cell. In MCM-based NOMA techniques, the transmitted super-positioned message at the m^{th} subcarrier and the k^{th} time domain symbol is written as follows:

$$x_{m,k} = \sqrt{\alpha} d_{edge,m,k} + \sqrt{1-\alpha} d_{center,m,k} \tag{5.1}$$

$d_{edge,m,k}, d_{center,m,k} \in \mathbb{C}$ are the symbols transmitted at the m^{th} subcarrier and the k^{th} time symbol of the edge and the center users, respectively. α is the power allocation factor of the NOMA edge user. By allocating $1-\alpha$ power to the center user, we assure a normalized transmitted power $E\left[|x_{m,k}|^2\right] = 1$. $d_{m,k} \in \mathbb{R}$ is the possible special case *e.g.*, PAM.

At the receiver, the demodulated signal $\boldsymbol{y}_u$ at the users terminals can be written as follows

$$\boldsymbol{y}_{\mathfrak{u}} = \underbrace{\boldsymbol{Q}^H \boldsymbol{H}_{\mathfrak{u}} \boldsymbol{G}}_{\mathcal{D}_{\mathfrak{u}}} \boldsymbol{x} + \boldsymbol{Q}^H \boldsymbol{\eta}_{\mathfrak{u}} \tag{5.2}$$

where $\mathfrak{u} \in \{\text{center, edge}\}$ indicates the user we are dealing with. $\boldsymbol{H}_u \in \mathbb{C}^{N \times N}$ is the time variant channel convolution matrix at user $\mathfrak{u}$. $\boldsymbol{Q} \in \mathbb{C}^{N \times MK}$ represents the multi-carrier demodulation matrix. $\boldsymbol{G} \in \mathbb{C}^{N \times MK}$ is the multi-carrier modulation matrix. $\mathcal{D}_u$ is the resulting STM at user $\mathfrak{u}$. $\boldsymbol{\eta} \in \mathbb{C}^{N \times 1}$ is the additive white Gaussian noise.

At the center user, SIC is performed in two steps. First, edge user data $\boldsymbol{d}_{\{EatC\}}$ is detected while considering the center user signal as interference.

$$\hat{\boldsymbol{d}}_{\{EatC\}} = \mathcal{M}\left(\frac{1}{\sqrt{\alpha}} \boldsymbol{A}^H_{\{EatC\}} \boldsymbol{y}_{center}\right) \tag{5.3}$$

where $\boldsymbol{A}_{\{EatC\}}$ denotes the adopted equalizer that estimates edge user data at center user. $\mathcal{M}()$ is the nearest neighbor symbol detection method. Second, detected edge user data $\hat{\boldsymbol{d}}_{\{EatC\}}$ will be removed from the received signal at the center user $\boldsymbol{y}_{\text{center}}$. This allows the detection of center user data at the center user $\boldsymbol{d}_{\{CatC\}}$ as follows:

$$\hat{\boldsymbol{d}}_{\{CatC\}} = \mathcal{M}\left(\frac{1}{\sqrt{1-\alpha}} \boldsymbol{A}^H_{\{CatC\}} \left(\boldsymbol{y}_{center} - \mathcal{D}\sqrt{\alpha}\hat{\boldsymbol{d}}_{\{EatC\}}\right)\right) \tag{5.4}$$

$\boldsymbol{A}_{\{CatC\}}$ represents the equalizer used to estimate center user data at the center user.

At the edge user, center user data will be ignored and treated as interference. Hence, edge user data $\boldsymbol{d}_{\{EatE\}}$ will be detected directly as follows:

$$\hat{\boldsymbol{d}}_{\{EatE\}} = \mathcal{M}\left(\frac{1}{\sqrt{\alpha}}\boldsymbol{A}^{H}_{\{EatE\}}\boldsymbol{y}_{edge}\right) \tag{5.5}$$

where $\boldsymbol{A}_{\{EatE\}}$ is the equalizer used to estimate edge user data at the edge user.

5.4 On the Sum Rate

In this section, we analyze the multi-carrier modulation technology combined with both non-orthogonal multiple access and the conventional orthogonal multiple access technologies. MCM-based NOMA and MCM-based OMA systems are compared in terms of the total sum rate in doubly selective channel where an analytical development is presented. In order to perform fair comparisons, we take into consideration all the different parameters among the MCM techniques, in addition to the distinct resource allocation in both NOMA and OMA systems. Furthermore, the performance of both MCM-based NOMA and MCM-based OMA systems is analyzed at different speeds. The sum rate, which represents the overall data rate achieved in both edge and center users, is written as follows:

$$R_{\text{sum}} = R_{edge} + R_{center} \tag{5.6}$$

where R_{edge} and R_{center} express the achieved data rate of the edge and the center users, respectively. These data rates are calculated differently in the NOMA and OMA cases. The fact that FBMC-OQAM uses the real part of the received signal only requires special treatment. In what follows, we handle each of these cases independently before evaluating and comparing their sum rate performance.

5.4.1 NOMA Case

In the NOMA case, the achieved data rate at user $u \in \{\text{edge, center}\}$ is given as follows

$$R_{\text{u}} = \gamma\beta\frac{MK}{KT}\log_2\left(1 + \text{SINR}_{\text{u}}\right) \tag{5.7}$$

where SINR_{u} is taken at one symbol that is situated in the middle of the resource grid. This assures considering the effects of all surrounding interference components. By multiplying with MK, we get the data rate of the whole resource grid where we assume that all time frequency positions has the same data rate. In addition, this implies the fact that, in NOMA, users share the same MK time and frequency resources. In complex constellation based waveforms, *e.g.*, OFDM,

WOLA, F-OFDM, we give $\gamma = 1$, while in real constellation based waveforms, FBMC-OQAM, $\gamma = 1/2$. In addition, we should mention that the noise power in one FBMC-OQAM symbol is half that of one OFDM, WOLA, or F-OFDM symbol.

$$P_n^{FBMC} = \frac{1}{2} P_n^{\text{OFDM,WOLA,F-OFDM}} \tag{5.8}$$

In order to calculate the SINR of the i^{th} symbol, we start by writing the i^{th} row of the corresponding STM as follows

$$\mathcal{D}_{\text{u}}(i,:) = \boldsymbol{Q}^H(:,i)\boldsymbol{H}_{\text{u}}\boldsymbol{G} = \left(\boldsymbol{G}^H \sum_{l=0}^{L-1} diag\left(\boldsymbol{Q}^{(l)}(:,i)\right) \boldsymbol{h}_{\text{u},l}^H \right)^H \tag{5.9}$$

where

$$\boldsymbol{Q}^{(l)}(:,n) = \begin{cases} \boldsymbol{Q}(:,n-l), & 0 \leq n-l < N \\ 0, & otherwise \end{cases} \tag{5.10}$$

Using Equation (5.9), we can calculate the covariance matrix of the STM i^{th} row $\nabla_{\text{u}} = E\left[\mathcal{D}_{\text{u}}(i,:)^H \mathcal{D}_{\text{u}}(i,:)\right]$ as follows:

$$\nabla_{\text{u}} = \boldsymbol{G}^H \left(\sum_{l=0}^{L-1} \boldsymbol{R}_{q_l} \odot \boldsymbol{R}_{h_l}^{\text{u}} \right) \boldsymbol{G} \tag{5.11}$$

where

$$\boldsymbol{R}_{q_l} = \boldsymbol{Q}^{(l)}(:,i)\boldsymbol{Q}^{(l)}(:,i)^H \tag{5.12}$$

At the edge user

In order to calculate the SINR at the edge user, we need to calculate the power of the useful signal P_{useful}, the power of the intra-user interference P_{intra} , and the power of the inter-user interference P_{inter}

$$P_{\text{useful}} = \alpha \boldsymbol{\nabla}_{\text{edge}}(i,i) \tag{5.13}$$

$$P_{\text{intra}} = \alpha\big(tr\{\boldsymbol{\nabla}_{\text{edge}}\} - \boldsymbol{\nabla}_{\text{edge}}(i,i)\big) \tag{5.14}$$

$$P_{\text{inter}} = (1-\alpha) tr\{\boldsymbol{\nabla}_{\text{edge}}\} \tag{5.15}$$

Hence

$$\text{SINR}_{\text{edge}} = \frac{P_{\text{useful}}}{P_{\text{intra}} + P_{\text{inter}} + P_n} \tag{5.16}$$

At the center user

At the center user, the SIC process is implemented. By assuming a perfect SIC, the inter-user interference component will be deleted. This allows us to write the

corresponding SINR as follows:

$$\mathrm{SINR}_{\mathrm{center}} = \frac{P_{\mathrm{useful}}}{P_{\mathrm{intra}} + P_n} \tag{5.17}$$

where

$$P_{\mathrm{useful}} = (1-\alpha)\boldsymbol{\nabla}_{\mathrm{center}}(i,i) \tag{5.18}$$

$$P_{\mathrm{intra}} = (1-\alpha)\big(tr\{\boldsymbol{\nabla}_{\mathrm{center}}\} - \boldsymbol{\nabla}_{\mathrm{center}}(i,i)\big) \tag{5.19}$$

5.4.2 OMA Case

In the OMA case, users do not share the same time and frequency resources. By assuming fair distribution of resources among users, the edge and center users will have access to $MK/2$ resources each. Hence, we write the bit rate $R_{\mathfrak{u}}^{OMA}$ at user $\mathfrak{u}$ as follows:

$$R_{\mathfrak{u}}^{OMA} = \gamma \frac{MK}{2KT} \log_2\left(1 + \mathrm{SINR}_{\mathfrak{u}}^{\mathrm{OMA}}\right) \tag{5.20}$$

It should be noted that $\mathrm{SINR}_{\mathfrak{u}}^{\mathrm{OMA}} = 2\,\mathrm{SINR}_{\mathfrak{u}}^{\mathrm{NOMA}}$. This is due to the fact that $P_n^{\mathrm{OMA}} = (1/2)P_n^{\mathrm{NOMA}}$

5.4.3 FBMC-OQAM Based (N)OMA Case

In FBMC-OQAM, the useful signal resides the real part while the imaginary component represents a built-in interference and should be eliminated. Hence, to well calculate the corresponding SINR values, a phase compensation step has be to done. To do that, we perform a matrix decomposition of the covariance matrix $\boldsymbol{\nabla}_{\mathfrak{u}}$, as in [58]:

$$\boldsymbol{\nabla}_{\mathfrak{u}} = \boldsymbol{\Omega}_{\mathfrak{u}}\boldsymbol{\Omega}_{\mathfrak{u}}^H \tag{5.21}$$

Afterward, we conduct a phase compensation process regarding the i^{th} desired symbol, which is represented by the i^{th} row of $\boldsymbol{\Omega}_{\mathfrak{u}}$, hence we write:

$$\tilde{\boldsymbol{\Omega}}_{\mathfrak{u}}(j,u) = \boldsymbol{\Omega}_{\mathfrak{u}}(j,u)e^{-j\phi_{i,u}} \tag{5.22}$$

where $\phi_{i,u}$ is the phase component of the (i,u) element in $\Omega_{\mathfrak{u}}$. The FBMC-OQAM power matrix of the i^{th} symbol could be written as:

$$\tilde{\boldsymbol{\nabla}}_{\mathfrak{u}} = \Re\{\tilde{\boldsymbol{\Omega}}_{\mathfrak{u}}\}\Re\{\tilde{\boldsymbol{\Omega}}_{\mathfrak{u}}\}^T \tag{5.23}$$

After that, the same calculations of Equations (5.13-5.20) regarding the NOMA and OMA cases are implemented but by using $\tilde{\boldsymbol{\nabla}}_{\mathfrak{u}}$ instead of $\boldsymbol{\nabla}_{\mathfrak{u}}$.

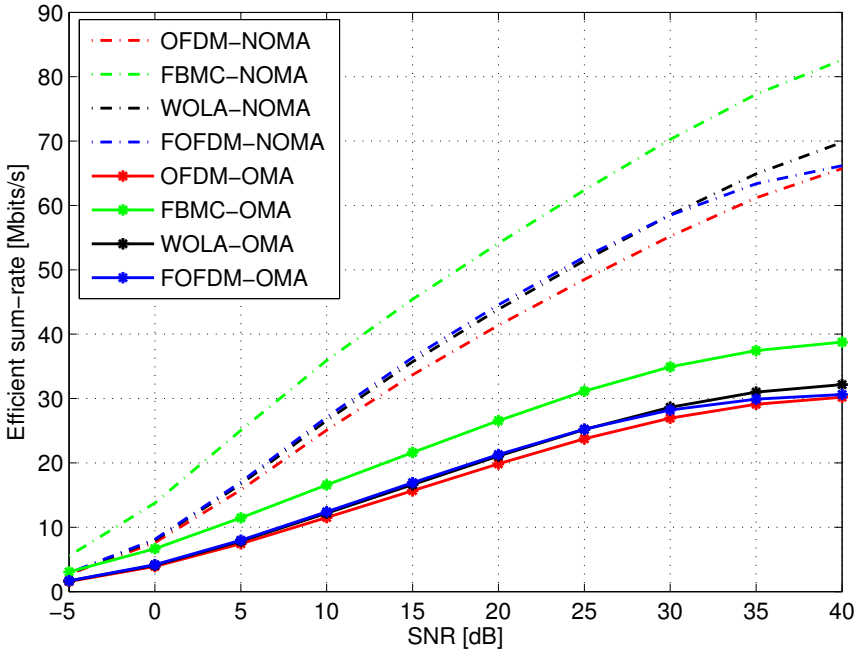

Figure 5.1: Efficient Sum Rate vs SNR of different MCM-based (N)OMA

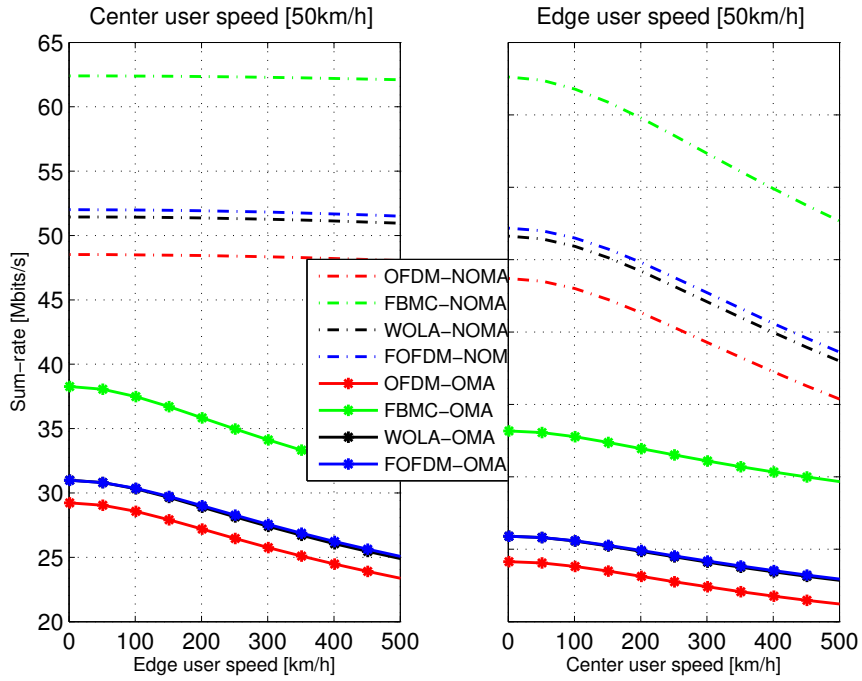

Figure 5.2: Sum Rate over edge user / center user speeds with fixed center/edge user speed of 50 [km/h] and an SNR value of 25 dB

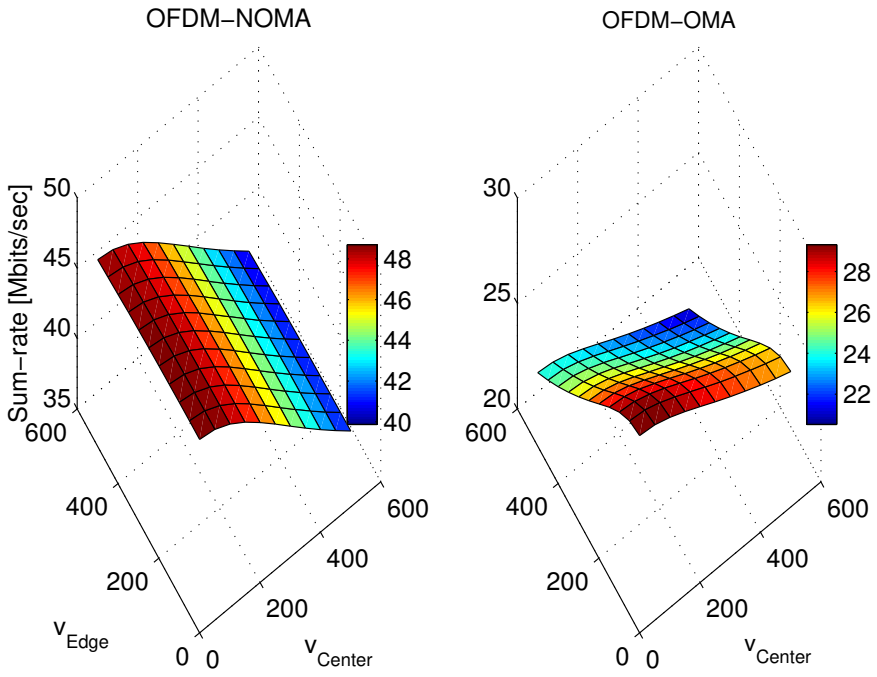

Figure 5.3: 3D plot of OFDM-(N)OMA sumrate over user terminals speeds

5.4.4 Numerical Simulations

To evaluate the sum rate of the different MCM techniques, we start by reconsidering the plotted power spectral density of Figure 2.5. We noted that for a given bandwidth of 5 MHz at 2.5 GHz, and a subcarrier spacing of 15 kHz, the CP-OFDM used only 300 subcarriers. FBMC-OQAM used 331 subcarriers, 324 subcarriers for F-OFDM while WOLA needed 318 subcarriers. That was for an OOB emission threshold of -25 dB. Using the MCM settings of table 5.1, we consider a NOMA power allocation factor of $\alpha = 0.7$ and a doubly selective channel with Vehicular-A power delay profile and Jakes Doppler spectrum model.

	CP-OFDM	WOLA	F-OFDM	FBMC
Nr. Subcarriers	300	318	324	331
Nr. Symbols	14	14	14	30
TF	1.07	1.07	1.07	1
Constellation	4-QAM	4-QAM	4-QAM	2-PAM
Filtering / Windowing	sinc	Raised Cosine [59]	Soft-truncated sinc [57]	Hermite [58]

Table 5.1: MCM-based NOMA simulation parameters for sumrate evaluation

In Figure 5.1, we plot the efficient sumrate versus SNR. This happens for

the different MCM-based NOMA techniques and their corresponding MCM-based OMA ones. By efficient sum rate, we mean that the data rate of the edge and center user in Equation (5.6) are multiplied with the success rate $\big(1 - \text{BER}\big)$.

$$R_{\text{sum}}^{\text{Efficient}} = (1 - BER_{\text{edge}})\, R_{\text{edge}} + (1 - BER_{\text{center}})\, R_{\text{center}} \tag{5.24}$$

In our efficient sum rate definition, we consider the BER in the place of frame error rate [7] for simulations simplicity. We conduct 500 Monte-Carlo repetitions where we assume a perfect SIC and we use a one tap equalizer at both center and edge users. From the resulting Figure 5.1, we can note the accompanied gains of the NOMA technique compared with the OMA case. In addition, we see how in both cases, FBMC-OQAM can deliver higher sum rates than other MCM waveforms. This Figure has been drawn under a center user speed of $v_{center} = 50\,[km/h]$ and an edge user speed of $v_{edge} = 100\,[km/h]$.

In Figure 5.2, we present the sum rate variations against edge and center users mobility and at a fixed SNR value of 25 dB. We can remark the robustness of the NOMA technique to the edge user mobility. This could be rendered to the fact that inter-user interference in NOMA is dominant over the intra-user interference component in Equation (5.16).

To better visualize this fact, we consider the NOMA and OMA cases of the OFDM waveform only and we draw 3D plot in Figure 5.3 to show their sum rate robustness against edge and center users mobility. While OMA sensitivity to edge and center user mobility is almost equal, it is clear how NOMA technique presents high robustness to the edge user mobility.

5.5 Joint Iterative Inter-User and Intra-User Interference Cancellation

In the previous section, we have assumed a perfect SIC implementation at the center user where we evaluated the accompanied MCM-based NOMA gains. However, this is not practical since it requires the center user to have perfect knowledge of the edge user data. In fact, the center user has to start by decoding edge user data to use it after in the SIC process, where a residual interference component is expected. In this section, we treat the imperfect SIC case and we evaluate the performance of NOMA combined with different MCM techniques in doubly selective wireless channel. In addition, we propose a novel joint iterative interference cancellation scheme that cancels both the NOMA induced inter-user interference and the MCM and the doubly selective channel induced intra-user interference. The performance of the proposed algorithm is evaluated with different design parameters and channel scenarios. Using numerical simulations, the algorithm proves to perform close to the PSIC case while maintaining fast convergence rate, hence low complexity.

5.5.1 The Proposed Algorithm

We have mentioned previously in Section 5.3, that SIC is implemented at the center user by first detecting edge user data through Equation (5.3). This happens by the use of the equalizer $\boldsymbol{A}_{EatC}$. Then the detected edge user data will be removed from the received signal to finally estimate center user data as done in Equation (5.4). This happens by using the equalizer $\boldsymbol{A}_{CatC}$.

A simple choice of the equalizers $\boldsymbol{A}_{EatC}$ and $\boldsymbol{A}_{CatC}$ is the one tap equalizer.

$$\boldsymbol{A}_{XatC}^{H} = diag(\mathcal{D}_{center})^{-1} \tag{5.25}$$

However, and as we explained previously, the STM in doubly selective channels and non-orthogonal MCM techniques becomes non-diagonal, hence, leading to poor performance of the one tap equalizer. In addition, the detection error of edge user data will propagate to the detection of center user data which deteriorates the performance even more. In this contribution, we build on the non-diagonal interference cancellation scheme of [113] to propose a joint iterative algorithm that cancels both inter-user and intra-user interference and that could be implemented for different MCM-based NOMA combinations.

Hence, we write the demodulated signal at the center user after the i^{th} iteration as follows:

$$\bar{\boldsymbol{y}}_{EatC}^{(i)} = \boldsymbol{y}_{\text{center}} - \underbrace{ndiag(\mathcal{D})\sqrt{\alpha}\hat{\boldsymbol{d}}_{edge}^{(i-1)}}_{\text{intra-user interference}} - \underbrace{\boldsymbol{\mathcal{D}}\sqrt{1-\alpha}\hat{\boldsymbol{d}}_{center}^{(i-1)}}_{\text{inter-user interference}} \tag{5.26}$$

where $\bar{\boldsymbol{y}}_{EatC}^{(i)}$ represents the result of the i^{th} iteration that will be used to detect edge user data, at the center user. In the Right-Hand Side (RHS) of Equation (5.26), the second and third terms represent the intra-user and inter-user interference cancellation components, respectively. From the second term, we note that the detected edge user data of the $(i-1)^{th}$ iteration will be used to cancel the non-diagonal induced interference. On the other hand, the third term shows that the detected center user data of the $(i-1)^{th}$ iteration will be used to cancel the interference caused by the NOMA scheme.

Afterward, the signal $\bar{\boldsymbol{y}}_{EatC}^{(i)}$ will be used to detect edge user data, as in Equation (5.3), which we re-write for the i^{th} iteration as follows:

$$\hat{\boldsymbol{d}}_{edge}^{(i)} = \mathcal{M}\left(\frac{1}{\sqrt{\alpha}} diag(\mathcal{D})^{-1}\bar{\boldsymbol{y}}_{EatC}^{(i)}\right) \tag{5.27}$$

After detecting $\hat{\boldsymbol{d}}_{edge}^{(i)}$, we remove edge user induced interference and the channel doubly selectivity induced interference from the demodulated signal $\boldsymbol{y}$

$$\bar{\boldsymbol{y}}_{CatC}^{(i)} = \boldsymbol{y} - \underbrace{ndiag(\mathcal{D})\sqrt{1-\alpha}\hat{\boldsymbol{d}}_{center}^{(i-1)}}_{\text{intra-user interference}} - \underbrace{\mathcal{D}\sqrt{\alpha}\hat{\boldsymbol{d}}_{edge}^{(i)}}_{\text{inter-user interference}} \tag{5.28}$$

$\bar{\boldsymbol{y}}_{CatC}^{(i)}$ represents the results of the i^{th} iteration that will be used to detect center user data, at the center user. In the right-hand side of Equation (5.28),the second term expresses the intra-user interference cancellation step with the use of the detected center user data of the $(i-1)^{th}$. The third RHS term expresses the inter-user interference cancellation step that uses the detected edge user data of the i^{th} iteration. Now, center user data is ready to be detected by the use of the following equation

$$\hat{\boldsymbol{d}}_{center}^{(i)} = \mathcal{M}\left(\frac{1}{\sqrt{1-\alpha}} diag(\mathcal{D})^{-1} \bar{\boldsymbol{y}}_{CatC}^{(i)}\right) \tag{5.29}$$

The proposed algorithm is summarized in Algorithm 1

Algorithm 1 Proposed iterative algorithm

{**Initial state (i=0)**}
1) Detect edge user data at center user using Equation (5.3)
2) Remove edge user induced interference from received signal and detect center user data using Equation (5.4)
{**Start the iteration process**}
for (i < Number of iterations) **do**
1) i++
2) Remove STM and center user induced interference from received signal using Equation (5.26)
3) Detect edge user data using Equation (5.27).
4) Remove STM and edge user induced interference from received signal using Equation (5.28)
5) Detect center user data using Equation (5.29).
end for

5.5.2 Numerical Simulations

In this section, we simulate the performance of the proposed joint iterative inter-user and intra-user interference cancellation algorithm. The algorithm is evaluated for different MCM-based NOMA systems. In other words, we consider all the aforementioned waveforms, CP-OFDM, WOLA, F-OFDM, and the FBMC-OQAM. We use a subcarrier spacing of 15 kHz and a carrier frequency of 2.5 GHz. We use the same simulations settings of Table 5.1, but for simulations simplicity we use 24 subcarriers only. We conduct Monte Carlo simulations with 1500 repetitions while adopting a channel model with Vehicular-A power delay profile and Jakes Doppler spectrum model. Unless stated otherwise, we consider a power allocation factor of $\alpha = 0.9$, an SNR value of 25 dB, 4 iterations of our proposed algorithm, and a center user speed of 200 [km/h].

Figure 5.4 plots the BER of our proposed algorithm versus different SNR values at the center user. Its performance is compared with the case where use the one

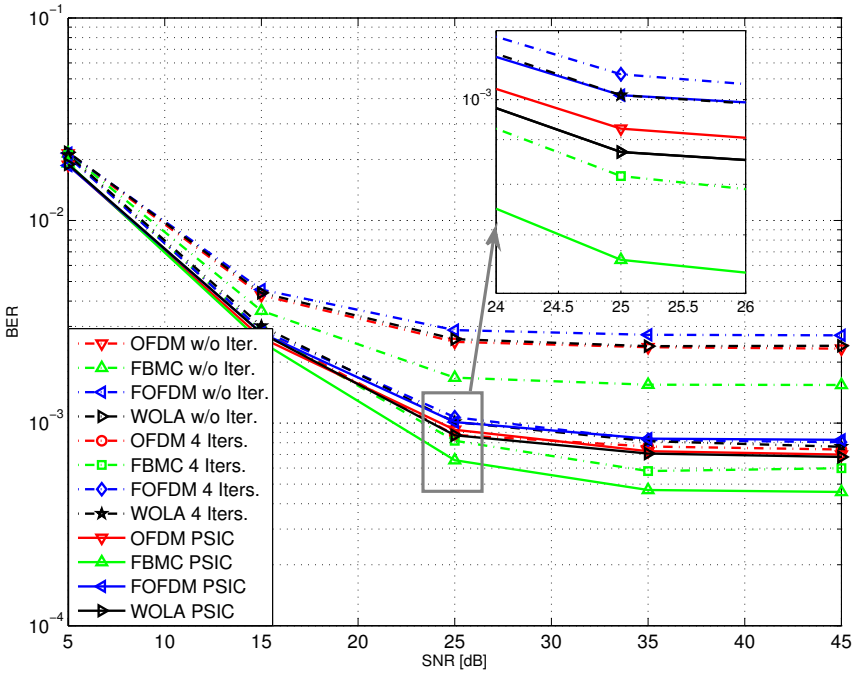

Figure 5.4: BER vs SNR with $\alpha = 0.9$ and center user speed of 200 [km/h] for different MCM-based NOMA techniques

tap equalizer without any iteration. In addition, we consider the PSIC case where we assume that edge user data are perfectly cancelled at the center user. We first note that the proposed algorithm has a small performance gap compared to the perfect SIC case while the gap is big with the no iteration case. In addition, one can notice that the algorithm works well for the different MCM techniques with FBMC-OQAM having the best performance.

In Figure 5.5, we evaluate the BER performance for different center user speed values while fixing the SNR to 25 dB. We can see that the proposed iterative algorithm still perform close to the perfect SIC case regardless of center user speed. We observe also that FBMC-OQAM has the worst performance at low speed values. Starting from about 100 [km/h], FBMC-OQAM outperforms the other studied MCM schemes.

Another advantage of the proposed iterative algorithm is its fast convergence. This fact is presented by Figure 5.6 where we can note that after 2 to 3 iterations the algorithm will converge for the all studied waveforms with FBMC-OQAM being the first to converge.

In Figure 5.7, we illustrate the BER performance versus different NOMA power allocation values. We note that for the adopted simulation parameters, the performance gap between our algorithm and the no iteration case is quite small for low values of α. Starting with a power allocation value of 0.7, the gap will start

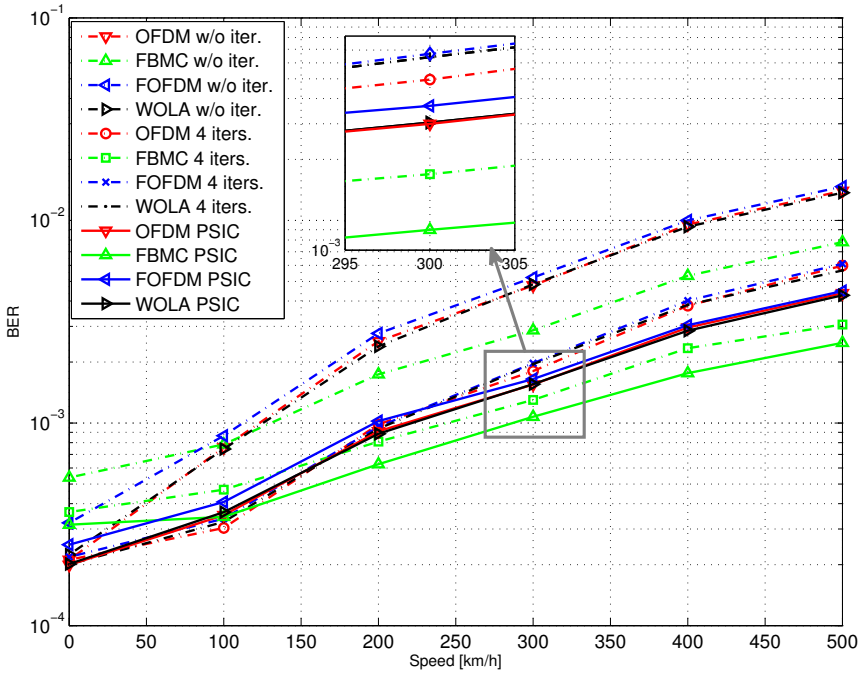

Figure 5.5: BER vs Speed with $\alpha = 0.9$ and SNR= 25 dB for different MCM-based NOMA techniques

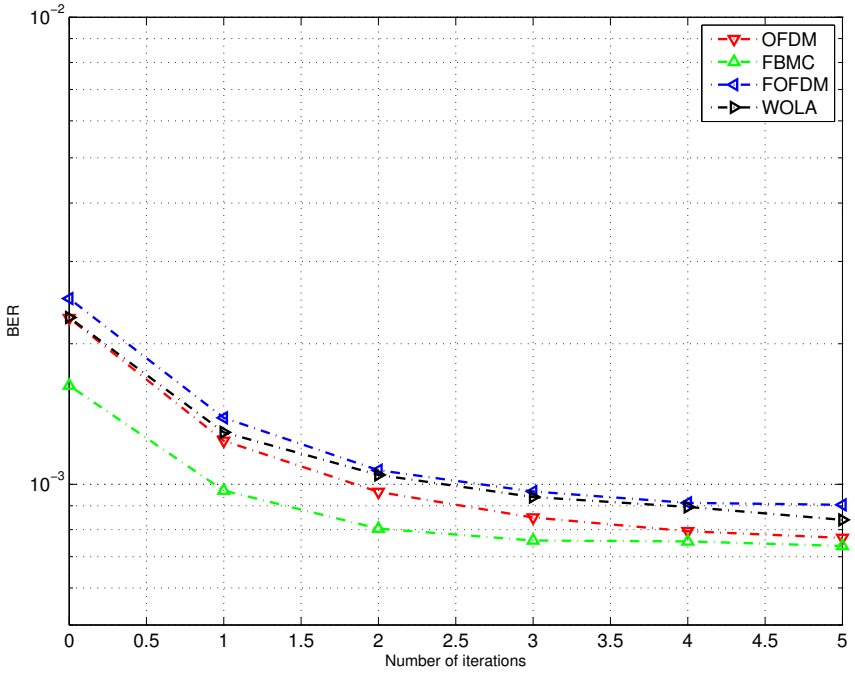

Figure 5.6: BER vs Number of iterations with $\alpha = 0.9$, SNR= 25 dB, and terminal speed of 200 [km/h] for different MCM-based NOMA techniques

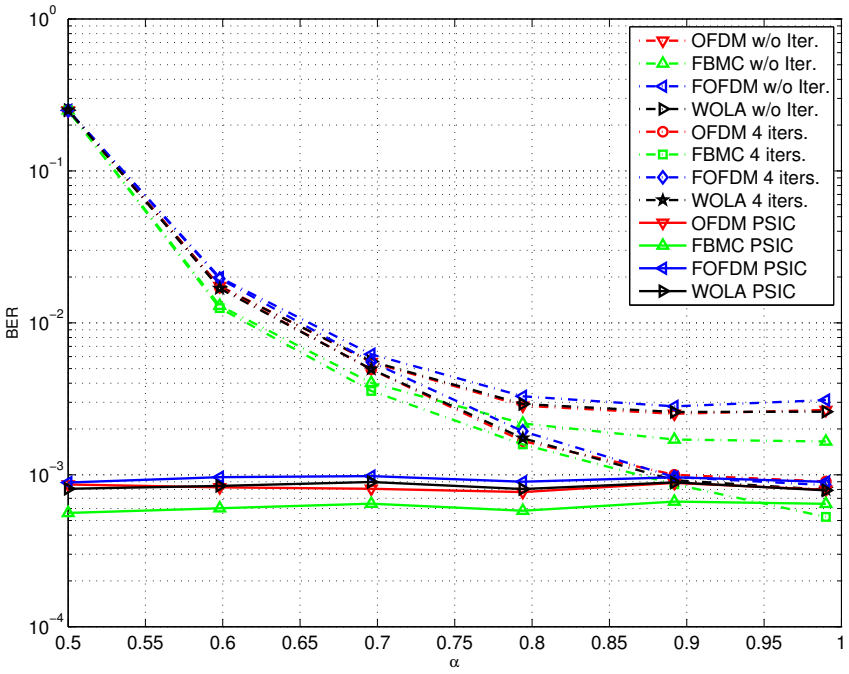

Figure 5.7: BER vs α with SNR= 25 dB and terminal speed of 200 [km/h] for different MCM-based NOMA techniques

increasing till the BER performance of the iterative technique reaches almost the same performance as that of the perfect SIC. This happens happens at around $\alpha = 0.94$. For $\alpha > 0.94$, we note that the proposed algorithm outperforms the PSIC case where this could be rendered to the embedded intra-user interference cancellation scheme that the proposed iterative technique has.

5.6 Conclusion

NOMA technique has forced itself as a critical enabling technology for future communication systems. Combined with the MCM technology, MCM-based NOMA systems could offer outstanding features from different perspectives, *e.g.*, frequency localization and spectral efficiency. In this chapter, we study the overall MCM-based NOMA system while considering different MCM technologies, namely the CP-OFDM, WOLA, F-OFDM and FBMC waveforms. Besides their advantages, NOMA suffers from inter-user interference. At the center user, this inter-user interference is removed by means of a successive interference cancellation scheme. In addition, the MCM technique has its own built-in interference added to its suffering from the doubly selectivity of the wireless channel. In this chapter, we started by investigating the accompanied advantages of MCM-based NOMA systems compared with the traditional MCM-based OMA ones. It was shown

that MCM-based NOMA system outperforms the MCM-based OMA system for all MCM techniques in terms of users sum rate. Moreover, the FBMC-NOMA combination has been proved to provide the highest sum rate at both high speed and low speed scenarios. However, we should insist that these gains come with the assumption of perfect SIC at the center user. In fact, this is not totally correct since edge user interference is not totally cancelled at the center user.

In the second contribution of this chapter, we considered the imperfect SIC case in addition to all other aforementioned sources of interference. Hence, we have proposed a joint iterative interference cancellation scheme that cancels both NOMA induced interference and the non-diagonal STM induced interference. The algorithm is developed with a general model so that it could be implemented with different MCM techniques. We proved through numerical simulations that the proposed algorithm performs closely to the perfect SIC case with high power allocation factors. Whereas it performs close to the one tap equalizer with low power allocation factors. In addition, the proposed algorithm has proved to have a fast convergence rate, thus leading to low computational complexity and low latency. Furthermore, we noted again that FBMC-OQAM based NOMA outperforms other MCM-based NOMA combinations in high speed scenarios.

Based on the presented results, future works include the proposal of adaptive receivers that can decide either to adopt or not the iterative mode. This could be based on the users channel conditions that will in-turn affect the power allocation values. For high power allocations, iterative mode shown to bring critical improvements while guarding the sample one tap equalizer is preferred for low power allocation values.

General Conclusions and Perspectives

Nowadays, the railway sector is witnessing an increasing demand on information exchange among railway stakeholders in order to support the various critical and non-critical applications and services. Hence, and in order to face the obsolescence of current railway communications systems *e.g.,* GSM-R, the idea of a railway adaptable communication system has emerged at a European level. To this end, different wireless communication technologies are supposed to cooperate to achieve the desirable key performance indicators. Recently, the wireless communication sector has witnessed various technological evolutions where many key enabling technologies have been proposed and studied for future 5G and Beyond communications systems. In this Ph.D, we have considered two key enabling technologies that could satisfy various needs of the railway sector, namely, the multi-carrier modulation and non-orthogonal multiple access technologies.

In what follows, we summarize the key topics discussed in this Ph.D thesis and we highlight our main contributions and conclusions. Thereafter, we present the possible perspectives that could be pursued.

Summary and Conclusions

In Chapter 1, we discussed the problematic, the context, and the motivations of this Ph.D. We started by giving a record of the railway communications needs. While the obsolete GSM-R system is still deployed in the railway sector, different industrial and academical research projects have been triggered in Europe and abroad to build an Adaptable Communication System for Railways. This system will be IP based and will support the cooperation between different technologies while being resilient to technological evaluations. To this end, we have presented different key enabling technologies that were proposed and analyzed within the framework of 5G and Beyond, and that could answer altogether the different railway needs. Among these technologies, we have presented the advantages of the Multi-Carrier Modulation and the Non-Orthogonal Multiple-Access technologies in terms of achieving an efficient utilization of the available spectrum and the

enhancement of the overall data exchange capacity.

In Chapter 2, we started by considering the Multi-Carrier Modulation technology where we provided the historical motivations and needs. Afterward, we explained the MCM working principles and we explore several MCM schemes by adopting a generalized system model. This allowed us to evaluate and compare different MCM schemes while considering a doubly selective channel scenario and an impulsive noise assumption that exist in high speed railway scenarios. The Filter-Bank Multi-Carrier Modulation technique shows high frequency localization and efficient spectrum utilization. In addition, simulations proved that FBMC-OQAM is robust against high mobility scenarios where it has superior performance compared to other studied MCM schemes. On the other hand, FBMC-OQAM performs relatively bad in low mobility scenarios. Also, we noted that MCM schemes perform closely after being impaired by the impulsive noise. The performance gap is restored after the use of IN blanking and clipping schemes.

These facts have urged us to conduct more analysis and comparisons on the doubly selective channel estimation aspect of different MCM schemes in general, and the FBMC-OQAM in particular. Thus, we started in Chapter 3 by generalizing the sliding window TD-LMMSE channel estimation technique so that it could be implemented on different MCM schemes. Besides, we developed the technique in order to exploit multi-paths and multi-antennas correlation, once they exist. Although this results in performance enhancements for the corresponding MCM schemes, the so called FBMC-OQAM was performing the worst. This is due to its built-in interference. Hence, we proposed an FBMC-OQAM channel estimation technique that, in contrast to others, it is able to exploit the power spread patterns of different FBMC-OQAM prototype filters. This offered performance enhancements while guarding low computational complexity, compared to other studies in the literature. Thereafter, we have used the developed FBMC-OQAM channel estimation concept within a more general framework while considering the equalization block. Hence, we have proposed in Chapter 4, and for the first time, an FBMC-OQAM equalizer that can exploit the channel estimation errors, thus giving superior performance accuracy. Also, we showed that in some scenarios, such as the high speed railway context, the proposed enhancements could come without additional computational complexity.

In addition to the different MCM techniques, the NOMA enabling technology has forced itself recently as key player in future wireless communications systems. In Chapter 5, we dealt with the overall MCM based NOMA system. We first evaluated the advantages of the MCM based NOMA technology compared to the traditional MCM based OMA. We conduct this study for different MCM technologies. The FBMC-OQAM based NOMA combination proved to bring enormous gains in terms of overall achieved data rate. We have also seen the MCM-based NOMA gains, in general, compared to the MCM based OMA systems. However, these gains where presented under assumption of the perfect cancellation of NOMA induced interference. In the second main contribution of Chapter 5, we propose

a joint iterative inter-user (NOMA induced) and intra-user (MCM and channel induced) interference cancellation scheme. We proved through numerical simulations that the proposed algorithm performs closely to the perfect SIC case with high power allocation factors. Whereas it performs close to the one tap equalizer with low power allocation factors. In addition, the proposed algorithm has proved to have a fast convergence rate, thus leading to low computational complexity and low latency.

Perspectives

In this section, we present our visions and perspectives for further questions and studies that still need to be developed and investigated.

- Although the Generalized sliding window TD-LMMSE technique has shown for improvements or different MCM techniques, it performed poorly with the FBMC-OQAM waveform. This is due to the fact that FBMC-QOAM has a built-in interference component. To this end, iterative interference cancellation schemes should be implemented and with SW TD-LMMSE to enhance its performance. Also, the transmitted pilot signal should go through an optimization process to minimize the interference coming from surrounding data symbols. This should be done while considering different FBMC-OQAM prototype filters.

- The proposed efficient LMMSE equalizer of Chapter 4 exploits the channel estimation errors and leads to performance improvements. This developed equalizer should be implemented in a joint iterative model where channel estimation errors and hard or soft detection errors will be exchanged iterativly to remove the residual error floor.

- In this Ph.D, we considered the LMMSE technique to realize different channel estimation and equalization schemes. A more realistic option of an environment such as the HSR is to consider an adaptive version of the LMMSE filter, the Kalman filter.

- We have assumed that channel statistics are perfectly known at the receiver. A natural development is to estimate needed channel statistics before the implementation of the LMMSE filter. Also, another option is to consider different filters that do not require channel statistics such as the Least Mean Square filter.

- In the NOMA technology, we have considered 2 users case. Further developments of our proposed techniques should consider the more general case of N users. Increasing the number of users affect the achieved gains. This should be evaluated while considering the MCM challenges also.

- The channel estimation aspect of MCM based NOMA system should be evaluated. The fact that different users are sharing the same time and frequency grids results in more degrees of freedoms where pilots knowledge should be shared between the different users. Different pilots patterns could be given to different users allowing to cover the whole resource grid and hence resulting in performance enhancements.

- Afterall, the evaluation of all proposed algorithms should be evaluated in impulsive noise scenario where different IN cancellations schemes could be considered.

- Finally, the hardware implementation on SDR cards of our developed techniques needs to be conducted. This will allow the potential measurements and verification of the performance accuracy of our proposed techniques in a railway environment.

Bibliography

[1] P. Fraga-Lamas, T. M. Fernández-Caramés, and L. Castedo, "Towards the internet of smart trains: A review on industrial iot-connected railways," in *Sensors*, 2017.

[2] FRMCS Functional Working Group, *Future Railway Mobile Communication System, User Requirements Specification, FU-7100*, January 2019.

[3] *UIC. Railway Mobile Communication System User Requirement. International Railway Union, Technical report, October 2010.*

[4] *ERA. Evolution of GSM-R - Final Report. European Railway Agency, Technical report, ERA/2014/04/ERTMS/OP, April 2015.*

[5] *FP7 NTGC Project http:// www.ngtc.eu.*

[6] J. Moreno, J. M. Riera, L. d. Haro, and C. Rodriguez, "A survey on future railway radio communications services: challenges and opportunities," *IEEE Communications Magazine*, vol. 53, no. 10, pp. 62–68, October 2015.

[7] L. Brunel, H. Bonneville, and A. Charaf, "Throughput performance of 3gpp lte system in railway environment," in *International Workshop on Communication Technologies for Vehicles*. Springer, 2017, pp. 60–71.

[8] R. He, B. Ai, G. Wang, K. Guan, Z. Zhong, A. F. Molisch, C. Briso-Rodriguez, and C. P. Oestges, "High-speed railway communications: From gsm-r to lte-r," *IEEE Vehicular Technology Magazine*, vol. 11, no. 3, pp. 49–58, 2016.

[9] B. Ai, K. Guan, M. Rupp, T. Kurner, X. Cheng, X.-F. Yin, Q. Wang, G.-Y. Ma, Y. Li, L. Xiong *et al.*, "Future railway services-oriented mobile communications network," *IEEE Communications Magazine*, vol. 53, no. 10, pp. 78–85, 2015.

[10] D. Mottier, "How 5g technologies could benefit to the railway sector: challenges and opportunities," in *Mitsubishi Electric R&D Centre Europe–France*, 2018.

[11] *https:// www.shift2rail.org.*

[12] *https://projects.shift2rail.org/s2r_ip2_n.aspx?p=X2RAIL-1*.

[13] *https://projects.shift2rail.org/s2r_ip2_n.aspx?p=X2RAIL-3*.

[14] U. Geier, M. Mikulandra, K. Kernstock, and B. Allen, "Adaptable communication system for all railways," 2019.

[15] *Shift2Rail Joint Undertaking. Multi-Annual Action Plan, Part-B, 20-05-2019.*

[16] "5gppp architecture working group, white paper: View on 5g architecture, december 2017," Tech. Rep.

[17] I. F. Akyildiz, S. Nie, S.-C. Lin, and M. Chandrasekaran, "5g roadmap: 10 key enabling technologies," *Computer Networks*, vol. 106, pp. 17–48, 2016.

[18] D. He, B. Ai, K. Guan, Z. Zhong, B. Hui, J. Kim, H. Chung, and I. Kim, "Channel measurement, simulation, and analysis for high-speed railway communications in 5g millimeter-wave band," *IEEE Transactions on Intelligent Transportation Systems*, vol. 19, no. 10, pp. 3144–3158, 2017.

[19] Y. Cui and X. Fang, "Performance analysis of massive spatial modulation mimo in high-speed railway," *IEEE Transactions on Vehicular Technology*, vol. 65, no. 11, pp. 8925–8932, 2016.

[20] *FP7 PHYDYAS Project. http://www.ict-phydyas.org*.

[21] *FP7 METIS 2020 Project https://www.metis2020.com*.

[22] *FP7 5GNOW Project, http://www.5gnow.eu/*.

[23] *FP7 EMPhAtiC Project, http://www.ict-emphatic.eu/*.

[24] M. Doelz, E. Heald, and D. Martin, "Binary data transmission techniques for linear systems," *Proceedings of the IRE*, vol. 45, no. 5, pp. 656–661, 1957.

[25] Y. Cai, Z. Qin, F. Cui, G. Y. Li, and J. A. McCann, "Modulation and multiple access for 5g networks," *IEEE Communications Surveys Tutorials*, vol. 20, no. 1, pp. 629–646, Firstquarter 2018.

[26] X. Zhang, W. Cheng, and H. Zhang, "Full-duplex transmission in phy and mac layers for 5g mobile wireless networks," *IEEE Wireless Communications*, vol. 22, no. 5, pp. 112–121, 2015.

[27] *F.C.C. 15-138, Notice Of Proposed Rulemaking, Use of Spectrum Bands Above 24 Ghz For Mobile Radio Services, 2015.*

[28] Z. Qingling and J. Li, "Rain attenuation in millimeter wave ranges," in *2006 7th International Symposium on Antennas, Propagation & EM Theory.* IEEE, 2006, pp. 1–4.

[29] M. Samimi, K. Wang, Y. Azar, G. N. Wong, R. Mayzus, H. Zhao, J. K. Schulz, S. Sun, F. Gutierrez Jr, and T. S. Rappaport, "28 ghz angle of arrival and angle of departure analysis for outdoor cellular communications using steerable beam antennas in new york city." in *VTC Spring*, 2013, pp. 1–6.

[30] T. S. Rappaport and S. Deng, "73 ghz wideband millimeter-wave foliage and ground reflection measurements and models," in *2015 IEEE International Conference on Communication Workshop (ICCW)*. IEEE, 2015, pp. 1238–1243.

[31] T. S. Rappaport, Y. Xing, G. R. MacCartney, A. F. Molisch, E. Mellios, and J. Zhang, "Overview of millimeter wave communications for fifth-generation (5g) wireless networks—with a focus on propagation models," *IEEE Transactions on Antennas and Propagation*, vol. 65, no. 12, pp. 6213–6230, Dec 2017.

[32] T. S. Rappaport, Y. Xing, O. Kanhere, S. Ju, A. Madanayake, S. Mandal, A. Alkhateeb, and G. C. Trichopoulos, "Wireless communications and applications above 100 ghz: Opportunities and challenges for 6g and beyond," *IEEE Access*, vol. 7, pp. 78 729–78 757, 2019.

[33] M. Shafi, J. Zhang, H. Tataria, A. F. Molisch, S. Sun, T. S. Rappaport, F. Tufvesson, S. Wu, and K. Kitao, "Microwave vs. millimeter-wave propagation channels: Key differences and impact on 5g cellular systems," *IEEE Communications Magazine*, vol. 56, no. 12, pp. 14–20, December 2018.

[34] T. L. Marzetta *et al.*, "Noncooperative cellular wireless with unlimited numbers of base station antennas," *IEEE Transactions on Wireless Communications*, vol. 9, no. 11, p. 3590, 2010.

[35] D. Ying, F. W. Vook, T. A. Thomas, and D. J. Love, "Hybrid structure in massive mimo: Achieving large sum rate with fewer rf chains," in *2015 IEEE International Conference on Communications (ICC)*. IEEE, 2015, pp. 2344–2349.

[36] K. Zheng, S. Ou, and X. Yin, "Massive mimo channel models: A survey," *International Journal of Antennas and Propagation*, vol. 2014, 2014.

[37] J. Mitola, G. Q. Maguire *et al.*, "Cognitive radio: making software radios more personal," *IEEE personal communications*, vol. 6, no. 4, pp. 13–18, 1999.

[38] S. Haykin, "Cognitive radio: brain-empowered wireless communications," *IEEE journal on selected areas in communications*, vol. 23, no. 2, pp. 201–220, 2005.

[39] A. Amanna, M. Gadnhiok, M. J. Price, J. H. Reed, W. P. Siriwongpairat, and T. K. Himsoon, "Railway cognitive radio," *IEEE Vehicular Technology Magazine*, vol. 5, no. 3, pp. 82–89, Sep. 2010.

[40] "Architecture générique de gestion des ressources et des protocoles associés, urban planing for radio communications, urc-sp1-d1,2,3, november 2017," Tech. Rep.

[41] "Multi-technology vehicular cooperative system based on software defined radio (sdr), 5th workshop on communication technologies for vehicles, nets4cars," 2013.

[42] K. Bouallegue, I. Dayoub, M. Gharbi, and K. Hassan, "Blind spectrum sensing using extreme eigenvalues for cognitive radio networks," *IEEE Communications Letters*, vol. 22, no. 7, pp. 1386–1389, July 2018.

[43] K. Hassan, R. Gautier, I. Dayoub, M. Berbineau, and E. Radoi, "Multiple-antenna-based blind spectrum sensing in the presence of impulsive noise," *IEEE Transactions on Vehicular Technology*, vol. 63, no. 5, pp. 2248–2257, Jun 2014.

[44] S. Kharbech, I. Dayoub, M. Zwingelstein-Colin, and E. P. Simon, "Blind digital modulation identification for mimo systems in railway environments with high-speed channels and impulsive noise," *IEEE Transactions on Vehicular Technology*, vol. 67, no. 8, pp. 7370–7379, Aug 2018.

[45] *https://www.nt.tuwien.ac.at/christian-doppler-laboratory/cd-download/.*

[46] *"Orthogonal Frequency Division Multiplexing," U.S. Patent No. 3,488,4555, filed November 14, 1966, issued January 6, 1970.*

[47] J. A. Bingham *et al.*, "Multicarrier modulation for data transmission: An idea whose time has come," *IEEE Communications magazine*, vol. 28, no. 5, pp. 5–14, 1990.

[48] Z. Wang and G. B. Giannakis, "Wireless multicarrier communications," *IEEE signal processing magazine*, vol. 17, no. 3, pp. 29–48, 2000.

[49] R. v. Nee and R. Prasad, *OFDM for wireless multimedia communications*. Artech House, Inc., 2000.

[50] P. Banelli, S. Buzzi, G. Colavolpe, A. Modenini, F. Rusek, and A. Ugolini, "Modulation formats and waveforms for 5g networks: Who will be the heir of ofdm?: An overview of alternative modulation schemes for improved spectral efficiency," *IEEE Signal Processing Magazine*, vol. 31, no. 6, pp. 80–93, 2014.

[51] G. Berardinelli, F. M. Tavares, T. B. Sørensen, P. Mogensen, and K. Pajukoski, "Zero-tail dft-spread-ofdm signals," in *2013 IEEE Globecom Workshops (GC Wkshps)*. IEEE, 2013, pp. 229–234.

[52] A. Sahin, R. Yang, M. Ghosh, and R. L. Olesen, "An improved unique word dft-spread ofdm scheme for 5g systems," in *2015 IEEE Globecom Workshops (GC Wkshps)*. IEEE, 2015, pp. 1–6.

[53] G. Berardinelli, K. I. Pedersen, T. B. Sorensen, and P. Mogensen, "Generalized dft-spread-ofdm as 5g waveform," *IEEE Communications Magazine*, vol. 54, no. 11, pp. 99–105, 2016.

[54] R. Zayani, Y. Medjahdi, H. Shaiek, and D. Roviras, "Wola-ofdm: A potential candidate for asynchronous 5g," in *2016 IEEE Globecom Workshops (GC Wkshps)*. IEEE, 2016, pp. 1–5.

[55] X. Zhang, L. Chen, J. Qiu, and J. Abdoli, "On the waveform for 5g," *IEEE Communications Magazine*, vol. 54, no. 11, pp. 74–80, 2016.

[56] V. Vakilian, T. Wild, F. Schaich, S. ten Brink, and J.-F. Frigon, "Universal-filtered multi-carrier technique for wireless systems beyond lte," in *2013 IEEE Globecom Workshops (GC Wkshps)*. IEEE, 2013, pp. 223–228.

[57] X. Zhang, M. Jia, L. Chen, J. Ma, and J. Qiu, "Filtered-ofdm-enabler for flexible waveform in the 5th generation cellular networks," in *2015 IEEE Global Communications Conference (GLOBECOM)*. IEEE, 2015, pp. 1–6.

[58] R. Nissel, S. Schwarz, and M. Rupp, "Filter bank multicarrier modulation schemes for future mobile communications," *IEEE Journal on Selected Areas in Communications*, 2017.

[59] *Qualcomm Incorporated, "Waveform candidates," in 3GPP TSG-RAN WG1 84b, Busan, Korea, April 2016.*

[60] A. Aminjavaheri, A. Farhang, A. RezazadehReyhani, and B. Farhang-Boroujeny, "Impact of timing and frequency offsets on multicarrier waveform candidates for 5g," in *2015 IEEE Signal Processing and Signal Processing Education Workshop (SP/SPE)*. IEEE, 2015, pp. 178–183.

[61] M. Van Eeckhaute, A. Bourdoux, P. De Doncker, and F. Horlin, "Performance of emerging multi-carrier waveforms for 5g asynchronous communications," *EURASIP Journal on wireless communications and networking*, vol. 2017, no. 1, p. 29, 2017.

[62] A. I. Pérez-Neira, M. Caus, R. Zakaria, D. Le Ruyet, E. Kofidis, M. Haardt, X. Mestre, and Y. Cheng, "Mimo signal processing in offset-qam based filter bank multicarrier systems," *IEEE Transactions on Signal Processing*, vol. 64, no. 21, pp. 5733–5762, 2016.

[63] E. Kofidis, D. Katselis, A. Rontogiannis, and S. Theodoridis, "Preamble-based channel estimation in ofdm/oqam systems: A review," *Signal Processing*, vol. 93, no. 7, pp. 2038–2054, 2013.

[64] F. Schaich, T. Wild, and Y. Chen, "Waveform contenders for 5g-suitability for short packet and low latency transmissions," in *2014 IEEE 79th Vehicular Technology Conference (VTC Spring)*. IEEE, 2014, pp. 1–5.

[65] M. Bellanger, "Efficiency of filter bank multicarrier techniques in burst radio transmission," in *2010 IEEE Global Telecommunications Conference GLOBECOM 2010*. IEEE, 2010, pp. 1–4.

[66] M. Bellanger, M. Renfors, T. Ihalainen, and C. A. da Rocha, "Ofdm and fbmc transmission techniques: a compatible high performance proposal for broadband power line communications," in *ISPLC2010*. IEEE, 2010, pp. 154–159.

[67] F. Wang, D. Qu, T. Jiang, and B. Farhang-Boroujeny, "Tail shortening by virtual symbols in fbmc-oqam signals," in *2015 IEEE Signal Processing and Signal Processing Education Workshop (SP/SPE)*. IEEE, 2015, pp. 157–161.

[68] B. Farhang-Boroujeny, A. Farhang, A. RezazadehReyhani, A. Aminjavaheri, and D. Qu, "A comparison of linear fbmc and circularly shaped waveforms," in *2016 IEEE/ACES International Conference on Wireless Information Technology and Systems (ICWITS) and Applied Computational Electromagnetics (ACES)*. IEEE, 2016, pp. 1–2.

[69] H. G. Feichtinger and T. Strohmer, *Gabor analysis and algorithms: Theory and applications*. Springer Science & Business Media, 2012.

[70] B. Farhang-Boroujeny, "Ofdm versus filter bank multicarrier," *IEEE signal processing magazine*, vol. 28, no. 3, pp. 92–112, 2011.

[71] M. Bellanger, D. Le Ruyet, D. Roviras, M. Terré, J. Nossek, L. Baltar, Q. Bai, D. Waldhauser, M. Renfors, T. Ihalainen *et al.*, "Fbmc physical layer: a primer," *Phydyas*, vol. 25, no. 4, pp. 7–10, 2010.

[72] S. Dudoyer, V. Deniau, R. Adriano, M. N. B. Slimen, J. Rioult, B. Meyniel, and M. Berbineau, "Study of the susceptibility of the gsm-r communications face to the electromagnetic interferences of the rail environment," *IEEE Transactions on electromagnetic compatibility*, vol. 54, no. 3, pp. 667–676, 2011.

[73] K. Hassan, R. Gautier, I. Dayoub, M. Berbineau, and E. Radoi, "Multiple-antenna-based blind spectrum sensing in the presence of impulsive noise," *IEEE Transactions on Vehicular Technology*, vol. 63, no. 5, pp. 2248–2257, 2013.

[74] Q. Zheng, F. Wang, B. Ai, and Z. Zhong, "Multicarrier downlink transmission for high-speed railway in non-gaussian noise channels," *IEEE Access*, vol. 6, pp. 52 607–52 615, 2018.

[75] S. Kharbech, I. Dayoub, M. Zwingelstein-Colin, and E. P. Simon, "Blind digital modulation identification for mimo systems in railway environments with high-speed channels and impulsive noise," *IEEE Transactions on Vehicular Technology*, vol. 67, no. 8, pp. 7370–7379, 2018.

[76] C.-H. Yih, "Iterative interference cancellation for ofdm signals with blanking nonlinearity in impulsive noise channels," *IEEE Signal Processing Letters*, vol. 19, no. 3, pp. 147–150, 2012.

[77] P. Yang, Y. L. Guan, X. B. Liu, and Z. Liu, "An improved hybrid turbo equalizer for single carrier transmission with impulsive noise and isi," *IEEE Transactions on Vehicular Technology*, vol. 66, no. 11, pp. 9852–9861, 2017.

[78] S. V. Zhidkov, "Analysis and comparison of several simple impulsive noise mitigation schemes for ofdm receivers," *IEEE Transactions on Communications*, vol. 56, no. 1, pp. 5–9, 2008.

[79] F. H. Juwono, Q. Guo, D. Huang, and K. P. Wong, "Deep clipping for impulsive noise mitigation in ofdm-based power-line communications," *IEEE Transactions on Power Delivery*, vol. 29, no. 3, pp. 1335–1343, 2014.

[80] P. G. Georgiou, P. Tsakalides, and C. Kyriakakis, "Alpha-stable modeling of noise and robust time-delay estimation in the presence of impulsive noise," *IEEE transactions on multimedia*, vol. 1, no. 3, pp. 291–301, 1999.

[81] M. K. Ozdemir and H. Arslan, "Channel estimation for wireless ofdm systems," *IEEE Communications Surveys & Tutorials*, vol. 9, no. 2, pp. 18–48, 2007.

[82] D. Kong, D. Qu, and T. Jiang, "Time domain channel estimation for oqam-ofdm systems: Algorithms and performance bounds." *IEEE Trans. Signal Processing*, vol. 62, no. 2, pp. 322–330, 2014.

[83] B. Ai, X. Cheng, T. Kürner, Z.-D. Zhong, K. Guan, R.-S. He, L. Xiong, D. W. Matolak, D. G. Michelson, and C. Briso-Rodriguez, "Challenges toward wireless communications for high-speed railway," *IEEE transactions on intelligent transportation systems*, vol. 15, no. 5, pp. 2143–2158, 2014.

[84] R. Gerzaguet, N. Bartzoudis, L. G. Baltar, V. Berg, J.-B. Doré, D. Kténas, O. Font-Bach, X. Mestre, M. Payaró, M. Färber *et al.*, "The 5g candidate waveform race: a comparison of complexity and performance," *EURASIP Journal on Wireless Communications and Networking*, vol. 2017, no. 1, p. 13, 2017.

[85] G. B. Giannakis and C. Tepedelenlioglu, "Basis expansion models and diversity techniques for blind identification and equalization of time-varying channels," *Proceedings of the IEEE*, vol. 86, no. 10, pp. 1969–1986, 1998.

[86] Z. Tang, R. C. Cannizzaro, G. Leus, and P. Banelli, "Pilot-assisted time-varying channel estimation for ofdm systems," *IEEE Transactions on Signal Processing*, vol. 55, no. 5, pp. 2226–2238, 2007.

[87] D. K. Borah and B. Hart, "Frequency-selective fading channel estimation with a polynomial time-varying channel model," *IEEE Transactions on Communications*, vol. 47, no. 6, pp. 862–873, 1999.

[88] Y. E. H. Shehadeh and S. Sezginer, "Fast varying channel estimation in downlink lte systems," in *21st Annual IEEE International Symposium on Personal, Indoor and Mobile Radio Communications*. IEEE, 2010, pp. 608–613.

[89] S. O. Haykin, *Adaptive filter theory*. Pearson Higher Ed, 2013.

[90] Y. Li, L. J. Cimini, and N. R. Sollenberger, "Robust channel estimation for ofdm systems with rapid dispersive fading channels," *IEEE Transactions on communications*, vol. 46, no. 7, pp. 902–915, 1998.

[91] S. Y. Park, Y. G. Kim, and C. G. Kang, "Iterative receiver for joint detection and channel estimation in ofdm systems under mobile radio channels," *IEEE Transactions on Vehicular Technology*, vol. 53, no. 2, pp. 450–460, 2004.

[92] R. Nissel, E. Zochmann, and M. Rupp, "On the influence of doubly-selectivity in pilot-aided channel estimation for fbmc-oqam," in *Vehicular Technology Conference (VTC Spring), 2017 IEEE 85th*. IEEE, 2017, pp. 1–5.

[93] K. Zhong, X. Lei, B. Dong, and S. Li, "Channel estimation in ofdm systems operating under high mobility using wiener filter combined basis expansion model," *EURASIP Journal on Wireless Communications and Networking*, vol. 2012, no. 1, p. 186, 2012.

[94] H. Hijazi and L. Ros, "Joint data qr-detection and kalman estimation for ofdm time-varying rayleigh channel complex gains," 2010.

[95] M. Aldababseh and A. Jamoos, "Estimation of fbmc/oqam fading channels using dual kalman filters," *The Scientific World Journal*, vol. 2014, 2014.

[96] A. Kalakech, M. Berbineau, I. Dayoub, and E. P. Simon, "Time-domain lmmse channel estimator based on sliding window for ofdm systems in high-mobility situations," *IEEE Transactions on Vehicular Technology*, vol. 64, no. 12, pp. 5728–5740, 2015.

[97] C. Sgraja and J. Lindner, "Estimation of rapid time-variant channels for ofdm using wiener filtering," in *IEEE International Conference on Communications, 2003. ICC'03.*, vol. 4. IEEE, 2003, pp. 2390–2395.

[98] R. Nissel, F. Ademaj, and M. Rupp, "Doubly-selective channel estimation in fbmc-oqam and ofdm systems," in *2018 IEEE 88th Vehicular Technology Conference (VTC-Fall)*. IEEE, 2018, pp. 1–5.

[99] Y. Cocheril, M. Berbineau, P. Combeau, and Y. Pousset, "On the importance of the mimo channel correlation in underground railway tunnels," *Journal of Communication*, vol. 4, no. 4, pp. 224–231, 2009.

[100] B. Zhang, Z. Zhong, R. He, K. Guan, J. Ding, and C. Briso-Rodríguez, "Empirical correlation property of multi-path for high-speed railways in composite propagation scenario," in *2015 IEEE International Symposium on Antennas and Propagation & USNC/URSI National Radio Science Meeting*. IEEE, 2015, pp. 91–92.

[101] A. Paier, T. Zemen, L. Bernadó, G. Matz, J. Karedal, N. Czink, C. Dumard, F. Tufvesson, A. F. Molisch, and C. F. Mecklenbrauker, "Non-wssus vehicular channel characterization in highway and urban scenarios at 5.2 ghz using the local scattering function," in *2008 International ITG Workshop on Smart Antennas*. IEEE, 2008, pp. 9–15.

[102] J.-P. Javaudin, D. Lacroix, and A. Rouxel, "Pilot-aided channel estimation for ofdm/oqam," in *Vehicular Technology Conference, 2003. VTC 2003-Spring. The 57th IEEE Semiannual*, vol. 3. IEEE, 2003, pp. 1581–1585.

[103] C. Lélé, R. Legouable, and P. Siohan, "Channel estimation with scattered pilots in ofdm/oqam," in *Signal Processing Advances in Wireless Communications, 2008. SPAWC 2008. IEEE 9th Workshop on*. IEEE, 2008, pp. 286–290.

[104] R. Nissel and M. Rupp, "On pilot-symbol aided channel estimation in fbmc-oqam," in *Acoustics, Speech and Signal Processing (ICASSP), 2016 IEEE International Conference on*. IEEE, 2016, pp. 3681–3685.

[105] W. Cui, D. Qu, T. Jiang, and B. Farhang-Boroujeny, "Coded auxiliary pilots for channel estimation in fbmc-oqam systems," *IEEE Transactions on Vehicular Technology*, vol. 65, no. 5, pp. 2936–2946, 2016.

[106] M. Fuhrwerk, S. Moghaddamnia, and J. Peissig, "Scattered pilot-based channel estimation for channel adaptive fbmc-oqam systems," *IEEE Transactions on Wireless Communications*, vol. 16, no. 3, pp. 1687–1702, 2017.

[107] M. Caus, A. I. Pérez-Neira *et al.*, "Transmitter-receiver designs for highly frequency selective channels in mimo fbmc systems." *IEEE Transactions on Signal Processing*, vol. 60, no. 12, p. 6519, 2012.

[108] X. Mestre and D. Gregoratti, "Parallelized structures for mimo fbmc under strong channel frequency selectivity," *IEEE Transactions on Signal Processing*, vol. 64, no. 5, pp. 1200–1215, 2015.

[109] D. S. Waldhauser, L. G. Baltar, and J. A. Nossek, "Mmse subcarrier equalization for filter bank based multicarrier systems," in *Signal Processing Advances in Wireless Communications, 2008. SPAWC 2008. IEEE 9th Workshop on*. IEEE, 2008, pp. 525–529.

[110] M. Bellanger, "Fs-fbmc: An alternative scheme for filter bank based multicarrier transmission," in *2012 5th International Symposium on Communications, Control and Signal Processing*. IEEE, 2012, pp. 1–4.

[111] A. Ikhlef and J. Louveaux, "Per subchannel equalization for mimo fbmc/oqam systems," in *2009 IEEE Pacific Rim Conference on Communications, Computers and Signal Processing*. IEEE, 2009, pp. 559–564.

[112] L. Marijanović, S. Schwarz, and M. Rupp, "Mmse equalization for fbmc transmission over doubly-selective channels," in *Wireless Communication Systems (ISWCS), 2016 International Symposium on*. IEEE, 2016, pp. 170–174.

[113] R. Nissel, M. Rupp, and R. Marsalek, "Fbmc-oqam in doubly-selective channels: A new perspective on mmse equalization," in *Signal Processing Advances in Wireless Communications (SPAWC), 2017 IEEE 18th International Workshop on*. IEEE, 2017, pp. 1–5.

[114] M. Saideh, I. Dayoub, and M. Berbineau, "Efficient equalization for fbmc-oqam under doubly selective channel estimation errors," *IEEE Communications Letters*, vol. 23, no. 5, pp. 863–866, 2019.

[115] ITU, "Recommendation itu-r m.1225: Guidelines for evaluation of radio transmission technologies for imt-2000," *tech. rep., ITU, 1997*.

[116] G. Wunder, P. Jung, M. Kasparick, T. Wild, F. Schaich, Y. Chen, S. Ten Brink, I. Gaspar, N. Michailow, A. Festag *et al.*, "5gnow: non-orthogonal, asynchronous waveforms for future mobile applications." *IEEE Communications Magazine*, vol. 52, no. 2, pp. 97–105, 2014.

[117] Y. Saito, A. Benjebbour, Y. Kishiyama, and T. Nakamura, "System-level performance evaluation of downlink non-orthogonal multiple access (noma)," in *2013 IEEE 24th Annual International Symposium on Personal, Indoor, and Mobile Radio Communications (PIMRC)*. IEEE, 2013, pp. 611–615.

[118] A. Li, A. Harada, and H. Kayama, "A novel low computational complexity power assignment method for non-orthogonal multiple access systems," *IEICE Transactions on Fundamentals of Electronics, Communications and Computer Sciences*, vol. 97, no. 1, pp. 57–68, 2014.

[119] H. Weingarten, Y. Steinberg, and S. S. Shamai, "The capacity region of the gaussian multiple-input multiple-output broadcast channel," *IEEE transactions on information theory*, vol. 52, no. 9, pp. 3936–3964, 2006.

[120] Y. Saito, Y. Kishiyama, A. Benjebbour, T. Nakamura, A. Li, and K. Higuchi, "Non-orthogonal multiple access (noma) for cellular future radio access," in *2013 IEEE 77th vehicular technology conference (VTC Spring)*. IEEE, 2013, pp. 1–5.

[121] Z. Ding, F. Adachi, and H. V. Poor, "Performance of mimo-noma downlink transmissions," in *2015 IEEE Global Communications Conference (GLOBECOM)*. IEEE, 2015, pp. 1–6.

[122] M. Zeng, A. Yadav, O. A. Dobre, G. I. Tsiropoulos, and H. V. Poor, "On the sum rate of mimo-noma and mimo-oma systems," *IEEE Wireless Communications Letters*, vol. 6, no. 4, pp. 534–537, 2017.

[123] Y. Alsaba, C. Y. Leow, and S. K. A. Rahim, "Full-duplex cooperative non-orthogonal multiple access with beamforming and energy harvesting," *IEEE Access*, vol. 6, pp. 19 726–19 738, 2018.

[124] J. G. Andrews and T. H. Meng, "Optimum power control for successive interference cancellation with imperfect channel estimation," *IEEE Transactions on Wireless Communications*, vol. 2, no. 2, pp. 375–383, 2003.

[125] A. Maatouk, E. Çalışkan, M. Koca, M. Assaad, G. Gui, and H. Sari, "Frequency-domain noma with two sets of orthogonal signal waveforms," *IEEE Communications letters*, vol. 22, no. 5, pp. 906–909, 2018.

[126] Y. Fu, L. Salaün, C. W. Sung, and C. S. Chen, "Subcarrier and power allocation for the downlink of multicarrier noma systems," *IEEE Transactions on Vehicular Technology*, vol. 67, no. 12, pp. 11 833–11 847, 2018.

[127] F. Fang, Z. Ding, W. Liang, and H. Zhang, "Optimal energy efficient power allocation with user fairness for uplink mc-noma systems," *IEEE Wireless Communications Letters*, 2019.